Dynamics of Systems of Charged Particles Sedimenting in a Viscous Fluid

Christopher I Trombley

Doctoral thesis advisor:
Maria L. Ekiel-Jezewska

Institute Of Fundamental Technological Research,
Polish Academy of Sciences

Warsaw
June 25, 2021

Contents

Abstract

This thesis consists of three publications, a review chapter on the basic concepts of Stokes flows and two original papers on charged particles sedimenting under gravity in a Stokes flow.

It has been known from the literature that for certain initial conditions, two uncharged spherical particles with different densities and radii sedimenting in a Stokes flow can stay close together even after long periods of time. Uncharged stationary relative positions have the line of particle centers either aligned with or at a right angle with the direction of gravity. The bounded relative orbits consist of periodic orbits and heteroclinics. However, these bounded relative orbits and stationary relative positions are at best neutrally stable. Also, the volume of initial conditions in which the relative distance of uncharged particles stays bounded is small.

In this thesis it is shown that electrostatic interaction changes the qualitative dynamics of the pair of particles settling under gravity in a viscous fluid. In particular, two charged particles settling in a Stokes flow may have configurations which are asymptotically stable to perturbations. Thus Earnshaw's Theorem, which states that there is no stable steady configuration of charged particles in a vacuum, does not generalize to the case of charged particles in a fluid.

A pair of charged particles can have stable stationary relative positions with a line of particle centers aligned with gravity or inclined. There are no periodic orbits for pair of charged particles settling under gravity in a Stokes flow. In addition, there can be multiple stable stationary relative positions. For given values of the parameters, there can exist two stable stationary relative position with line of particle centers aligned with gravity. If there exists a stable stationary relative position with line of particle centers inclined with gravity then there are two found symmetrically across the line of symmetry.

Stable doublets only form between particles of different densities and different radii, but can exist even if the charge is arbitrarily small. In fact, analyzing the conditions when stable and non-overlapping doublets can exist gives bounds on particle parameters - ratio of particle densities relative to the fluid density, ratio of particle radii and the ratio of characteristic electrostatic force to characteristic gravitational force. Phase space diagrams are given describing bounds of the ratio of Stokes velocities and particle radii. The region consistent with the existence of a stable stationary relative position is given, as well as regions in which stability to some but not all perturbations can exist. A diagram is

also provided which shows the maximum distance between the pair of particles given the ratio of Stokes velocity and ratio of particle radii.

The larger particle is always above the smaller particle at the stable stationary relative position. For there to exist a stable stationary state, either the particles must be both denser than the fluid or both less dense than the fluid. If the particles are denser than the fluid, then the smaller particle must be denser than the larger one and if they are less dense then the smaller particle must be less dense than the larger one. When the line of particle centers is inclined with respect to gravity, the Stokes velocities must be such that the isolated larger particle would sediment faster than the smaller particle, but when the line of particle centers is aligned with gravity there are examples where the isolated larger particle could have greater or lower Stokes velocity than the smaller one.

There are stable stationary relative positions for arbitrarily large separations between the particles. For large separations, the upper particle must have a slightly greater Stokes velocity than the lower one. Additionally, the characteristic electrostatic force must be large in comparison to the characteristic gravitational force. It is also shown that if the particles have both very close Stokes velocities and very close densities, then the ratio of characteristic forces consistent with a stable stationary relative position can be very small.

The basin of attraction of the stationary relative position is can have a horizontal cross section radius large in comparison to the sum of particle radii and is unbounded above. The set of relative orbits which stay bounded is separated from the relative orbits which go to infinity by a seperatrix curve. On this seperatrix there is a saddle point stationary relative position. The distance between particles when they are at this saddle point is a good measure of the radius of the cross-section of the basin of attraction of the stable stationary relative position. The qualitative dynamics are established using the Poincare-Bendixson theorem.

The existence and large basins of attraction of such stable doublets of charged sedimenting particles is fundamental. With the broad range of parameters consistent with the existence of stable doublets, these results may be significant for dilute charged particulate systems in biological, medical and industrial contexts.

Streszczenie

Na niniejszy doktorat składają się: jeden artykuł przeglądowy na temat podstawowych pojęć przepływów Stokesa i dwie oryginalne publikacje poświęcone cząstkom naładowanym sedymentującym w przepływie Stokesa.

Z literatury wiadomo, że dla pewnych warunków początkowych dwie nienaładowane cząstki sferyczne o różnych gęstościach i promieniach opadające grawitacyjnie w przepływie Stokesa mogą pozostawać blisko siebie nawet na długich skalach czasu. Stacjonarne względne położenia nienaładowanych cząstek są takie, że linia prosta łącząca środki cząstek jest równoległa lub prostopadła do grawitacji. Ograniczone względne trajektorie to orbity periodyczne i heterokliniki. Jednakże zarówno ograniczone względne trajektorie jak i punkty stacjonarne są co najwyżej neutralnie stabilne. Poza tym objętość zbioru położeń początkowych prowadzących do ograniczonych względnych trajektorii jest niewielka.

W niniejszym doktoracie zostało pokazane, że oddziaływanie elektrostatyczne jakościowo zmienia dynamikę pary cząstek opadających grawitacyjnie w lepkim płynie. A mianowicie, dwie naładowane cząstki opadające w płynie opisywanym przybliżeniem Stokesa mogą tworzyć konfiguracje asymptotycznie stabilne względem zaburzeń. A zatem dla układu cząstek w naładowanym płynie nie można uogólnić twierdzenia Earnshawa, które orzeka, że w próżni nie ma stabilnych stacjonarnych konfiguracji cząstek naładowanych.

Para cząstek naładowanych może tworzyć stabilną konfigurację o pionowej lub nachylonej linii łączącej środki cząstek, natomiast nie może wykonywać ruchów periodycznych. W dodatku dla ustalonych wartości parametrów, możliwe jest istnienie więcej niż jednej stabilnej stacjonarnej konfiguracji względnych położeń cząstek. W takim przypadku linie proste łącząca środki cząstek mogą być zarówno wzdłuż kierunku grawitacji jak i względem niego nachylone.

Stabilne pary mogą tworzyć tylko takie cząstki naładowane, które mają różne gęstości i promienie, natomiast ich ładunek może być dowolnie mały. W pracy podane zostały ograniczenia na wartości parametrów układu – stosunku gęstości względnych cząstek, stosunku promieni oraz stosunku charakterystycznej siły elektrostatycznej do charakterystycznej siły grawitacji – konieczne do spełnienia aby zaistniała możliwość utworzenia przez cząstki naładowane stabilnej pary. Wyznaczono diagram fazowy w

przestrzeni stosunku promieni i oraz stosunku prędkości Stokesa, podając obszary, dla których możliwe jest istnienie stabilnych stanów stacjonarnych, a także obszary, gdzie występują konfiguracje stabilne tylko ze względu na niektóre (nie wszystkie) zaburzenia. Dodatkowo pokazane zostało jakich wartości odległości między cząstkami w stabilnym stanie stacjonarnym można oczekiwać dla jakich stosunków prędkości Stokesa i promieni.

W stabilnej konfiguracji stacjonarnej, większa cząstka jest zawsze powyżej cząstki mniejszej, a poza tym obie cząstki muszą mieć większe gęstości niż płyn, lub obie mniejsze. Jeśli cząstki są gęstsze niż płyn, to w stabilnej konfiguracji stacjonarnej mniejsza cząstka musi być gęstsza niż większa cząstka. Jeśli zaś cząstki są mniej gęste od płynu, to w stabilnej konfiguracji stacjonarnej mniejsza cząstka musi być mniej gęsta niż większa cząstka. Gdy w stabilnym stanie stacjonarnym linia prosta łącząca środki cząstek jest nachylona względem kierunku grawitacji, to prędkości Stokesa są takie, że izolowana większa cząstka opadałaby szybciej niż mniejsza. Jeśli jednak linia prosta łącząca środki cząstek jest równoległa do kierunku grawitacji, to są przykłady pokazujące na to, że izolowana większa cząstka może mieć zarówno większą jak i mniejszą prędkość Stokesa od cząstki mniejszej.

Istnieją stabilne stacjonarne położenia względne dla dowolnie dużych odległości między cząstkami. Dla dużych odległości, górna cząstka musi mieć nieco większą prędkość Stokesa od niższej cząstki. Ponadto charakterystyczna siła elektrostatyczna musi być duża w porównaniu z charakterystyczną siłą grawitacji. Pokazano także, że jeśli prędkości Stokesa obu cząstek bardzo nieznacznie różnią się od siebie, a ich gęstości są niemal równe, to stabilne stacjonarne konfiguracje są osiągane dla bardzo małych wartości opisanego powyżej stosunku sił charakterystycznych.

Basen przyciągania stanów stacjonarnych względnych położeń jest nieograniczony od góry, przy czym promień poziomego przekroju czynnego może być duży w porównaniu z sumą promieni cząstek. Zbiór ograniczonych orbit ruchu względnego jest oddzielony saparatrysą od orbit dążących do nieskończoności. Na tej saparatrysie ruchów względnych znajduje się punkt stacjonarny będący siodłem. Odległość między cząstkami w tym punkcie jest w przybliżeniu taka jak promień przekroju czynnego dla trajektorii przyciąganych do stabilnego punktu stacjonarnego. Jakościowa dynamika jest wyznaczona z użyciem twierdzenia Poincaré-Bendixsona.

Istnienie dużych basenów przyciągania stabilnych par naładowanych cząstek opadających w lepkim płynie jest fundamentalne. Zważywszy na to, że stabilne stacjonarne konfiguracje par wystepują dla szerokiego zakresu parametrów, wyniki niniejszego doktoratu mogą być znaczące dla rozrzedzonych układów cząstek w kontekstach biologicznych, medycznych i przemysłowych.

1 Motivation

This thesis is made up of three publications. The publications are a review chapter on the basic concepts of Stokes flows [1] and two original papers on charged particles sedimenting under gravity in a Stokes flow [2, 3].

Non-inertial "Stokes flows", introduced in [4] , have a central place in sedimentation [5, 6, 7] and the dynamics of micro and nanoparticles more generally [8, 9, 10, 11, 12, 13, 14, 15].

The dynamics of hydrodynamically interacting particles in a Stokes flow can become complicated. Large scale spontaneous self-organization into ordered structures has been observed in, for instance, many drops in a Hele-Shaw cell [16, 17] and many magnetically active rollers near a repelling wall [18]. Spontaneous organization has applications such as the design of micro swimmers which can capture cargo [19] for, e.g., drug delivery [20]. Smaller scale organization of particles in Stokes flows has been observed such as formation of doublets for drops in a Hele-Shaw cell [21], pairs of magnetically active rollers near a repelling wall [22] and many others.

It has been shown [23] there is a set of initial conditions for two uncharged spherical particles of different radii and different masses settling under gravity in a Stokes flow for which the particles do not tend to separate. The relative orbits generated by these initial conditions consist of periodic orbits and heteroclinic orbits. The bounded relative orbits and stationary relative positions are at best neutrally stable. Further the set of initial conditions which lead to these orbits is bounded. The set is small enough that capture will probably have no significant effect on the dynamics of sedimenting suspensions e.g. [24, 25, 26, 27].

The question that motivates this thesis is if it is possible for new forces, such as electrostatic forces, to stabilize pairs of sedimenting particles. Electrostatically stabilized pairs of sedimenting particles are interesting for the simple reason that charged particles in fluids are very common. However, electrostatic forces in a vacuum are destablizing by Earnshaw's Theorem, introduced in [28]. Geometrically, Earnshaw's theorem holds because the electrostatic field is a harmonic function away from the charges [29] and therefore the strong maximum principle (see 6.4.2 in [30]) implies there can be no minimum to the electrostatic potential away from the boundary. It will be shown in this thesis that this theorem does not generalize to the presence of a fluid.

2 Goal & Structure Of The Thesis

The goal of this thesis is to utilize a simple "point particle" model to understand the conditions under which charged particles sedimenting under gravity in a Stokes flow can form stable doublets with large basins of attraction. In order to accomplish this goal, this thesis consists of three publications [1, 2, 3].

A. Trombley, C.I. and Ekiel-Jeżewska, M.L., 2019. Basic Concepts of Stokes Flows. In Flowing Matter (pp. 35-50). Editors: Toschi, F. and Sega, M., Springer, Cham. `https://doi.org/10.1007/978-3-030-23370-9_2`

   - Abstract: Various properties essential to the understanding of Stokes flow are discussed, including reversibility, negligibility of inertial forces and minimum energy dissipation theorem. Illustrative examples related to these properties are provided: inertial terms for the fluid flow generated by a rotating cylinder, force on a rotating cylinder close to a solid plane wall, Stokes paradox, energy dissipation for particles of different shapes. The meaning and the limits of the Stokes approximation are discussed in the context of more general equations.
   - This work was supported in part by Narodowe Centrum Nauki under grant No. 2014/15/B/ST8/04359. We acknowledge scientific benefits from COST Action MP1305.

B. Trombley, C.I. and Ekiel-Jeżewska, M.L., 2018. Stable Configurations of Charged Sedimenting Particles. Physical Review Letters, 121(25), p.254502. `https://doi.org/10.1103/PhysRevLett.121.254502`

   - Abstract: The qualitative behavior of charged particles in a vacuum is given by Earnshaw's theorem, which states that there is no steady configuration of charged particles in a vacuum that is asymptotically stable to perturbations. In a viscous fluid, examples of stationary configurations of sedimenting uncharged particles are known, but they are unstable or neutrally stable—they are not attractors. In this Letter, it is shown by example that two charged particles settling in a fluid may have a configuration that is asymptotically stable to perturbations for a wide range of charges, radii, and densities.

The existence of such "bound states" is essential from a fundamental point of view and it can be significant for dilute charged particulate systems in various biological, medical, and industrial contexts.

- The supplemental material to this article is also included. The supplemental material was published at `https://journals.aps.org/prl/supplemental/10.1103/PhysRevLett.121.254502`
- This Letter was supported in part by Narodowe Centrum Nauki under Grant No. 2014/15/B/ST8/04359. We acknowledge scientific benefits from COST Action MP1305.

C. Trombley, C.I. and Ekiel-Jezewska, M.L., 2021. Relative trajectories of two charged sedimenting particles in a Stokes flow. Journal of Physics Communications. Accepted Manuscript online 27 May 2021 . `https://doi.org/10.1088/2399-6528/ac060c`

- Abstract: We study the dynamics of two charged point particles settling in a Stokes flow. We find what ranges of initial relative positions and what ranges of system parameters lead to formation of stable doublets. The system is parameterized by the ratio of radii, ratio of masses and the ratio of electrostatic to gravitational force. We focus on opposite charges. We find a new class of stationary states with the line of the particle centers inclined with respect to gravity and demonstrate that they are always locally asymptotically stable. Stability properties of stationary states with the vertical line of the particle centers are also discussed. We find examples of systems with multiple stable stationary states. We show that the basin of attraction for each stable stationary state has infinite measure, so that particles can capture one another even when they are very distant, and even if their charge is very small. This behavior is qualitatively different from the uncharged case where there only exists a bounded set of periodic relative trajectories. We determine the range of ratios of Stokes velocities and ratio masses which give rise to non-overlapping stable stationary states (given the appropriate ratio of electrostatic to gravitational force). For non-overlapping stable inclined or vertical stationary states the larger particle is always above the smaller particle. The non-overlapping stable inclined stationary states exist only if the larger particle has greater Stokes velocity, but there are non-overlapping stable vertical stationary states where the larger particle has higher or lower Stokes velocity.
- This work was supported in part by the National Science Centre under grant UMO2018/31/B/ST8/03640.

For the remainder of this introduction, these three publications will be referred to as article A [1], article B [2] and article C [3]. In section 3, the background of Stokes Flows from article A and the point particle model analyzed in article B and article C are expounded. In section 4 there is a brief

overview of some of the original results in article B & article C. A summary and some general conclusions are drawn in section 5. Full-text articles along with supplementary materials are provided in section 7. Signed declarations of author contributions are provided in Section 8.

3 Methods & Model

3.1 Stokes Flows

Many fluid systems have weak inertial fluid forces in comparison to viscous forces. Stokes flows are fluid flows in which inertial forces are dominated by viscous forces to the point that inertial forces are negligible. Many high quality introductions to Stokes flows have been written such as those in [8, 9, 10, 11, 12, 13, 14, 15, 31]. The Stokes equations of an incompressible fluid are

$$\mu\nabla^2\mathbf{u} - \nabla p = 0 \tag{3.1}$$
$$\nabla \cdot \mathbf{u} = 0 \tag{3.2}$$

where μ is the dynamic viscosity, $\mathbf{u}$ is the fluid velocity and p is the fluid pressure.

Article A is a review chapter on the basic concepts of incompressible Stokes flow. This subsection will follow that paper. In article A, two approaches to Stokes flow are given: 1) starting from the Navier-Stokes equations and moving to the limit of low Reynolds number & 2) finding the differentiable and solenoidal vector field which attains the minimum of the extensive energy dissipation rate for given boundary conditions. In addition, article A covers topics such as reversibility of Stokes flows and the relation between Stokes and other fluid flow equations.

For now, I will discuss the Stokes equations using the "variational" approach as in section 2.4 of article A, while also drawing on 3.4 of [8] and section 2.2 of [11]. There are many interesting comments on variational methods in fluid mechanics in general in [32].

Let the flow $\mathbf{u}$ be a vector field which is continuously differentiable and solenoidal - that is, $\mathbf{u}$ obeys equation (3.2) - within a volume V and with given boundary conditions on ∂V. Further, let $\mathbf{e^u}$ be the rate of strain tensor given component-wise as

$$e^{\mathbf{u}}_{ij} = \frac{1}{2}(\frac{\partial u_i}{\partial x_j} + \frac{\partial u_j}{\partial x_i}) \tag{3.3}$$

.

An integral of $\mathbf{e^u}$ multiplied by itself is the extensive energy dissipation rate E

$$E = \int 2\mu \mathbf{e^u} : \mathbf{e^u} dV \tag{3.4}$$

where : is the double dot product. In article A, there is a brief demonstration that the differentiable & solenoidal minimizer of this integral subject to boundary conditions solves Stokes equations (3.1) & (3.2) with the same boundary conditions. Similar demonstrations can be found in [11] and other sources. In fact, the minimum energy dissipation principle, introduced in [33], states that a necessary and sufficient condition for a differentiable solenoidal vector field to minimize integral (3.4) subject to given boundary conditions is for $\mathbf{u}$ to solve the Stokes equations (3.1) & (3.2) for the same boundary conditions.

This variational point of view can be useful for reasoning about Stokes flows. One might wonder if an object with a jagged boundary experiences more drag (i.e. force component antiparallel with motion) than its convex hull. But because Stokes flows minimize the extensive energy dissipation rate E, they exhibit inclusion monotonicity [34]. One consequence of inclusion monotonicity is that a large particle which could include a smaller particle must experience at least as much drag as the small particle when undergoing the same translation in a fluid with the same boundary conditions. Therefore, for instance, making a particle convex by filling in the jagged bits cannot reduce the drag on a particle. For more discussion see section 2.4 of article A.

This concludes the material from article A which will be used in this introduction. However, one can also observe that (3.1) & (3.2) are linear partial differential equations. Therefore they can be solved by Green's function methods. For an unbounded fluid which is at rest far from the particles, the Green Tensor $\mathbf{G}/8\pi\mu$ to find $\mathbf{u}$ at a given point $\mathbf{r}$ is

$$\frac{1}{8\pi\mu}\mathbf{G}(\mathbf{r}) = \frac{1}{8\pi\mu|\mathbf{r}|}(\mathbf{I} + \frac{\mathbf{r}\otimes\mathbf{r}}{|\mathbf{r}|^2}) \tag{3.5}$$

where $\mathbf{I}$ is the identity tensor. Notice that $\mathbf{G}$ is symmetric under the mapping $\mathbf{r} \to -\mathbf{r}$. The product of this tensor with an external force gives a velocity field, or "Stokeslet". There is also a Green tensor for the pressure [11]. The Green tensor (3.5) - which is also sometimes called the Oseen tensor - will be used in our analysis of the dynamics of a pair of charged settling particles in a Stokes flow.

3.2 Charged Point Particles Settling Under Gravity In A Stokes Flow

In article B & article C, a model was introduced in order to examine the dynamics of a pair of charged particles with radii a_1 & a_2, masses M_1 & M_2 and

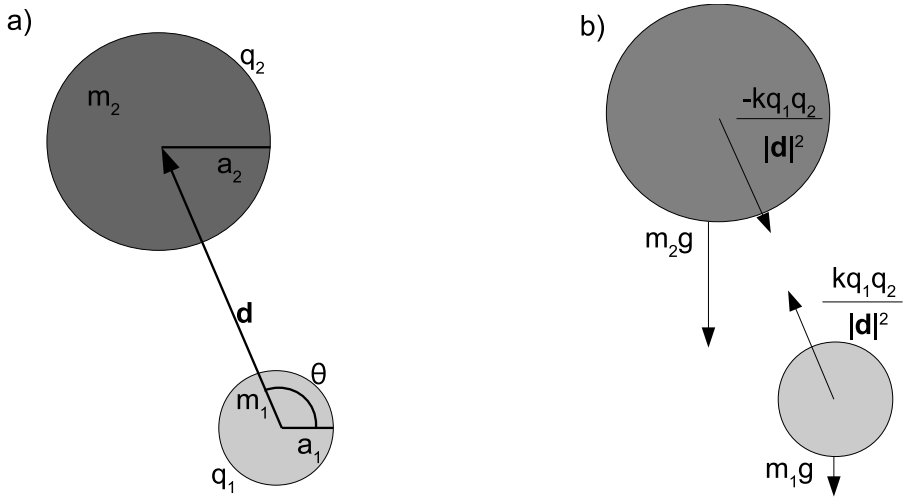

Figure 3.1: (a) Geometric coordinates chosen for a pair of charged particles sedimenting in a viscous fluid under gravity with radii a_1 & a_2, reduced masses m_1 & m_2 and charges q_1 & q_2. Interparticle position $\mathbf{d}$ and its angle θ from the direction perpendicular to gravity is also shown. (b) Diagram of external forces on the same system.

charges q_1 & q_2 sedimenting under constant gravity in a Stokes flow with density ρ and dynamic viscosity μ. Particle labels are chosen so that $a_1 \leq a_2$. To take care of buoyancy, the reduced mass $m_i = M_i - \frac{4}{3}\pi a_i^3 \rho$ is used for particle $i = 1, 2$. This system is illustrated in figure 3.1(a).

The model is constructed using the "point particle approximation" where the forces are assumed to act on the centers of the particles. The point particle approximation may be physically accurate if the particles are not too close.

With external force $\mathbf{f}_i$ acting on particle i and assuming the fluid velocity goes to zero far from the pair of particles we can use (3.5) to find the Stokeslet of particle i at the location of the center of particle $3 - i$

$$\frac{1}{8\pi\mu}\boldsymbol{G}(\mathbf{d}) \cdot \mathbf{f}_i \tag{3.6}$$

where $\mathbf{d}$ is the vector starting on the center of particle 1 and ending on the center of particle 2 as in 3.1(a). This is used as the interaction contribution to particle velocity.

The self-contribution of the particle to its own velocity comes from Stokes law

$$\frac{1}{6\pi\mu a_i}\mathbf{f}_i \tag{3.7}$$

The sum of (3.6) & (3.7) gives the velocity of each particle.

Moving on to the external forces $\mathbf{f}_i$: gravitational and electrostatic. The diagram of external forces is in figure 3.1(b). A unit vector $\hat{z}$ is chosen so that the gravitational force $\mathbf{f}_{m,i}$ on particle i is

$$\mathbf{f}_{m,i} = -m_i g \hat{z}. \tag{3.8}$$

where g is the acceleration due to gravity. In order to arrive at the simplest possible model and apply the point particle approximation consistently, the electrostatic force $\mathbf{f}_{q,i}$ in article B & article C was chosen to be Coulomb, i.e.

$$\mathbf{f}_{q,i}(\mathbf{d}) = (-1)^i k q_i q_{3-i} \frac{\mathbf{d}}{|\mathbf{d}|^3} \tag{3.9}$$

where k is Coulomb's constant. This approximation leaves out considerations such as anisotropy of charge, motile charges on the surface of the particle and screening. In total, the sum of the external forces acting on particle i is

$$\mathbf{f}_i(\mathbf{d}) = \mathbf{f}_{m,i} + \mathbf{f}_{q,i}(\mathbf{d}) \tag{3.10}$$

With those external forces, one can find the relative particle center velocity $\dot{\mathbf{d}}$ in the point particle approximation. The result is the following nonlinear vectorial ordinary differential equation

$$\dot{\mathbf{d}} = \left(\frac{1}{8\pi\mu}\boldsymbol{G}(\mathbf{d})\cdot\mathbf{f}_1(\mathbf{d}) + \frac{1}{6\pi\mu a_2}\mathbf{f}_2(\mathbf{d})\right) - \left(\frac{1}{8\pi\mu}\boldsymbol{G}(\mathbf{d})\cdot\mathbf{f}_2(\mathbf{d}) + \frac{1}{6\pi\mu a_1}\mathbf{f}_1(\mathbf{d})\right) \tag{3.11}$$

The term in the first parentheses is the velocity of particle 2 and the term in the second is the velocity of particle 1.

Reasoning about equation (3.11) is simplified by non-dimensionalization. The units chosen are a length unit L and velocity unit V_0.

$$L = a_1 + a_2, \tag{3.12}$$

$$V_0 = \frac{m_2 g}{6\pi\mu L} \tag{3.13}$$

From this one can define, e.g. a characteristic time scale $T = L/V_0$. Notice that looking at systems with different viscosity merely changes the units. This is because Stokes flows are always dynamically similar. One can also see the nondimensional separation vector between particle centers is

$$\boldsymbol{\alpha} = \frac{\boldsymbol{d}}{L} \tag{3.14}$$

It will also be helpful to define $\alpha = |\boldsymbol{\alpha}|$ as the norm of the nondimensional separation vector. In article B, it was found that the system depends on three non-dimensional parameters:

$$\beta = -\frac{kq_1q_2}{L^2m_2g} \tag{3.15}$$

$$\gamma = \frac{a_1}{a_2}, \tag{3.16}$$

$$\delta = \frac{m_1}{m_2} \tag{3.17}$$

One can see that β is a ratio of a characteristic gravitational force, γ is the ratio between particle radii and δ the ratio of reduced masses. Parameters β & γ are defined to be positive when the particles are denser than the fluid and the charges are opposite. For a discussion of how the system behaves when one or both particles are less dense than the fluid, see the supplemental material to article B. Equations (3.15) - (3.17) correspond to equations (6) in article B and equations (12)-(14) in article C. With these definitions, δ/γ is the ratio of Stokes velocities and δ/γ^3 is the ratio of reduced particle densities.

Nondimeninsionalizing equation (3.11) one gets the following non-dimensional nonlinear vector ordinary differential equation

$$\begin{aligned}\dot{\boldsymbol{\alpha}} &= \frac{3}{2|\boldsymbol{\alpha}|^3}\beta\,\boldsymbol{\mathcal{G}}\cdot\boldsymbol{\alpha} + \frac{3}{4}(1-\delta)\,\boldsymbol{\mathcal{G}}\cdot\hat{\mathbf{z}} - \beta\frac{(1+\gamma)^2}{\gamma|\boldsymbol{\alpha}|^3}\boldsymbol{\alpha} \\ &- \frac{(\gamma-\delta)(1+\gamma)}{\gamma}\hat{\mathbf{z}}\end{aligned} \tag{3.18}$$

where $\boldsymbol{\mathcal{G}}$ is the nondimensionalized Green's tensor

$$\boldsymbol{\mathcal{G}}(\boldsymbol{\alpha}) = \frac{1}{|\boldsymbol{\alpha}|}(\mathbf{I} + \frac{\boldsymbol{\alpha}\otimes\boldsymbol{\alpha}}{|\boldsymbol{\alpha}|^2}) \tag{3.19}$$

The results in article B & article C were established via mathematical analysis of equation (3.18), which is equation (9) in article B and equation (14) in article C.

There are two coordinate systems which are convenient to analyze (3.18) in. The first is a Cartesian coordinate system such that $\hat{x}$ is an unit vector orthogonal with $\hat{z}$ and in the plane with the particle centers and $\hat{z}$. Therefore, $\boldsymbol{\alpha} = \alpha_x\hat{x} + \alpha_z\hat{z}$. In this coordinate system equation (3.18) becomes the following nonlinear system of ordinary differential equations

$$\dot{\alpha}_x = 3\beta\frac{\alpha_x}{\alpha^4} - \beta\frac{(1+\gamma)^2}{\gamma}\frac{\alpha_x}{\alpha^3} + \frac{3(1-\delta)}{4}\frac{\alpha_x\alpha_z}{\alpha^3} \tag{3.20}$$

$$\dot{\alpha}_z = 3\beta\frac{\alpha_z}{\alpha^4} - \beta\frac{(1+\gamma)^2}{\gamma}\frac{\alpha_z}{\alpha^3} + \frac{3(1-\delta)}{4}\frac{\alpha_x^2+2\alpha_z^2}{\alpha^3} - \frac{(\gamma-\delta)(1+\gamma)}{\gamma} \tag{3.21}$$

which are equations (17) & (18) in article C.

The other convenient coordinate system is polar coordinates where $\alpha = |\boldsymbol{\alpha}|$ as earlier and θ is defined to be the angle from the horizontal. In this coordinate system, equation (3.18) becomes the following nonlinear system of ordinary differential equations

$$\dot{\alpha} = \frac{\beta}{\alpha^2}\left(\frac{3}{\alpha} - \frac{(1+\gamma)^2}{\gamma}\right) + \left(\frac{3(1-\delta)}{2\alpha} - \frac{(\gamma-\delta)(1+\gamma)}{\gamma}\right)\sin(\theta) \quad (3.22)$$

$$\alpha\dot{\theta} = \left(\frac{3(1-\delta)}{4\alpha} - \frac{(\gamma-\delta)(1+\gamma)}{\gamma}\right)\cos(\theta) \quad (3.23)$$

which are equations (21) & (22) in article C.

Equation (3.18) and its coordinate forms (3.20) - (3.23) are the basic equations of the dynamics investigated in article B & article C.

4 Overview Of Original Results

In this section I will summarize some of the original results in article B & article C. In article B, it was demonstrated from the vector ordinary differential equation (3.18) that the two settling charged point particles with particle centers aligned with gravity can have stable stationary relative positions, where stability is defined as returning to the original relative position after perturbation. By linearizing around a stationary relative position, necessary and sufficient conditions for the stability of a stationary relative position were given and analyzed. In article C, it was demonstrated that such stable stationary states exist also for systems where the line of particle centers is inclined with respect to gravity. Further, it was shown in article C that the basin of attraction for a stable stationary relative position can be large in comparison to the sum of particle radii. Article B & article C both find bounds on the region of parameter space of ratio of characteristic forces, ratio of reduced masses and ratio of radii consistent with the existence of non-overlapping stable stationary relative positions and estimate values of interparticle distance for given regions of parameter space.

4.1 Stationary States & Local Asymptotic Stability

Article B focuses on finding the stationary and stability conditions when the line of particle centers is aligned with gravity and particle 2 is above particle 1, i.e. $\boldsymbol{\alpha} = \alpha^* \hat{z}$, where $\alpha^* > 0$. There are no stable stationary relative positions on the ray $\theta = \frac{3\pi}{2}$, so there is no restriction in taking $\alpha^* > 0$. On the ray $\theta = \pi/2$, the right hand side of equation (3.23) is identically zero. Therefore, the stationary condition is

$$0 \quad = \quad 6\gamma\beta - 2\beta(1+\gamma)^2\alpha^* + 3\gamma(1-\delta)\alpha^{*2} - 2(\gamma-\delta)(1+\gamma)\alpha^{*3} \qquad (4.1)$$

which is equation (14) in article B and equation (39) in article C. This equation is linear in β and δ and non-linear in γ and α^*.

The stability conditions are found by linearizing around a stationary relative position. This intuitive approach is shown to be necessary and sufficient for local asymptotic stability in the supplemental material to article B by the Lypunov function method. Letting $\alpha = \alpha^* + \epsilon_r$ and $\theta = \frac{\pi}{2} + \epsilon_\theta$, the linear dynamics are

$$\begin{bmatrix} \dot{\epsilon}_r \\ \dot{\epsilon}_\theta \end{bmatrix} \approx -\frac{1}{\gamma\alpha^{*3}}\mathbf{A}\cdot\begin{bmatrix} \epsilon_r \\ \epsilon_\theta \end{bmatrix} \tag{4.2}$$

where

$$\mathbf{A} = \begin{bmatrix} \lambda_1 & 0 \\ 0 & \alpha^*\lambda_2 \end{bmatrix} \tag{4.3}$$

and

$$\lambda_1 = \beta(1+\gamma)^2 - 3\gamma(1-\delta)\alpha^* + 3(\gamma-\delta)(1+\gamma)\alpha^{*2} \tag{4.4}$$
$$\lambda_2 = 3\gamma(1-\delta) - 4(\gamma-\delta)(1+\gamma)\alpha^* \tag{4.5}$$

Linear ordinary differential equation with constant coefficients (4.2) is equivalent to equations (10) & (11) in article B and equations (34) & (35) in article C. Because of the spherical symmetry of the charge, the electrostatic force only effects the radial coordinate, not the angle. Because $\mathbf{A}$ is a diagonal matrix, the eigenvalues are simply the diagonal entries. Therefore the system is stable if and only if

$$0 < \beta(1+\gamma)^2 - 3\gamma(1-\delta)\alpha^* + 3(\gamma-\delta)(1+\gamma)\alpha^{*2} \tag{4.6}$$
$$0 < 3\gamma(1-\delta) - 4(\gamma-\delta)(1+\gamma)\alpha^* \tag{4.7}$$

These inequalities are equivalent to inequalities (15) & (16) in article B and are inequalities (36) & (37) in article C. The stationary and stability conditions in those articles are equivalent, but are in different coordinate systems (Cartesian in article B, radial in article C).

In article C, the equivalents of (4.1) - (4.7) are found for particles in arbitrary orientations. Consider the case of an inclined stationary relative position with separation vector $\alpha^\dagger = |\boldsymbol{\alpha}|$ and angle $\theta^\dagger \neq \pi/2$. The stationary conditions can be read off equations (3.22) & (3.23). One sees that the inclined stationary relative positions are at

$$\alpha^\dagger = \frac{3(1-\delta)\gamma}{4(\gamma-\delta)(1+\gamma)} \tag{4.8}$$
$$\sin(\theta^\dagger) = \beta\frac{4(1+\gamma)(1+3\delta-3\gamma-\delta\gamma)}{3\gamma(1-\delta)^2\alpha^\dagger} \tag{4.9}$$

which are equations (44) & (45) in article C. Interestingly, the charge only effects the angle, not the interparticle distance. This is because of our assumption of spherical symmetry of the charge. Further, the sine of the angle of the particle centers is proportional to the ratio of characteristic electrostatic force to characteristic gravitational force.

The same linearization method as (4.2) is used to find the conditions for local asymptotic stability in this case. Letting $\alpha = \alpha^\dagger + \epsilon_r$ and $\theta = \theta^\dagger + \epsilon_\theta$ and linearizing one gets

$$\begin{bmatrix} \dot{\epsilon}_r \\ \dot{\epsilon}_\theta \end{bmatrix} \approx \begin{bmatrix} -\frac{3\beta}{\alpha^{\dagger 4}} & \frac{(\gamma-\delta)(1+\gamma)}{\gamma}\cos(\theta^\dagger) \\ -\frac{(\gamma-\delta)(1+\gamma)}{\alpha^{\dagger 2}\gamma}\cos(\theta^\dagger) & 0 \end{bmatrix} \begin{bmatrix} \epsilon_r \\ \epsilon_\theta \end{bmatrix} \tag{4.10}$$

which corresponds to equations (46) & (47) in article C. Notice that the matrix in (4.10) does not have $\mathbf{A}$ as a limit as $\theta \to \frac{\pi}{2}$.

Now to find the stability condition from (4.10). A real 2×2 matrix has eigenvalues with negative real parts if and only if the determinant is positive and the trace is negative. Doing some algebra one can see the stability condition for non-identical particles with an inclined stationary relative position is simply $\beta > 0$, i.e. opposite charges, which is inequality (50) in article C.

4.2 Necessary Conditions On Parameters For Non-Overlapping Stable Stationary Relative Positions

Having found the necessary and sufficient conditions for a locally asymptotically stable stationary relative position for with line of particle centers either aligned with gravity or inclined, the question is now: what ranges of parameters - ratio of reduced masses δ, ratio of radii γ or ratio of characteristic forces β - are consistent with the existence of a stable stationary relative position? Articles B & C both concentrated on the case when the particles are non-overlapping at the stable stationary relative position, i.e.

$$\alpha^* > 1 \tag{4.11}$$

$$\alpha^\dagger > 1 \tag{4.12}$$

Inequality (4.11) is inequality (17) in article B and inequality (53) in article C.

The question of parameters must be broken into two sub-questions: (a) "What ranges of parameters are consistent with the existence of a stable stationary relative position with line of particle centers aligned with gravity?" and (b) "What ranges of parameters are consistent with the existence of a stable stationary relative position with line of particle centers inclined with gravity?".

I will start with stable stationary relative positions with line of particle centers aligned with gravity, following article B & section 7 in article C. Manipulating (4.6) & (4.7) it can be shown that some necessary conditions for vertically aligned stable stationary states are

$$\delta > 0 \tag{4.13}$$

$$\frac{\delta}{\gamma^3} > 1 \tag{4.14}$$

$$\beta > 0 \tag{4.15}$$

$$1 \neq \gamma \tag{4.16}$$

These inequalities follow from inequalities (18) - (21) in article B. Inequality (4.13) shows that the sedimenting particles must either both be denser than the fluid or both less dense. Inequality (4.14) shows that the smaller particle must be denser than the larger particle if they are denser than the fluid or the contrary if less dense. There is further discussion of the case when particles are less dense than the fluid in the supplemental material to article B. Inequality (4.15) shows that opposite charges are necessary to stabilize the system. Finally, inequality (4.16) demonstrates the particles must have different radii. This is shown in the supplemental material to article B.

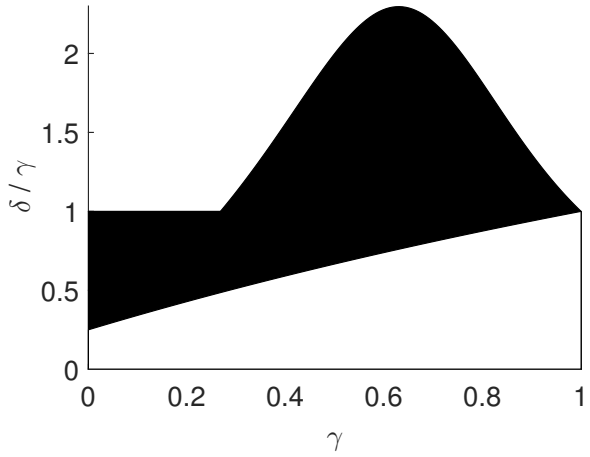

Figure 4.1: Phase diagram of vertical stationary states in the parameter space of the ratio of particle radii γ and the ratio of the particle Stokes velocities δ/γ. Non-overlapping stable stationary relative positions can exist in the black but not in the white region.

More detailed bounds on the ratio of Stokes velocities δ/γ & ratio of radii γ are discussed in detail in section 7 of article C. A simplified phase diagram is shown in figure 4.1. In the black area of figure 4.1, stable stationary relative positions can exist. The angular stability condition (4.7) and the feasibility condition (4.11) give a lower bound of the black area

$$\frac{\delta}{\gamma} > \frac{4\gamma + 1}{4 + \gamma} \tag{4.17}$$

which is inequality (59) in article C. The upper bound comes from using the stationary condition (4.1) to eliminate β from the radial stability condition (4.6) and solving for δ/γ. The upper bound is

$$\frac{\delta}{\gamma} < \max\left\{\frac{18\gamma + 4(1+\gamma)^3 - 3(1+\gamma)(1+7\gamma)}{18\gamma^2 + 4(1+\gamma)^3 - 3\gamma(1+\gamma)(7+\gamma)}, 1\right\} \tag{4.18}$$

which is equation (63) in article C. Inequalities (4.17) & (4.18) specify the range of the ratio of Stokes velocities and ratio of radii consistent with the existence of a stable stationary relative position.

Moving on to the parameters consistent with stable stationary relative positions with line of particle centers inclined with gravity, it has already been noted that if an inclined stationary relative position exists then

$$\beta > 0 \tag{4.19}$$

is a necessary and sufficient condition for stability. From the stationary condition on interparticle distance for inclined particles (4.8) and the fact that the separation vector must have positive norm one gets

$$(1-\delta)(\gamma-\delta) > 0 \tag{4.20}$$

which is equation (24) in article C. Further, the stationary condition (4.8) & the feasibility condition (4.12) entail

$$\frac{4\gamma+1}{4+\gamma} < \frac{\delta}{\gamma} < 1 \tag{4.21}$$

The lower bound is the same as in figure 4.1 The above and equation (4.20) entail

$$\delta < 1 \tag{4.22}$$

Now that some bounds on the parameter set have been established, some relations which hold for stable stationary relative positions with large separations - i.e. $\alpha^* \gg 1$ & $\alpha^\dagger \gg 1$ - can be outlined.

Again I will start with the case when the line of particle centers is aligned with gravity, following article B. From the stationary condition (4.1) and stability conditions (4.6) & (4.7) in the limit of $\alpha^* \gg 1$ the following relations hold

$$1 - \frac{\delta}{\gamma} \approx \frac{3(1-\gamma)}{4(1+\gamma)}\frac{1}{\alpha^*} \ll 1 \tag{4.23}$$

$$\beta \approx \frac{3\gamma(1-\gamma)}{4(1+\gamma)^2}\alpha^* \gg 1 \tag{4.24}$$

Relation (4.23) means that large stable stationary interparticle distances with line of particle centers aligned with gravity require the Stokes velocities of

the particles to be approximately the same. The second relation means that the ratio of characteristic electrostatic to characteristic gravitational force must be large in order to have a large separation for stable stationary relative distances with a line of particle centers aligned with gravity.

Finally, for the case when the line of particle centers is inclined with gravity one can see from (4.8) that $\alpha^\dagger \gg 1$ if

$$1 - \frac{\delta}{\gamma} \approx 0 \tag{4.25}$$

$$1 - \delta \approx 1 \tag{4.26}$$

As in the case when particle centers are aligned with gravity, the Stokes velocities must be approximately the same for large separations at a stable stationary relative position. Unlike that case, it is also required the reduced masses be similar.

The necessary conditions on parameters for the existence of stable stationary relative positions with line of particle centers aligned with gravity (4.15)-(4.18) or inclined with gravity (4.19)-(4.22) help understand when to expect stable doublets to form. Relations (4.23)-(4.26) can help guide experimental work as the point particle model is expected to be accurate for distant particles.

4.3 Example Of Stable Stationary Relative Positions & Their Basins Of Attraction

With the relations on parameters in the previous subsection as a guide, it is now possible to talk about the dynamics of systems with stable stationary relative positions. A comparison between the dynamics of an uncharged not stable system and a charged stable system is given in figure 4.2, which is made up of figures 2(b) and 3(a) from article C.

In 4.2(a), an example of relative trajectories of an uncharged system is shown. This is example H' from article B. The parameters chosen are $\delta = .986$ & $\gamma = .988$. One can see that when the particles are sufficiently close together, closed periodic orbits are formed. This is expected from classical results [23]. The stationary states with line of particle centers aligned with gravity are saddle points connected by heteroclinic orbits. These orbits form the seperatrix between bounded relative orbits and unbounded relative orbits. In article C section 3, an exact solution is given for this seperatrix. The horizontal stationary states are neutrally stable and surrounded by periodic orbits. See article C section 3 for more details.

In 4.2(b), a small charge is added so that $\beta = .01$ to the system with the same values of δ & γ. This is similar to example H from article B. This creates a vertical stable stationary relative position at $\alpha^* = 2.31....$ There are not stable stationary relative positions with the larger particle directly below the smaller one - that is, $\theta = 3\pi/2$ - at $\alpha = 6.56...$ and $\alpha = .588....$ The stationary relative

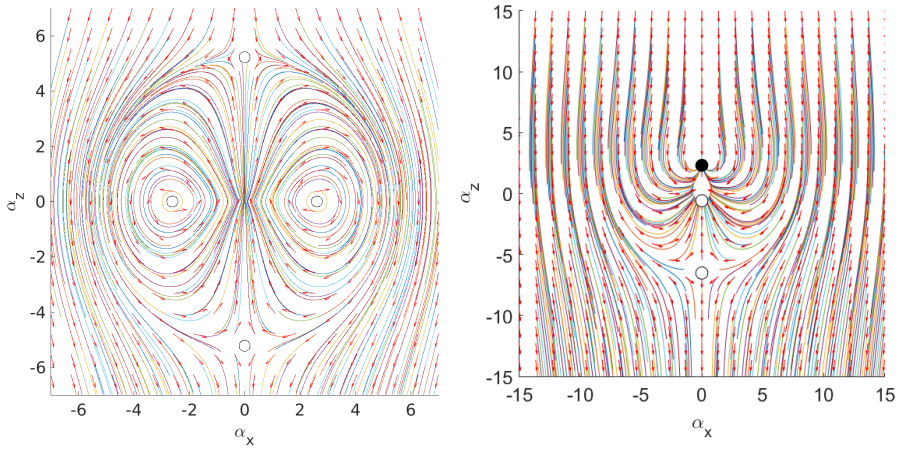

Figure 4.2: Examples of relative trajectories (a) $\beta = 0$ (uncharged), $\delta = .986$ & $\gamma = .988$. The orbits of the larger particle are shown in the reference frame on the center of the smaller particle. The open circles represent not stable stationary relative positions. The colors are used to facilitate tracing streamlines close to each other. (b) $\beta = .01$, $\delta = .986$ & $\gamma = .988$. The black circle at $\alpha_z = 2.31...$ is a stable steady relative position.

positions on the ray $\theta = 3\pi/2$ are saddle points. In particular, the stationary relative position $\alpha = .588...$ is stable against perturbations in the direction with gravity and the stationary relative position at $\alpha = 6.56...$ is stable against horizontal perturbations.

The basin of attraction of the stable stationary relative position is unbounded above. This can be seen by considering the of orbits that end on the lowest saddle point. These orbits form the seperatrix between bounded and unbounded relative orbits: almost every relative orbit which begins on the interior of this curve goes to the stable stationary relative position. Every relative orbit outside the seperatrix goes toward infinity. In fact, in article C section 5, the Poincare-Bendixson theorem is used to show this and a stronger result: all orbits in the interior of the seperatrix must go to a stationary relative position. There are no periodic orbits as seen in the uncharged case.

The horizontal cross-section of the basin of attraction in figure 4.2(b) is bigger than six times the sum of the particle radii. Therefore even well-separated particles can end up at the stable stationary relative position. Figure 3(b) in article C gives an example with a cross section radius and separation distance that is even larger. In fact, in article C, it is observed that the cross-section radius scales with the vertical position of the saddle point on the seperatrix.

In article C section 5, the same results are shown for other cases, such as two stable stationary relative positions with line of particle centers aligned with gravity, when the line of particle centers at the stable relative positions are inclined with respect to gravity and when there are both stable stationary

relative positions aligned with gravity and stable stationary relative positions inclined with gravity.

The qualitative dynamics in these cases are similarly established by the Poincare-Bendixson theorem. In fact, the qualitative dynamics for systems with multiple and inclined stable stationary relative positions are similar to the case of a single stable relative position. In all cases, the relative orbits either go to a stationary relative position or seperate. Further, there is in each case a seperatrix which separates the bounded and unbounded relative orbits with a saddle point stationary relative position.

5 Conclusions

This section summarizes some of the results in the review article A [1] and some of the original results in article B [2] & article C [3] and draws some general conclusions.

In article A, basic concepts of Stokes flow such as reversibility, negligibility of inertial forces and minimum energy dissipation theorem are analyzed. Applications of each concept are given as well as their interrelations. For example, it is shown that the minimum energy dissipation theorem entails reversibility but reversibility does not imply the minimum energy dissipation theorem. Illustrative examples are given for each concept.

Article B is concerned with showing there exist stable relative positions of pairs of charged particles settling under gravity in a Stokes flow by the analysis of a point particle model. This research drew inspiration from classical results showing there can exist a small set of at best neutrally stable bounded relative orbits between two uncharged particles sedimenting under gravity in a Stokes flow [23]. The stabilization of stationary relative positions by electrostatic force was unexpected because Earnshaw's Theorem means that electrostatic forces are destabilizing in a vacuum. The stable stationary relative positions considered in article B have a line of particle centers aligned with gravity. The interparticle separation at the stable stationary relative position can be arbitrarily large. This means that the point particle approximation may be physically reasonable. Charged particles must have different radii in order for stable doublets to form. When charged particles have a line of centers aligned with gravity, the larger or the smaller particle could have greater Stokes Velocity.

It is further shown in article B that for large separations of charged particles at a stable stationary relative position, the ratio of Stokes velocities must be near unity and the ratio of characteristic electrostatic to characteristic gravitational force must be large. Also for large separations of charged particles at a stable stationary relative position, the upper particle must have a greater Stokes velocity than the lower particle. The particles must have different densities and radii to have a stable stationary relative position, but in the limit of very similar particles - in the sense of having similar Stokes velocities and densities - the ratio of characteristic electrostatic to characteristic gravitational force consistent with a stable stationary relative position can be arbitrarily small.

Article C analyzes the point particle model in order to find the dynamics of a pair of charged particles settling under gravity in a Stokes flow. Using the

Poincare-Bendixson Theorem, it is shown that there are two qualitative kinds of dynamics in the point particle model: either the particles go to a stationary relative position or they separate.

Further, in article C it is shown that the set of initial conditions which give rise to relative orbits that do not separate over time is unbounded (unlike the bounded set seen for uncharged particles). The set of relative orbits which stay together is segregated from the set of relative orbits which go to infinity by a seperatrix curve. The seperatrix has a saddle point stationary relative position on it. The distance between particle centers at the saddle point can be used as a proxy for the cross section radius. This cross section radius can be several times the sum of particle radii. The large size of the set of relative orbits in which the particles stay together both in measure and in cross-section and the large particle separation at the stable stationary relative position suggest the relevant particle dynamics could be well-approximated by the point-particle model.

It is also shown in article C that, unlike the uncharged case, there are no periodic orbits for pairs of charged point particle sedimenting under gravity in a Stokes flow in the model examined. Further, there can be stable stationary states with a line of charged particle centers inclined with respect to gravity with charged point particle sedimenting under gravity in a Stokes flow, but not for uncharged particles. Phase space diagrams were used to describe bounds on the ratio of Stokes velocities and particle radii for stable stationary relative positions with line of charged particle centers either aligned or inclined with respect to gravity.

The point particle model makes the prediction of stable doublets and absence of periodic relative orbits. These qualitative features could be confirmed by future experiments. If confirmed, the existence of stable doublets could have consequences for dilute charged suspensions, as it is well known that the effect of the relative diffusion of doublet pairs can have a singular perturbing effect on the suspension [24]. Because charged matter in a viscous fluid is very common in scientific, biological, medical and industrial contexts, the results in this thesis are fundamental.

Bibliography

[1] Trombley C I and Ekiel-Jeżewska M L 2019 Basic concepts of Stokes flows *Flowing Matter* (Springer, Cham) pp 35–50

[2] Trombley C I and Ekiel-Jeżewska M L 2018 Stable configurations of charged sedimenting particles Phys. Rev. Lett. **121**(25) 254502

[3] Trombley C I and Ekiel-Jezewska M L 2021 Relative trajectories of two charged sedimenting particles in a stokes flow Journal of Physics Communications. Accepted May 2021

[4] Stokes G G 1851 On the effect of the internal friction of fluids on the motion of pendulums Trans. Camb. Phil. Soc. **9** 8–94

[5] Witten T A and Diamant H 2020 A review of shaped colloidal particles in fluids: Anisotropy and chirality Reports on Progress in Physics **83** 116601

[6] Ramaswamy S 2001 Issues in the statistical mechanics of steady sedimentation Advances in Physics **50** 297–341

[7] Guazzelli E and Hinch J 2011 Fluctuations and instability in sedimentation Annual review of fluid mechanics **43** 97–116

[8] Batchelor G K 2000 An introduction to fluid dynamics (Cambridge University Press)

[9] Russel W B, Russel W, Saville D A and Schowalter W R 1991 Colloidal Dispersions (Cambridge University Press)

[10] Pozrikidis C 1992 Boundary integral and singularity methods for linearized viscous flow (Cambridge University Press)

[11] Kim S and Karrila S J 2013 Microhydrodynamics: principles and selected applications (Courier Corporation)

[12] Guazzelli E and Morris J F 2011 A physical introduction to suspension dynamics (Cambridge University Press)

[13] Happel J and Brenner H 2012 Low Reynolds number hydrodynamics: with special applications to particulate media vol 1 (Springer Science & Business Media)

[14] Duprat C and Stone H A 2015 Fluid-structure interactions in low-Reynolds-number flows (Royal Society of Chemistry)

[15] Graham M D 2018 Microhydrodynamics, Brownian motion, and complex fluids (Cambridge University Press)

[16] Zurita-Gotor M, Bławzdziewicz J and Wajnryb E 2007 Swapping trajectories: a new wall-induced cross-streamline particle migration mechanism in a dilute suspension of spheres Journal of Fluid Mechanics **592** 447–469

[17] Singha S, Malipeddi A R, Zurita-Gotor M, Sarkar K, Shen K, Loewenberg M, Migler K B and Blawzdziewicz J 2019 Mechanisms of spontaneous chain formation and subsequent microstructural evolution in shear-driven strongly confined drop monolayers Soft Matter **15** 4873–4889

[18] Driscoll M, Delmotte B, Youssef M, Sacanna S, Donev A and Chaikin P 2017 Unstable fronts and motile structures formed by microrollers Nat. Phys. **13** 375–379

[19] Chamolly A, Lauga E and Tottori S 2020 Irreversible hydrodynamic trapping by surface rollers Soft Matter **16** 2611–2620

[20] Gao W, Kagan D, Pak O S, Clawson C, Campuzano S, Chuluun-Erdene E, Shipton E, Fullerton E E, Zhang L, Lauga E *et al.* 2012 Cargo-towing fuel-free magnetic nanoswimmers for targeted drug delivery small **8** 460–467

[21] Shen B, Leman M, Reyssat M and Tabeling P 2014 Dynamics of a small number of droplets in microfluidic Hele–Shaw cells Exp. Fluids **55** 1–10

[22] Delmotte B 2019 Hydrodynamically bound states of a pair of microrollers: A dynamical system insight Phys. Rev. Fluids **4** 044302

[23] Wacholder E and Sather N 1974 The hydrodynamic interaction of two unequal spheres moving under gravity through quiescent viscous fluid J. Fluid Mech. **65** 417–437

[24] Batchelor G 1982 Sedimentation in a dilute polydisperse system of interacting spheres. part 1. general theory J. Fluid Mech **119** 379–408

[25] Batchelor G and Wen C S 1982 Sedimentation in a dilute polydisperse system of interacting spheres. part 2. numerical results J. Fluid Mech **124** 495–528

[26] Davis R H 1984 The rate of coagulation of a dilute polydisperse system of sedimenting spheres J. Fluid Mech **145** 179–199

[27] Bürger R, Karlsen K H, Tory E M and Wendland W L 2002 Model equations and instability regions for the sedimentation of polydisperse suspensions of spheres ZAMM-Journal of Applied Mathematics and Mechanics/Zeitschrift für Angewandte Mathematik und Mechanik: Applied Mathematics and Mechanics **82** 699–722

[28] Earnshaw S 1842 On the nature of the molecular forces which regulate the constitution of the luminferous ether Trans. Camb. Phil. Soc. **7** 97–112

[29] Abanov A, Hayford N, Khavinson D and Teodorescu R 2021 Around a theorem of F. Dyson and A. Lenard: Energy equilibria for point charge distributions in classical electrostatics Expositiones Mathematicae **39** 182–196

[30] Evans L C 2010 Partial differential equations (American Mathematical Society)

[31] Lamb H 1945 Hydrodynamics (Dover Books)

[32] Arnold V I and Khesin B A 1998 Topological methods in hydrodynamics vol 125 (Springer)

[33] Helmholtz H v 1868 Zur theorie der stationären ströme in reibenden flüssigkeiten Wiss. Abh **1** 223–230

[34] Hill R and Power G 1956 Extremum principles for slow viscous flow and the approximate calculation of drag The Quarterly Journal of Mechanics and Applied Mathematics **9** 313–319

7 Publications

Federico Toschi • Marcello Sega
Editors

Flowing Matter

cost
EUROPEAN COOPERATION
IN SCIENCE & TECHNOLOGY

Springer Open

Funded by the Horizon 2020 Framework Programme
of the European Union

Editors
Federico Toschi
Department of Applied Physics
University of Technology Eindhoven
Eindhoven, The Netherlands

Marcello Sega
Forschungszentrum Jülich
Helmholtz Institute Erlangen-Nürnberg
for Renewable Energy
Nuremberg, Germany

Funded by the Horizon 2020 Framework Programme of the European Union

This article/publication is based upon the work from COST Action MP1305, supported by COST (European Cooperation in Science and Technology).

COST (European Cooperation in Science and Technology; www.cost.eu) is a funding agency for research and innovation networks. Our Actions help connect research initiatives across Europe and enable scientists to grow their ideas by sharing them with their peers. This boosts their research, career and innovation.

ISSN 2213-1736 ISSN 2213-1744 (electronic)
Soft and Biological Matter
ISBN 978-3-030-23369-3 ISBN 978-3-030-23370-9 (eBook)
https://doi.org/10.1007/978-3-030-23370-9

This Springer imprint is published by the registered company Springer Nature Switzerland AG.
The registered company address is: Gewerbestrasse 11, 6330 Cham, Switzerland

Chapter 2
Basic Concepts of Stokes Flows

Christopher I. Trombley and Maria L. Ekiel-Jeżewska

2.1 Introduction

Stokes flows have many applications in both physical theory and practice. For example, they have been used to describe dynamics of complex fluids in microfluidics, lab-on-chip technologies [1], medical applications [2, 3], design of innovative materials [4–6] and micro-devices—e.g. to carry drugs [7, 8] or act as fuel cells [9]—and in biological systems [10–15].

In this chapter, we discuss some fundamental properties of Stokes flows, namely: negligibility of inertial forces, reversibility and the minimum energy dissipation theorem. First we will briefly discuss how the neglecting of inertial forces simplifies the nonlinear Navier–Stokes equations to the linear Stokes equations. We then discuss two basic aspects of Stokes flows: reversibility and the minimum energy dissipation theorem. In order to bring out the nature of the three principles, we will demonstrate by example how these properties can be used to obtain conclusions about investigated fluid systems without laborious construction of analytical solutions. We then move beyond the Stokes approximation in various ways in order to see how the principles work in a general context. Finally, we conclude by discussing the logical structure of the principles as revealed by the examples considered.

C. I. Trombley · M. L. Ekiel-Jeżewska (✉)
Institute of Fundamental Technological Research, Polish Academy of Sciences, Warsaw, Poland
e-mail: mekiel@ippt.gov.pl

F. Toschi, M. Sega (eds.), *Flowing Matter*, Soft and Biological Matter,
https://doi.org/10.1007/978-3-030-23370-9_2

2.2 Navier–Stokes and Stokes Equations

2.2.1 Navier–Stokes Equations

We start with the general Navier–Stokes equations for an incompressible fluid. These are [16–18]

$$\rho \frac{\partial \mathbf{u}}{\partial t} + \rho(\mathbf{u} \cdot \nabla)\mathbf{u} = \mu \nabla^2 \mathbf{u} - \nabla p + \mathbf{F} \tag{2.1}$$

$$\nabla \cdot \mathbf{u} = 0 \tag{2.2}$$

where ρ is the density of the fluid, $\mathbf{u}$ is the velocity field of a fluid, μ is the dynamic viscosity of the fluid, p is the fluid pressure field,[1] and $\mathbf{F}$ captures the effects of external forces. The left-hand side of this equation is the inertial forces, that is, the acceleration of a fluid element with unit volume. The right-hand side is sum of the viscous and pressure forces, $\mu\nabla^2\mathbf{u}$ and ∇p, respectively, exerted on surfaces of this fluid element, and any external body forces $\mathbf{F}$ acting on the fluid element. The second equation is based on the conservation of mass of a fluid element and achieves its simple form because of incompressibility of the fluid element.

We use non-dimensionalisation in order to capture the relative scale of the forces. Define U to be a characteristic velocity of the fluid and L to be a characteristic length scale. Other characteristic dimensional scales of the flow, for instance, a time scale $T = L/U$, can be defined implicitly from these scales. There is still some freedom when normalising pressure p and body forces $\mathbf{F}$. We choose to normalise pressure by a characteristic viscous force per unit area and $\mathbf{F}$ by a characteristic viscous force per unit volume as in [18]. Using a star to denote non-dimensionalised objects, this results in the following definitions:

$$\begin{aligned} \mathbf{u}^* &= \frac{\mathbf{u}}{U} \\ \nabla^* &= L\nabla \\ \frac{\partial}{\partial t^*} &= \frac{L}{U}\frac{\partial}{\partial t} \\ p^* &= \frac{L}{\mu U} p \\ \mathbf{F}^* &= \frac{L^2}{\mu U}\mathbf{F} \end{aligned} \tag{2.3}$$

[1] In the presence of a gravitational field, p is the so-called modified pressure, which takes into account also gravitational potential energy per unit fluid volume.

With the above characteristic dimensional scales, the inertial force per unit volume is estimated by $\frac{\rho U^2}{L}$ and the scale of the viscous force per unit volume is $\frac{\mu U}{L^2}$. The Reynolds number, Re, a non-dimensional number defined as the ratio of inertial and viscous forces in a fluid, takes the form

$$Re = \frac{(\rho U^2)/L}{(\mu U)/L^2} = \frac{\rho U L}{\mu} \tag{2.4}$$

The end result is the following non-dimensional version of the Navier–Stokes equation (2.1):

$$Re\left(\frac{\partial \mathbf{u}^*}{\partial t^*} + \mathbf{u}^* \cdot \nabla^* \mathbf{u}^*\right) = \nabla^{*2}\mathbf{u}^* - \nabla^* p^* + \mathbf{F}^* \tag{2.5}$$

The left-hand side is the inertial force and the right-hand side is the viscous, pressure and body forces. Flows with the same Re are hydrodynamically similar [18].

A difficulty to using Eqs. (2.1) and (2.2) (or their non-dimensional form) in the analysis of fluids is that the inertial forces are nonlinear in $\mathbf{u}$. In terms of forces, the so-called Stokes approximation can be understood as when the viscous and pressure forces dominate the inertial forces absolutely. The Reynolds number allows one to test the applicability of Stokes approximation to fluids. The Stokes approximation holds exactly in the limit as this ratio goes to zero [17–22]. For this reason, Stokes flows are often called low Reynolds number, non-inertial or viscous flows.

2.2.2 Stokes Flows

Taking the limit $Re \to 0$ in Eq. (2.5) one obtains the non-dimensional steady Stokes equations. In dimensional form, without external body forces, sources or sinks, they read

$$\mu \nabla^2 \mathbf{u} - \nabla p = 0 \tag{2.6}$$

$$\nabla \cdot \mathbf{u} = 0 \tag{2.7}$$

The first equation states the balance of forces in a non-accelerating fluid. The second equation is, as in Eq. (2.2), the conservation of mass for incompressible fluids.

The Stokes equations (2.6) and (2.7) must be combined with boundary conditions appropriate to the physical situation. The so-called stick or no-slip boundaries for rigid walls and at the surfaces of particles are important examples. Consider a surface S moving with local velocity $\mathbf{w}$. It has no-slip boundary condition for the fluid velocity $\mathbf{u}$ if on S one has

$$\mathbf{u}(\mathbf{r}) = \mathbf{w}(\mathbf{r}) \qquad \text{for } \mathbf{r} \in S \tag{2.8}$$

There are many other important examples of boundary conditions, such as the boundaries for a free surface [18], but we will focus on the stick boundary conditions, which are sufficient for considering inertial forces, reversibility and the minimum energy dissipation. When considering reversibility especially, one must remember that boundaries can be time dependent. This means that the boundaries move, such as in the classical Taylor–Couette experiment involving a fluid between two rotating cylinders [23]. The Stokes equations (2.6) and (2.7) can also apply to unbounded flow problems by the selection of an appropriate boundary at infinity. For instance, a fluid can be constrained to be at rest at infinity, as in case of particles settling in a quiescent fluid.

Equations (2.6)–(2.7) are linear, so that any linear combination of solutions $(\mathbf{u}_1, p_1)$ and $(\mathbf{u}_2, p_2)$ is also a solution $(\mathbf{u}_1 + \mathbf{u}_2, p_1 + p_2)$. Linearity allows for classes of solutions to be constructed. One example is the case of flow around a rigid sphere, where a complete set of elementary solutions to Eqs. (2.6) can be constructed, as done by Lamb [16]. In his families of elementary solutions, the pressure p is expanded in spherical harmonics and the velocity field $\mathbf{u}$ is written as an infinite series of solid harmonics. This concept is used in the multipole method of solving the Stokes equations for systems of particles moving in fluids [20, 24–30].

2.3 Reversibility of Fluid Flows

Because Stokes equations (2.6)–(2.7) are steady and linear, the motion they predict is reversible in time. Mathematically, it means that the reversibility transformation of any solution, that is, $(\mathbf{u}(\mathbf{x}, t), p(\mathbf{x}, t)) \longmapsto -(\mathbf{u}(\mathbf{x}, t), p(\mathbf{x}, t))$, will also give a solution. This can be checked by simple algebraic manipulation of the governing equations. G.I. Taylor explained in his film *Low Reynolds Number Flows* [31] the physical meaning of reversibility—"low Reynolds number flows are reversible when the direction of motion of the boundaries which gave rise to the flow is reversed". Actually, a reversed fluid flow can result from reversing velocity of the boundary (equal to the fluid velocity at the surfaces of particles or walls) or from reversing directions of the external and the opposite hydrodynamic forces. In the following, we will show how reversibility allows to predict symmetries of fluid flows and motion of particles in fluids.

2.3.1 Examples of Reversibility

One of the most dramatic presentations of reversibility is seen in the film mentioned above [31]. In this experiment, the volume between two transparent cylinders is filled with glycerine. Dyes are injected which form a compact coloured volume into the glycerine to help visualise the flow. The inner cylinder is rotated causing the dyes to stir and apparently mix. The inner cylinder is then rotated in the

opposite direction and one sees the seemingly mixed fluids unstir themselves. This experiment demonstrates the difficulty of mixing low Reynolds number fluids, an important problem for microfluidics.

G.I. Taylor used this experiment to explain the concept of reversibility in the following way: "On reversal of the motion of the boundary, every particle retracts exactly the same path on its return journey as on the outward journey, and at every point its speed is the same fraction of the boundary speed as it was at the same point on its outward journey, so that when the boundary has returned to its original position every particle in the fluid has also done so and the original pattern of dye is reproduced" [32].

A very important consequence of reversibility in biology is that the ordinary swimming motion done by an idealised swimmer with a rigid tail could not produce forward motion in a non-inertial fluid, since any propulsion created by the swimmer when the tail moves left is exactly cancelled when it moves right, as demonstrated in [31]. This is a consequence of the "Scallop theorem" fundamental to the study of the locomotion of microscale organisms [11].

One can use reversibility to derive basic properties of solutions to the Stokes equations without finding the solutions explicitly. Take the case of a rotating, but not translating, sphere immersed in fluid governed by Eqs. (2.6) and (2.7). This situation is illustrated in Fig. 2.1. We might ask how much force such a sphere would feel. Here we mean the force exerted by the fluid on the sphere owing to stick boundary conditions on its surface. This hydrodynamic force needs to be balanced by the opposite external (non-hydrodynamic) force acting on the sphere. Through the use

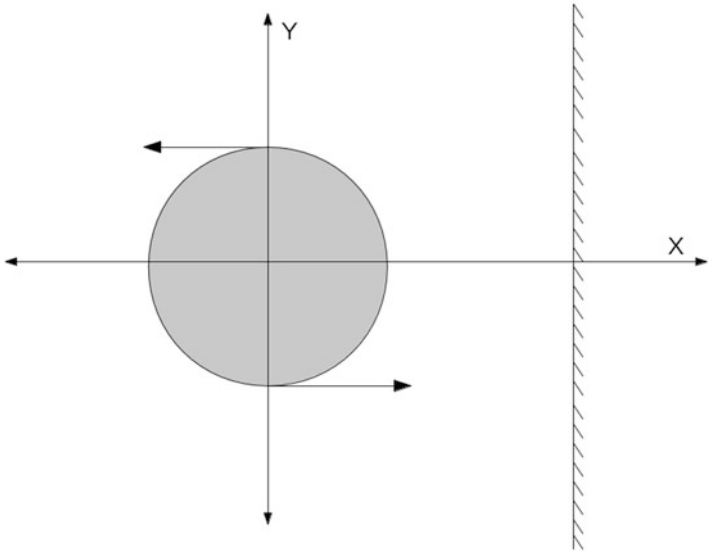

Fig. 2.1 A solid sphere rotating without translations near a solid wall. Reversibility implies that the sphere does not feel any external force perpendicular to the wall

of superposed reversibility and symmetry transformations, we can discover that in this situation the answer is that the sphere would not feel any hydrodynamic force in the direction perpendicular to the wall [33]. This can be proven by contradiction. Suppose $F_x \neq 0$. Notice that if we put the origin at the centre of the sphere, the system is symmetric for the transformation $y \longmapsto -y$. This reflection reverses the rotation of the sphere, but leaves the x-component of the force the same. Now apply the reversibility transformation. The rotation is now reversed back to the original sense. The force vector should have the opposite direction. The result is that the sphere is at the same position, has the same physical rotation, but opposite F_x. This is a contradiction. This argument shows how reversibility and symmetry arguments can be combined to put strong restrictions on Stokes flow [33, 34].

We can also apply reversibility arguments again to the case of a sphere which moves under a constant gravitational force parallel to a solid wall. Applying the time reversal, we now reverse also the direction of the sphere velocity and force. By the same argument above, i.e. by combining the time reversal with the reflection with respect to the plane $y = 0$, there will be no velocity in the direction perpendicular to the wall; the sphere will keep translating parallel to the wall [34]. This reasoning applies to the study of sedimentation of a slowly moving particle of any shape and material symmetric with respect to reflection in the plane $y = 0$ [33, 34]. We have demonstrated that reversibility has observable consequences which do not require elaborate constructions.

2.3.2 Irreversible Trajectories in Stokes Flow

Applying reversibility, one must take care that reversibility applies to time and forces. In particular, the paths that particles take need not be reversible in time even though the Stokes equation is reversible in time. As an example, consider the system shown in Fig. 2.2: two spheres of the same radii—one fixed and another one settling from above under gravity. For non-touching spheres, trajectories of the moving sphere centre are symmetric with respect to reflection in the plane $z = 0$. Under the time reversal, the gravitational force is reversed and the sphere centre moves backwards along the same trajectory. However, reversibility of the trajectories is broken when two spheres come so close to each other that their surfaces interact by direct forces, such as van der Waals attraction or mechanical reaction of rough surfaces at the contact [35–39]. The reason is that central direct forces are not symmetric with respect to superposition of the time reversal with reflection in the horizontal plane $z = 0$.

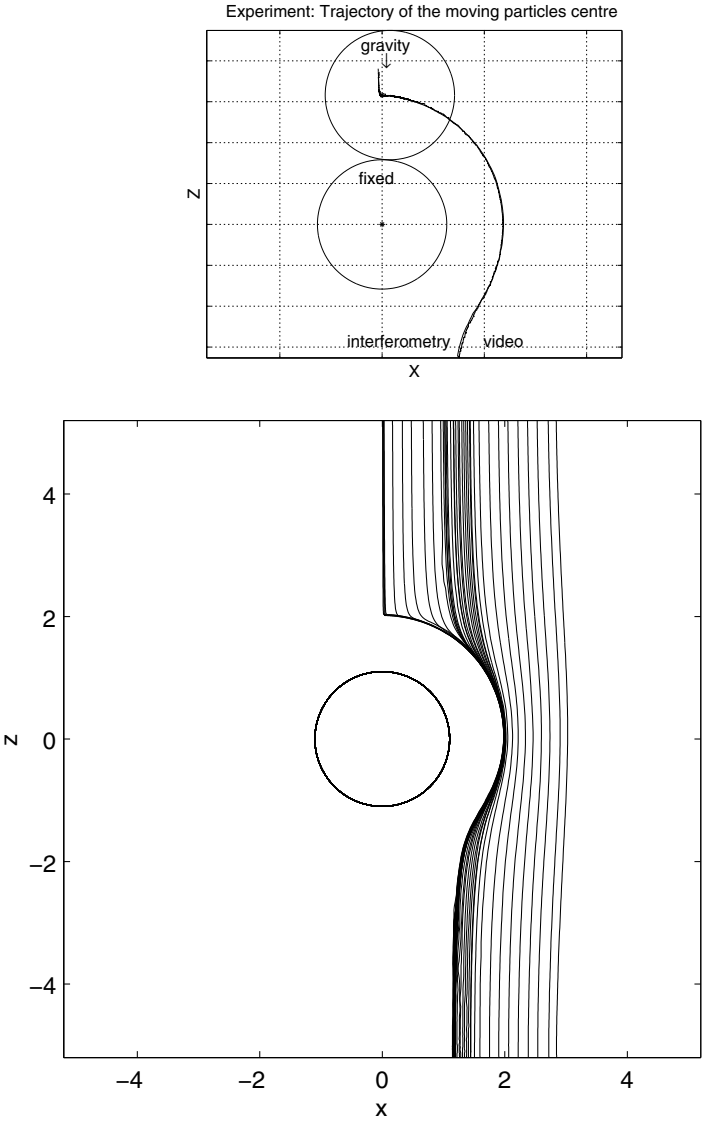

Fig. 2.2 Experimentally observed trajectories of the centre of sphere settling under gravity in a silicon oil towards another fixed sphere of the same radius. Top: reprinted by permission from Ref. [36]. Copyright Kluwer Academic Publisher (2002). Bottom: reprinted with permission from Ref. [37]. Initally, the line of the sphere centres is inclined with respect to gravity. For a large inclination, the surfaces of the spheres are always separated by a fluid, and the trajectories are reversible. However, if the initial inclination is small enough, after some time the surfaces come into contact and the resulting direct forces break the reversibility of the trajectories

2.4 Minimum Energy Dissipation Theorem

We will now give a "variational" view of Stokes flow. A solution to Stokes equations (2.6) and (2.7) is the unique divergence-free vector field that minimises the extensive energy dissipation rate (that is, the energy dissipated by the bulk of the fluid) [20]. In this section, we will state this minimum energy dissipation theorem precisely and sketch a proof. After that, we will apply it to derive "inclusion monotonicity", a principle about particles moving through Stokes flows.

2.4.1 Statement

Consider a fluid filling a volume V with an impermeable boundary $\partial V = S$. Let $\mathbf{u}$ be the velocity of a Stokes flow defined by Eqs. (2.6) and (2.7). Let $\mathbf{v}$ be a divergence-free vector field describing a flow in V with the same boundary conditions as $\mathbf{u}$. The minimum energy dissipation theorem is

$$\epsilon^{\mathbf{u}} \leq \epsilon^{\mathbf{v}} \tag{2.9}$$

where $\epsilon^{\mathbf{u}}$ is the extensive energy dissipation rate of the Stokes flow and $\epsilon^{\mathbf{v}}$ is the extensive energy dissipation rate of the other flow.

For an excellent discussion of how these relations for the change of internal energy over time are established physically, see section 3.4 of [18]. For now we will simply use the fact that for an incompressible fluid, the intensive energy dissipation rate (i.e. the energy dissipated per unit volume) Φ is

$$\Phi^{\mathbf{u}} = 2\mu \mathbf{e}^{\mathbf{u}} : \mathbf{e}^{\mathbf{u}} \tag{2.10}$$

$$\Phi^{\mathbf{v}} = 2\mu \mathbf{e}^{\mathbf{v}} : \mathbf{e}^{\mathbf{v}} \tag{2.11}$$

where $\mathbf{e}$ is the rate of strain tensor for the Stokes flow $\mathbf{u}$ given component-wise as $e^{\mathbf{u}}_{ij} = \frac{1}{2}(\frac{\partial u_i}{\partial x_j} + \frac{\partial u_j}{\partial x_i})$ (and similarly for $e^{\mathbf{v}}_{ij}$) and : is the double dot product. Integrating Φ over V gives the extensive energy dissipation rates ϵ, so that

$$\epsilon^{\mathbf{u}} = \int \Phi^{\mathbf{u}} dV \tag{2.12}$$

$$\epsilon^{\mathbf{v}} = \int \Phi^{\mathbf{v}} dV \tag{2.13}$$

Having thus connected the energy dissipation rate to the mechanical properties of the flow, we can now discuss the proof of Eq. (2.9). Because the minimum energy dissipation theorem is proven and discussed in many textbooks, such as [20], we will only give a brief outline. One starts by demonstrating

$$\int (e^{\mathbf{v}}_{ij} - e^{\mathbf{u}}_{ij}) e^{\mathbf{u}}_{ij} dV = 0 \tag{2.14}$$

from Green's theorem, the divergence theorem and Stokes equations (2.6) and (2.7). Then one subtracts Eq. (2.14) from the extensive energy dissipation rate for $\mathbf{v}$ and rearranges

$$2\mu \int e_{ij}^{\mathbf{v}} e_{ij}^{\mathbf{v}} dV = 2\mu \int \left(e_{ij}^{\mathbf{v}} e_{ij}^{\mathbf{v}} - (e_{ij}^{\mathbf{v}} - e_{ij}^{\mathbf{u}}) e_{ij}^{\mathbf{u}}\right) dV \tag{2.15}$$

$$= 2\mu \int \left(e_{ij}^{\mathbf{u}} e_{ij}^{\mathbf{u}} + (e_{ij}^{\mathbf{v}} - e_{ij}^{\mathbf{u}}) e_{ij}^{\mathbf{v}}\right) dV \tag{2.16}$$

$$= 2\mu \int \left(e_{ij}^{\mathbf{u}} e_{ij}^{\mathbf{u}} + (e_{ij}^{\mathbf{v}} - e_{ij}^{\mathbf{u}}) e_{ij}^{\mathbf{v}} - (e_{ij}^{\mathbf{v}} - e_{ij}^{\mathbf{u}}) e_{ij}^{\mathbf{u}}\right) dV \tag{2.17}$$

$$= 2\mu \int \left(e_{ij}^{\mathbf{u}} e_{ij}^{\mathbf{u}} + (e_{ij}^{\mathbf{v}} - e_{ij}^{\mathbf{u}})^2\right) dV \tag{2.18}$$

Which shows that $2\mu \int \left(e_{ij}^{\mathbf{v}} e_{ij}^{\mathbf{v}} - e_{ij}^{\mathbf{u}} e_{ij}^{\mathbf{u}}\right) dV \geq 0$, which by Eqs. (2.10) and (2.11) is the same as

$$\int \left(\Phi_{\mathbf{v}} - \Phi_{\mathbf{u}}\right) dV \geq 0 \tag{2.19}$$

By Eqs. (2.12) and (2.13), one sees that Eq. (2.19) is the same as Eq. (2.9), the minimum energy dissipation theorem.

2.4.2 An Application of the Minimum Energy Dissipation Theorem

One advantage of variational principles such as the minimum energy dissipation theorem is that they can be used to describe the behaviour of general rigid bodies in a Stokes flow. We will give an example through the principle of "inclusion monotonicity". If one particle is large enough to completely contain another particle, then we can compare the magnitude of the so-called drag force resulting from a Stokes flow. Inclusion monotonicity follows from the minimum energy dissipation theorem, which we will now show in a manner following [20].

Let a rigid particle 1 take up a volume V_1 with surface $\partial V_1 = S_1$ and compare with the flow around rigid particle 2 taking up a volume V_2 with a surface $\partial V_2 = S_2$. They are undergoing the same translational motion with velocity $\mathbf{w}$ without rotation. The fluid is described by Stokes equations (2.6) and (2.7). Further, the particles have no-slip boundary conditions on their surfaces. The forces the fluid flow exerts on these particles are

$$\mathbf{f}_1 = \oint \boldsymbol{\sigma}_1 \cdot \mathbf{n}_1 dS_1 \tag{2.20}$$

$$\mathbf{f}_2 = \oint \boldsymbol{\sigma}_2 \cdot \mathbf{n}_2 dS_2 \tag{2.21}$$

where $\boldsymbol{\sigma}_i$ is the fluid stress tensor and $\mathbf{n}_i$ is the normal coming out of surface of particle i. The force of the fluid on the particle has the same magnitude but opposite direction.

$$\textbf{Inclusion monotonicity principle: If} \quad V_2 \subset V_1, \quad \text{then} \quad \mathbf{f}_2 \cdot \mathbf{w} \leq \mathbf{f}_1 \cdot \mathbf{w} \tag{2.22}$$

The drag is the component of the fluid force on the particle in the direction of $\mathbf{w}$ [17]. One can see by dividing through by $|\mathbf{w}|$ that inclusion monotonicity relation Eq. (2.22) gives that the magnitude of the drag force on particle 1 is greater than magnitude of the drag force on particle 2. Proof of inclusion monotonicity principle Eq. (2.22) is illustrated in Fig. 2.3 and given below.

Let $\mathbf{u}_1$ be the Stokes flow around the larger particle 1 and $\mathbf{u}_2$ be the Stokes flow around the smaller particle 2. The energy dissipation rate per unit time in the fluid is proportional to the drag [20]

$$\epsilon^{\mathbf{u}_1} = \mathbf{f}_1 \cdot \mathbf{w} \tag{2.23}$$

$$\epsilon^{\mathbf{u}_2} = \mathbf{f}_2 \cdot \mathbf{w} \tag{2.24}$$

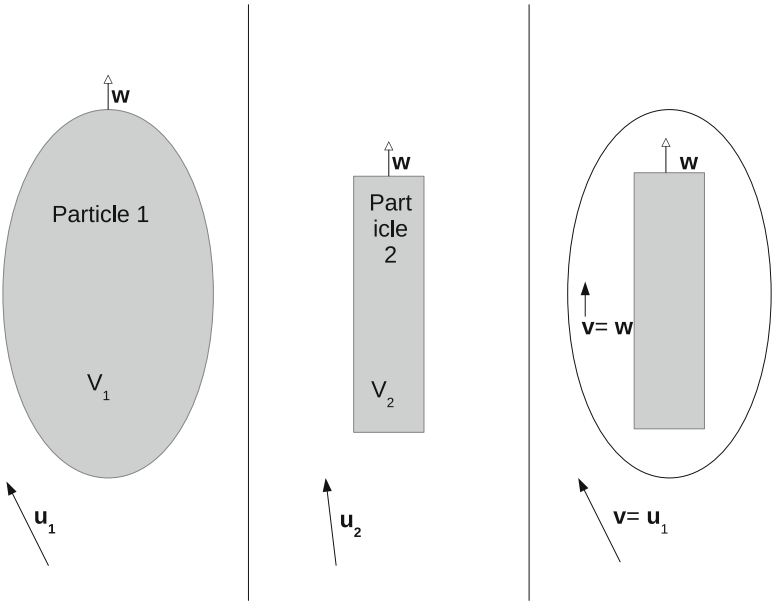

Fig. 2.3 Proof of inclusion monotonicity principle, illustrated. Three panels are drawn with particles in grey and fluid in white. In panel 1 and 2 particle 1 and particle 2 displace volumes such that $V_2 \subset V_1$. The particles are moving with the same velocity $\mathbf{w}$—shown with white tipped arrows—creating fluid velocity fields $\mathbf{u}_1$ and $\mathbf{u}_2$ shown with black tipped arrows. The last panel depicts a non-physical velocity field $\mathbf{v}$ which is equal to $\mathbf{u}_1$ outside of V_1 and $\mathbf{w}$ in $V_1 - V_2$

From the above equations it is easily seen that Eq. (2.22) is equivalent to $\epsilon^{\mathbf{u}_2} \leq \epsilon^{\mathbf{u}_1}$. However because these are Stokes flows for different geometries, the energy dissipation rates cannot be directly compared. Therefore, we will construct a (non-physical) vector field $\mathbf{v}$ in order to compare the energy dissipated by the motion of the two particles. Define $\mathbf{v}$ piecewise to be $\mathbf{u}_1$ outside of V_1 and $\mathbf{v} = \mathbf{w}$, the translational velocity, inside of $V_1 - V_2$. The vector field $\mathbf{v}$ is continuous because of the no-slip boundary condition. Now we will compare the energy dissipation rates of the different vector fields $\mathbf{u}_2$, $\mathbf{u}_1$ and $\mathbf{v}$.

We start by comparing $\mathbf{u}_1$ and $\mathbf{v}$. Because $\mathbf{v}$ is rigid body motion on $V_1 - V_2$, $\mathbf{v}$ does not dissipate any energy there. Outside that set, $\mathbf{v} = \mathbf{u}_1$. Therefore

$$\epsilon^{\mathbf{v}} = \epsilon^{\mathbf{u}_1} \tag{2.25}$$

We now move on to the comparison between $\mathbf{u}_2$ and $\mathbf{v}$. By definition, outside of V_1, $\mathbf{v} = \mathbf{u}_1$ which is a divergence-less vector field. On $V_1 - V_2$, $\mathbf{v}$ is constant, so it is automatically divergence free there. Therefore $\mathbf{v}$ is a divergence-free vector field defined on the same volume of fluid as $\mathbf{u}_2$. Therefore, by minimum energy dissipation theorem we have that $\mathbf{v}$ cannot dissipate less energy than $\mathbf{u}_2$, i.e.

$$\epsilon^{\mathbf{u}_2} \leq \epsilon^{\mathbf{v}} \tag{2.26}$$

Substituting the formulas for the energy dissipation rates Eqs. (2.23) and (2.24) into the above gives inclusion monotonicity Eq. (2.22).

2.5 Limits of the Stokes Approximation

2.5.1 Example of a System Where the Stokes Approximation Does Not Work

The examination of the validity of the Stokes approximation is very revealing of the logical structure of the features of Stokes flow (negligibility of inertial forces, reversibility and the minimum energy dissipation theorem). The most dramatic setting to consider is the famous "Stokes paradox". This paradox arises in the uniform Stokes flow past an infinite rigid cylinder. Suppose that such a cylinder is translating through a fluid with constant non-zero velocity $\mathbf{u}_0$ and has "no slip" on its surface. We suppose that very far from the cylinder, the fluid is at rest: $\mathbf{u}(\mathbf{x}) \to 0$ as $\mathbf{x} \to \infty$. Unfortunately, there is no solution to Eqs. (2.6) and (2.7) consistent with these boundary conditions [16, 19]. In a more general context, Stokes paradox occurs when a non-trivial two-dimensional solution of the Stokes equations (2.6) and (2.7) has no-slip boundary conditions on an object whose surface is a simple closed curve. The velocity is then necessarily logarithmically unbounded as one gets far from the object [18, 40]. More physically, Stokes paradox occurs because

the energy dissipated by the cylinder does not decline far from the particle—in other words, due to the minimum dissipation principle.

Other Linear Flow Equations

Because the Stokes approximation is not always justified and Navier–Stokes equations (2.1)–(2.2) are mathematically complicated, it is desirable to have other linear equation systems for fluid flow. We will very briefly give two such example systems in which Stokes paradox demonstrably does not occur but are still tractable: the Oseen and Brinkman equations.

We start with the well-known Oseen equations [19]. Let there be some constant background flow $\mathbf{u}_\infty$ imposed on the fluid. As mentioned before, the Navier–Stokes equations give that the inertial force have the nonlinear form $\rho(\mathbf{u}\cdot\nabla)\mathbf{u}$. If the characteristic velocity of the flow is much less than $|\mathbf{u}_\infty|$, then the main component of inertia is the resistance of the fluid flow against the background flow. We can decompose the local flow as $\mathbf{u}=\mathbf{u}_\infty+\mathbf{u}^O$ and call $\mathbf{u}^O$ the Oseen flow. The inertial force has therefore $\rho\left[(\mathbf{u}_\infty+\mathbf{u}^O)\cdot\nabla\right](\mathbf{u}^O+\mathbf{u}_\infty)=\rho(\mathbf{u}_\infty\cdot\nabla)\mathbf{u}^O+\rho(\mathbf{u}_\infty\cdot\nabla)\mathbf{u}_\infty+\rho(\mathbf{u}^O\cdot\nabla)\mathbf{u}_\infty+\rho(\mathbf{u}^O\cdot\nabla)\mathbf{u}^O$. Because $\mathbf{u}_\infty$ is constant, the middle terms are zero. Furthermore, we are looking for a linear equation, we assume that $|\mathbf{u}^O|\ll|\mathbf{u}_\infty|$. Therefore, we can neglect the nonlinear term. We use the term $\rho(\mathbf{u}_\infty\cdot\nabla)\mathbf{u}^O$ to incorporate inertial forces into linear equations. The equations resulting from the addition of this term to Eq. (2.6) are termed the Oseen equations [41, 42]. The Oseen equations for a steady, incompressible fluid have the form

$$\begin{aligned}\rho(\mathbf{u}_\infty\cdot\nabla)\mathbf{u}^O&=\mu\nabla^2\mathbf{u}^O-\nabla p^O\\ \nabla\cdot\mathbf{u}^O&=0\end{aligned}\tag{2.27}$$

where p^O is the pressure associated with such a flow.

There are considerations other than inertial forces that one can take into account for fluid motion in systems described by linear equations. For example, fluid flows in porous media can be described by linear equations. The solid skeleton causes an additional hydrodynamic resistance, which in the Brinkman model of porous media is introduced as a new term. This results in the following equations for fluid velocity $\mathbf{u}^B$ and fluid pressure p^B:

$$\begin{aligned}\mu\nabla^2\mathbf{u}^B-\nabla p^B&=c\mathbf{u}^B\\ \nabla\cdot\mathbf{u}^B&=0\end{aligned}\tag{2.28}$$

where c is the ratio of the fluid dynamic viscosity and the permeability of the porous media.

2.5.2 Departures from Reversibility Caused by Inertia

The Stokes approximation—which involves the deliberate neglecting of inertia—cannot be applied to systems in which inertial forces materially contribute to motion. This can be seen in flow visualisation. In symmetric environments, reversibility implies that the flow will also be symmetric [33]. For non-Stokes flows (i.e. $Re \gg 0$), the symmetry in the flow lines breaks down [43]. This departure from reversibility grows with the Reynolds number [44].

Reversible flow was shown in Sect. 2.3.1 to have the interesting property that a spherical particle under an external force parallel to a wall would not experience any lateral motion. In an inertial flow, however, a spherical particle tends to drift away from walls, breaking the reversibility, and causing the "tubular pinch effect" [44], with a different pattern of fluid streamlines.

In the analysis given in Sect. 2.3.1, a sphere rotating in a non-inertial fluid was considered. This leads to a reversible, time symmetric fluid flow [33]. However, a sphere (or a cylinder) which experiences inertial effects while rotating will create an irreversible flow. The inertial forces will cause the cylinder to irreversibly create vortices, which then interact with the rotation of the cylinder in a complex, non-time symmetric way, as shown in Ref. [45].

2.5.3 Accelerating Fluid Example

Even when the Stokes approximation is mathematically coherent, one should think with care how to interpret their results. As an illustrative example, consider a fluid contained within an infinite, impenetrable cylinder with radius R rotating with angular velocity Ω and with no-slip boundary conditions at its surface. The explicit solution of the Stokes equations has the form,

$$\mathbf{u}^S = \Omega r \hat{\boldsymbol{\theta}} \tag{2.29}$$

$$p^S = c \tag{2.30}$$

where c is a constant and $\hat{\boldsymbol{\theta}}$ is the unit vector in the azimuthal direction of the corresponding cylindrical coordinates. The flow velocity is, effectively, rigid body rotation. Pressure is constant in space and therefore there are clearly no centrifugal forces in the radial direction.

Moving on to consider the Navier–Stokes equations, we find that the solution becomes

$$\mathbf{u}^{NS} = \Omega r \hat{\boldsymbol{\theta}} \tag{2.31}$$

$$p^{NS} = \frac{1}{2}\rho\,\Omega^2 r^2 + c \tag{2.32}$$

Like the Stokes case, the fluid is undergoing rigid body rotation. But now a centrifugal force appears in the form of a pressure gradient in the radial direction. The Stokes solution ($\mathbf{u}^S$, p^S) has no forces in the radial direction, but in practice we would expect a centrifugal force in the presence of rotation. In the steady Navier–Stokes case, the centrifugal force per unit fluid volume is pressure gradient. Therefore, the centrifugal term p^{NS} is much more realistic than the constant term p^S.

2.6 Conclusions

Summarising, various properties essential to the understanding of Stokes flow, have been discussed, including negligibility of inertial forces, reversibility and the minimum energy dissipation theorem. Illustrative examples related to these properties have been provided: irreversible trajectories in Stokes flow, inertial terms for the fluid flow generated by a rotating cylinder, force on a rotating sphere close to a solid plane wall, Stokes paradox, energy dissipation for particles of different shapes. The meaning and the limits of the Stokes approximation have been discussed in the context of more general equations.

We will conclude with some analysis of the logical relationship between the assumption of the negligibility of inertial forces, the assumption of reversibility and the minimum energy dissipation theorem.

The assumption that a flow minimises the energy dissipation rate entails that the flow satisfies the Stokes equations. This means that minimum energy dissipation implies both reversibility and the negligibility of inertial forces. Stated contrapositively, irreversible flows or flows with inertial forces dissipate more energy than Stokes flows.

Furthermore, reversibility implies the negligibility of inertial forces. This is equivalent to saying that the presence of inertial forces implies irreversibility. Any term proportional to $\rho(\mathbf{u}\cdot\nabla)\mathbf{u}$, the inertial force term in the Navier–Stokes equation, will make a flow irreversible.

However, neither negligibility of inertial forces nor reversibility does not imply the minimum energy dissipation theorem. Like the Stokes equations (2.6) and (2.7), the Brinkman equations (2.28) and (2.29) are reversible and do not contain inertial terms. But one can now simply apply the proof in Sect. 2.4.1 by substituting $\mathbf{u}^B$ for the general solenoidal vector field $\mathbf{v}$ to find that the Brinkman flow dissipates more energy than the Stokes one. This also shows that, counterintuitively, reversibility is not sufficient to achieve the minimum energy dissipation achieved by Stokes flows.

Acknowledgements This work was supported in part by Narodowe Centrum Nauki under grant No. 2014/15/B/ST8/04359. We acknowledge scientific benefits from COST Action MP1305.

References

1. H.A. Stone, A. Stroock, A. Ajdari, Engineering flows in small devices: microfluidics toward a lab-on-a-chip. Annu. Rev. Fluid Mech. **36**, 381 (2004)
2. B.E. Rabinow, Nanosuspensions in drug delivery. Nat. Rev. Drug Discov. **3**(9), 785 (2004)
3. M. Peltomäki, G. Gompper, Sedimentation of single red blood cells. Soft Matter **9**(34), 8346 (2013)
4. J.K. Nunes, K. Sadlej, J.I. Tam, H.A. Stone, Control of the length of microfibers. Lab Chip **12**(13), 2301 (2012)
5. H.M. Shewan, J.R. Stokes, Review of techniques to manufacture micro-hydrogel particles for the food industry and their applications. J. Food Eng. **119**(4), 781 (2013)
6. A. Perazzo, J.K. Nunes, S. Guido, H.A. Stone, Flow-induced gelation of microfiber suspensions. Proc. Natl. Acad. USA **114**(41), E8557 (2017)
7. J.K. Oh, R. Drumright, D.J. Siegwart, K. Matyjaszewski, The development of microgels/nanogels for drug delivery applications. Prog. Polym. Sci. **33**(4), 448 (2008)
8. E. Kjeang, N. Djilali, D. Sinton, Microfluidic fuel cells: a review. J. Power Sources **186**(2), 353 (2009)
9. Y. Qiu, K. Park, Environment-sensitive hydrogels for drug delivery. Adv. Drug Deliv. Rev. **53**(3), 321 (2001)
10. N.A. Hill, M.A. Bees, Taylor dispersion of gyrotactic swimming micro-organisms in a linear flow. Phys. Fluids **14**(8), 2598 (2002)
11. E.M. Purcell, Life at low Reynolds number. Am. J. Phys. **45**(1), 3 (1977)
12. M. Garcia, S. Berti, P. Peyla, S. Rafaï, Random walk of a swimmer in a low-Reynolds-number medium. Phys. Rev. E **83**(3), 35301 (2011)
13. V. Kantsler, R.E. Goldstein, Fluctuations, dynamics, and the stretch-coil transition of single actin filaments in extensional flows. Phys. Rev. Lett. **108**(3), 38103 (2012)
14. A. Farutin, S. Rafaï, D.K. Dysthe, A. Duperray, P. Peyla, C. Misbah, Amoeboid swimming: a generic self-propulsion of cells in fluids by means of membrane deformations. Phys. Rev. Lett. **111**(22), 228102 (2013)
15. M. Harasim, B. Wunderlich, O. Peleg, M. Kröger, A.R. Bausch, Direct observation of the dynamics of semiflexible polymers in shear flow. Phys. Rev. Lett. **110**(10), 108302 (2013)
16. H. Lamb, *Hydrodynamics* (Cambridge University Press, Cambridge, 1932)
17. L.D. Landau, E.M. Lifshitz, *Fluid Mechanics: Course of Theoretical Physics*, vol. 6, 2nd edn. (Pergamon Press, Oxford, 1959)
18. G. Batchelor, *An Introduction to Fluid Dynamics* (Cambridge University Press, Cambridge, 2000)
19. J. Happel, H. Brenner, *Low Reynolds Number Hydrodynamics: With Special Applications to Particulate Media*, vol. 1 (Springer Science & Business Media, Dordrecht, 2012)
20. S. Kim, S.J. Karrila, *Microhydrodynamics: Principles and Selected Applications* (Dover, Downers Grove, 2005)
21. É. Guazzelli, J.F. Morris, *A Physical Introduction to Suspension Dynamics*, vol. 45 (Cambridge University Press, Cambridge, 2011)
22. M.D. Graham, *Microhydrodynamics, Brownian Motion, and Complex Fluids*, vol. 58 (Cambridge University Press, Cambridge, 2018)
23. G.I. Taylor, Stability of a viscous liquid contained between two rotating cylinders. Philos. Trans. R. Soc. London A Math. Phys. Eng. Sci. **223**(605–615), 289 (1923)
24. J.F. Brady, G. Bossis, Stokesian dynamics. Annu. Rev. Fluid Mech. **20**, 111 (1988)
25. B.U. Felderhof, Many-body hydrodynamic interactions in suspensions. Physica A **151**(1), 1 (1988)
26. A.J.C. Ladd, Hydrodynamic transport coefficients of random dispersions of hard spheres. J. Chem. Phys. **93**(5), 3484 (1990)
27. A.S. Sangani, G. Mo, Inclusion of lubrication forces in dynamic simulations. Phys. Fluids **6**(5), 1653 (1994)

28. B. Cichocki, B.U. Felderhof, K. Hinsen, E. Wajnryb, J. Bławzdziewicz, Friction and mobility of many spheres in Stokes flow. J. Chem. Phys. **100**, 3780 (1994)
29. B. Cichocki, M.L. Ekiel-Jeżewska, E. Wajnryb, Lubrication corrections for three-particle contribution to short-time self-diffusion coefficients in colloidal dispersions. J. Chem. Phys. **111**(7), 3265 (1999)
30. M.L. Ekiel-Jeżewska, E. Wajnryb, in *Theoretical Methods Micro Scale Viscous Flows*, ed. by F. Feuillebois, A. Sellier (Transworld Research Network, 2009), pp. 127–172
31. G.I. Taylor, *Low Reynolds Number Flows* (Educational Services Incorporated. Distributor: Encyclopaedia Britannica Educational Corporation, Chicago, Illinois, 1967)
32. G.I. Taylor, *Film Notes for "Low-Reynolds-Number Flows"* (National Committee for Fluid Mechanics Films, Education Development Center, Educational Services Incorporated. Distributor: Encyclopaedia Britannica Educational Corporation, Chicago, Illinois, 1967)
33. D.J. Jeffrey, in *Sedimentation of Small Particles in a Viscous Fluid*, ed. by E. Tory (Computational Mechanics Publications, Southampton, 1996)
34. D.J. Jeffrey, Y. Onishi, The slow motion of a cylinder next to a plane wall. Q. J. Mech. Appl. Math. **34**(2), 129 (1981)
35. K. Malysa, T. Dabros, T.G.M. de Ven, The sedimentation of one sphere past a second attached to a wall. J. Fluid Mech. **162**, 157 (1986)
36. M.L. Ekiel-Jeżewska, N. Lecoq, R. Anthore, F. Bostel, F. Feuillebois, in *Tubes, Sheets and Singularities in Fluid Dynamics*, ed. by K. Bajer, H.K. Moffatt (Kluwer Academic, Dordrecht, 2002), pp. 343–348
37. M.L. Ekiel-Jeżewska, F. Feuillebois, N. Lecoq, K. Masmoudi, R. Anthore, F. Bostel, E. Wajnryb, in *Third Conference on Multiphase Flow, ICMF 98, Lyon, France* (1998), pp. 1–8
38. K. Masmoudi, Etude des interactions hydrodynamiques particule-particules, particules-parois par interferometrie laser. Phd Thesis, Univ. Rouen, Rouen (1998)
39. M.L. Ekiel-Jeżewska, F. Feuillebois, N. Lecoq, K. Masmoudi, R. Anthore, F. Bostel, E. Wajnryb, Hydrodynamic interactions between two spheres at contact. Phys. Rev. E **59**(3), 3182 (1999)
40. I. Chang, R. Finn, On the solutions of a class of equations occurring in continuum mechanics, with application to the Stokes paradox. Arch. Ration. Mech. Anal. **7**(1), 388 (1961)
41. C.W. Oseen, Uber die Stokes' sche Formel und Uber eine verwandte Aufgabe in der Hydrodynamik. Ark. Mat., Astron. och Fys. **6**, 1 (1910)
42. H. Lamb, On the uniform motion of a sphere through a viscous fluid. Lond. Edinb. Dublin Philos. Mag. J. Sci. **21**(121), 112 (1911)
43. M.V. Dyke, *An Album of Fluid Motion* (Parabolic Press, Stanford, 1982)
44. E.G. Flekkøy, T. Rage, U. Oxaal, J. Feder, Hydrodynamic irreversibility in creeping flow. Phys. Rev. Lett. **77**(20), 4170 (1996)
45. A. Rao, B.E. Stewart, M.C. Thompson, T. Leweke, K. Hourigan, Flows past rotating cylinders next to a wall. J. Fluids Struct. **27**(5–6), 668 (2011)

Stable Configurations of Charged Sedimenting Particles

C. I. Trombley and M. L. Ekiel-Jeżewska*
Institute of Fundamental Technological Research, Polish Academy of Sciences, Pawińskiego 5b, 02-106 Warsaw, Poland

(Received 5 October 2018; revised manuscript received 27 November 2018; published 21 December 2018)

The qualitative behavior of charged particles in a vacuum is given by Earnshaw's theorem, which states that there is no steady configuration of charged particles in a vacuum that is asymptotically stable to perturbations. In a viscous fluid, examples of stationary configurations of sedimenting uncharged particles are known, but they are unstable or neutrally stable—they are not attractors. In this Letter, it is shown by example that two charged particles settling in a fluid may have a configuration that is asymptotically stable to perturbations for a wide range of charges, radii, and densities. The existence of such "bound states" is essential from a fundamental point of view and it can be significant for dilute charged particulate systems in various biological, medical, and industrial contexts.

DOI: 10.1103/PhysRevLett.121.254502

Earnshaw's theorem gives fundamental insights into the stability of charged systems. Introduced in Ref. [1], the theorem states that there is no stable equilibrium of charged particles distributed in a vacuum without a boundary. An informal reading is that electrostatic interactions are inherently destabilizing and one must add, e.g., boundaries or stabilizing forces [2]. Historically, Earnshaw's theorem informed the development of models of the stability of matter and studies of qualitative features of charged systems [2,3]. Finding the stable configurations allowed by Earnshaw's theorem when a spherical boundary is imposed—the "Thompson problem"—is an active field [4]. Earnshaw's theorem underpins classical models of Wigner crystallization (for instance, see Ref. [5]). It even allows one to find quantitative limits on parameters for stable classical models of complex molecules [6]. In this Letter, we show that the presence of an unbounded electrically neutral fluid can stabilize systems of charged microparticles.

At micro and nano scales, both active "agents" and passive objects, whether of biological [7–9] or inorganic materials [10,11], and naturally or artificially made, have been modeled theoretically as particles in a fluid. In general, such particles can have complex shapes and be deformable. Their rich dynamics have been extensively investigated [12–19]. The development of microfluidics, Lab-On-Chip technologies [20], and advances in medicine and the design of innovative materials and devices—e.g., to carry drugs [21] or treat wastewater [22]—depends on this research.

The concept of a noninertial "Stokes flow," introduced in Ref. [23], holds a central place in the theory of the dynamics of micro and nano particles [24,25]. In particular, Stokes equations are widely used to determine the influence of a viscous fluid on the dynamics of particles experiencing external forces, such as gravity or in a centrifuge [14,26–30]. For a single particle, Stokes flow is an appropriate model when the particle has reached its terminal velocity, its so-called Stokes velocity. The terminal velocity is reached swiftly at a microscale. In systems of microparticles in a Stokes flow, the velocity of each particle is a linear combination of the forces on every particle. The coefficients of this combination depend on positions of all the particles.

The goal of this Letter is to find asymptotically stable configurations of two sedimenting charged particles. The existence of such "attractive states" (configurations such that if the particles were disturbed from this configuration then they would tend to return) may be of a great significance for sedimenting suspensions that exhibit electrostatic interparticle interactions.

First, we briefly outline known results for uncharged particles. Owing to reversibility of Stokes equations, identical spherical sedimenting particles can form steady configurations, such as, e.g., horizontal regular polygons made of arbitrary numbers of particles [31]. More simply, any arrangement of two identical particles in free space is steady. However, these steady configurations are, at most, neutrally stable, and therefore are not attractive.

The more interesting case of two spherical uncharged sedimenting particles with different radii and densities was examined in the seminal paper [32]. If the particles are far enough from each other that their interaction can be neglected, then particle A with a larger Stokes velocity

will fall faster than particle B with a smaller Stokes velocity. Intuition may suggest that if particle A is above particle B with their centers in a vertical line, then they will tend to approach each other no matter what their distance. Counterintuitively, it was found that, in a certain range of parameters, the particles do not tend to touch each other (in an infinite time) but instead "capture" each other at a distance a bit larger than the sum of their radii [32]. Even more surprisingly, particle A can move slower than B if the interparticle distance is smaller than its steady value. In this uncharged system, vertical steady configurations are stable against vertical, but unstable with respect to horizontal, perturbations.

The main idea of this Letter is to introduce charge to such a system, to find a steady vertical configuration and check if electrostatic attraction between the particles will cause them to come back to the steady configuration if perturbed. In the following, we will show that indeed this is the case—we discover stable configurations. Counterintuitively to Earnshaw's theorem in vacuum, electrostatic interactions between charged particles in fluids can play a stabilizing role.

We now introduce a model of two charged, spherical particles settling under gravity in a fluid of dynamic viscosity μ. We assume that Brownian motion, fluid compressibility, and inertia are irrelevant, and we describe the fluid flow by the Stokes equations [24,25]. Thus, the external forces on the particles are in balance with the fluid resistance forces, and therefore the dynamics of particles is described by a system of first order differential equations.

We denote particle radii by a_1 and a_2. Let M_1 and M_2 represent the mass of particle 1 and 2. The reduced density of each particle is the difference between its density and the density ρ of the fluid. Similarly, $m_1 = M_1 - \frac{4}{3}\pi a_1^3\rho$ and $m_2 = M_2 - \frac{4}{3}\pi a_2^3\rho$ are the reduced masses. We assume $m_2 > 0$ with other cases covered in the Supplemental Material [33]. Let $\mathbf{r}_1$ and $\mathbf{r}_2$ be the positions of the centers of particle 1 and 2. Then the relative position is $\mathbf{d} = \mathbf{r}_2 - \mathbf{r}_1$. We choose a coordinate system so that the particle centers and the direction of gravity are in the plane $y = 0$ and $\hat{\mathbf{z}}$ is a unit vector pointing antiparallel to the constant gravitational field $\boldsymbol{g}$. We can now write the superposition of electrostatic and gravitational forces on the particles 1 and 2

$$\mathbf{f}_1 = -kq_1q_2\frac{\mathbf{d}}{|\mathbf{d}|^3} - m_1g\hat{\mathbf{z}} \tag{1}$$

$$\mathbf{f}_2 = kq_1q_2\frac{\mathbf{d}}{|\mathbf{d}|^3} - m_2g\hat{\mathbf{z}}, \tag{2}$$

where k is Coulomb's constant, q_1 and q_2 are the charges on particles 1 and 2, $|\mathbf{v}|$ is the length of any vector $\mathbf{v}$, and $g = |\boldsymbol{g}|$. Assuming pointlike charges, we consistently take a point particle approximation for the interaction with the fluid [25,34], and we obtain the following system of ordinary differential equations (ODEs):

$$\dot{\mathbf{r}}_1 = \frac{1}{8\pi\mu}\boldsymbol{G}\cdot\mathbf{f}_2 + \frac{1}{6\pi\mu a_1}\mathbf{f}_1 \tag{3}$$

$$\dot{\mathbf{r}}_2 = \frac{1}{8\pi\mu}\boldsymbol{G}\cdot\mathbf{f}_1 + \frac{1}{6\pi\mu a_2}\mathbf{f}_2, \tag{4}$$

where $G_{ij} = \delta_{ij}/|\mathbf{d}| + d_id_j/|\mathbf{d}|^3$ is the Green tensor for the Stokes equations in an unbounded fluid [25]. The total velocity of each particle has a mutual part that depends on the force on the other particle and a self-part that depends on the force on the particle itself. Notice that it is necessary to take into account the particle radii in the self-terms. Because of the translational invariance of the system $\boldsymbol{G}$ depends only on the relative position $\mathbf{d}$. We are interested in the relative motion, which satisfies the following ODEs

$$\dot{\mathbf{d}} = \frac{1}{8\pi\mu}\left(-\frac{2kq_1q_2}{|\mathbf{d}|^3}\boldsymbol{G}\cdot\mathbf{d} + (m_2 - m_1)g\boldsymbol{G}\cdot\hat{\mathbf{z}}\right) - \frac{1}{6\pi\mu}\left(-\frac{kq_1q_2}{|\mathbf{d}|^3}\left(\frac{1}{a_1}+\frac{1}{a_2}\right)\mathbf{d} + \left(\frac{m_2}{a_2}-\frac{m_1}{a_1}\right)g\hat{\mathbf{z}}\right). \tag{5}$$

Before we examine the properties of Eq. (5), we describe physical properties of the system using nondimensional parameters, which are independent of each other and constant during particle motion

$$\gamma = \frac{a_1}{a_2}, \qquad \delta = \frac{m_1}{m_2}, \qquad \beta = -\frac{kq_1q_2}{L^2m_2g}, \tag{6}$$

so that γ is the ratio of particle radii, δ is the ratio of reduced particle masses, and β is the ratio of characteristic Coulomb force $F_e = -kq_1q_2/L^2$ to the characteristic gravitational force $F_g = m_2g$. The sign of F_e is chosen to be positive when the charges attract each other. There are some physically interesting functions of these parameters. For instance, the ratio of reduced densities is δ/γ^3 and the ratio of Stokes velocities is δ/γ.

We now choose the units

$$L = a_1 + a_2, \qquad V = \frac{m_2g}{6\pi\mu L} \tag{7}$$

where L—the characteristic length—is the distance the particle centers would have if the particle surfaces were in contact, and V is a characteristic velocity. These scales define a characteristic timescale $T = L/V$. Notice that changing the viscosity μ modifies only the velocity and timescales. The nondimensional parameters [Eq. (6)] are invariant. In the Stokes regime, changes in viscosity do not alter the paths on which the particles move but only the rate at which they move on said paths [24,25].

Finally, we nondimensionalize the relative position

$$\alpha = \frac{\mathbf{d}}{L} \tag{8}$$

so that, if the particle surfaces were in contact, $|\boldsymbol{\alpha}| = 1$. We can now write Eq. (5) involving only the nondimensional ratios

$$\dot{\boldsymbol{\alpha}} = \frac{3}{2|\boldsymbol{\alpha}|^3}\beta\boldsymbol{\mathcal{G}}\cdot\boldsymbol{\alpha} + \frac{3}{4}(1-\delta)\boldsymbol{\mathcal{G}}\cdot\hat{\mathbf{z}} - \beta\frac{(1+\gamma)^2}{\gamma|\boldsymbol{\alpha}|^3}\boldsymbol{\alpha} - \frac{(\gamma-\delta)(1+\gamma)}{\gamma}\hat{\mathbf{z}}, \tag{9}$$

where $\mathcal{G}_{ij} = \delta_{ij}/|\boldsymbol{\alpha}| + \alpha_i\alpha_j/|\boldsymbol{\alpha}|^3$ and from now on the dot denotes derivative with respect to nondimensional time ratio t/T.

We now analyze Eq. (9) and discover a class of vertical configurations that are stable to any perturbation.

We denote a nondimensional stationary configuration by $\alpha^* = \alpha^*\hat{\mathbf{z}}$, with $\alpha^* > 0$. Our convention is then to assign label 2 to the particle with larger $\hat{z}$ component in the steady state. To examine the stability of such a configuration, we investigate how the system evolves if we have a first order perturbation ϵ in the direction perpendicular to gravity and a positive component α in the $\hat{z}$ direction (not necessarily close to α^*). If $\boldsymbol{\alpha} = \epsilon\hat{\mathbf{x}} + \alpha_z\hat{\mathbf{z}}$ and we neglect second and higher order terms in ϵ then $\alpha = |\boldsymbol{\alpha}| = \sqrt{\alpha_z^2 + \epsilon^2} \approx \alpha_z$. With this, Eq. (9) becomes

$$\dot{\epsilon} = g(\alpha)\epsilon \tag{10}$$

$$\dot{\alpha} = f(\alpha) \tag{11}$$

where

$$f(\alpha) = \frac{6\gamma\beta - 2\beta(1+\gamma)^2\alpha + 3\gamma(1-\delta)\alpha^2 - 2(\gamma-\delta)(1+\gamma)\alpha^3}{2\gamma\alpha^3} \tag{12}$$

$$g(\alpha) = \frac{12\gamma\beta - 4(1+\gamma)^2\beta\alpha + 3\gamma(1-\delta)\alpha^2}{4\gamma\alpha^4}. \tag{13}$$

In the numerator of f the four terms are, consecutively, the mutual and self-parts of velocity arising from electrostatic forces, and the mutual and self-parts of velocity arising from the gravitational forces. This is similar for g, except that there is no self-part of horizontal velocity arising from vertical gravitational force.

For any system of differential equations of the form (10) and (11), if g and f are continuous, then the condition for $\alpha^* = \alpha^*\hat{\mathbf{z}}$ to be an steady state is

$$f(\alpha^*) = 0. \tag{14}$$

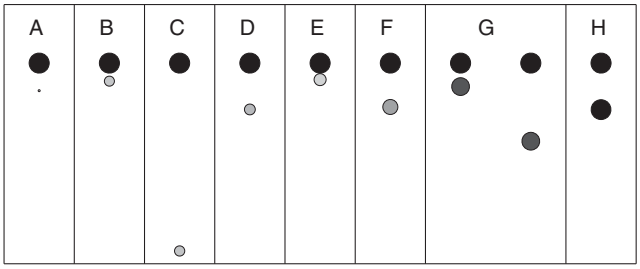

FIG. 1. Examples A–H illustrate stable stationary configurations of charged particles settling under gravity in a Stokes flow for the parameter values listed in Table I. Gravity points down.

If f is continuously differentiable and g is continuous in an open neighborhood of a steady state α^*, then $\boldsymbol{\alpha}^*$ is stable if and only if

$$g(\alpha^*) < 0 \tag{15}$$

$$f'(\alpha^*) < 0. \tag{16}$$

A proof that Eqs. (14)–(16) are necessary and sufficient for local asymptotic stability [35] is given in section II of the Supplemental Material [33].

Finally, we impose the feasibility condition

$$1 < \alpha^* \tag{17}$$

in order to rule out ghostlike overlapping particles.

We now demonstrate that there exist solutions to Eqs. (14)–(17). We provide examples of stable stationary feasible configurations in Fig. 1 with the parameters in Table I. In Fig. 1, the density of particle 2 is held constant and painted black, while brighter colors are used to represent denser particles. Similarly, radius a_2 of the upper particle is taken to be the same across columns and the radius a_1 of the lower particle is drawn to scale.

In case A, small δ and γ are chosen. This corresponds to the higher particle being much larger and more massive than the lower particle. Case B shows that stability is possible when $\delta = \gamma$. This corresponds to particles that

TABLE I. Positions and parameters of the stable stationary configurations shown in Fig. 1.

	α^*	β	δ	γ	δ/γ	δ/γ^3
A	2.5	0.160…	0.075	0.1	0.75	75
B	1.2	0.45	0.5	0.5	1	4
C	12.4	2.18…	0.5	0.51	0.980…	3.76…
D	3	0.361…	0.5	0.54	0.925…	3.17…
E	1.03	0.930…	1.1	0.6	1.83…	5.09…
F	2.5	0.523…	1	0.75	1.33…	2.37…
G	1.24…	0.125	0.875	0.885	0.988…	1.26…
	4.13…					
H	2.33…	0.009 97…	0.986	0.988	0.998…	1.02…

have identical Stokes velocities. Next we look at cases C and D where the separation distance α^* is large. Cases E and F give examples where $\delta/\gamma > 1$, so that the lower particle has a greater Stokes velocity than the upper particle. Case G illustrates that, for the same parameters, two distinct stable stationary configurations can exist. In case H, $\gamma \approx 1$, $\delta \approx 1$, and $\beta \approx 0$, showing that there are stable stationary configurations very close to the classic case of two identical uncharged particles.

Now that we know that the solution set is nonempty, we investigate the range of parameters consistent with a stable feasible steady configuration. The range will come directly from the necessary and sufficient conditions [Eqs. (14)–(17)]. The physical implications of these bounds will also be discussed.

We start with the ratio of characteristic electrostatic to characteristic gravitational force β. By manipulating the conditions [Eqs. (14)–(17)], one can see

$$\frac{3\beta}{\alpha^{*3}} = 3f(\alpha^*) - \alpha^*[f'(\alpha^*) + 2g(\alpha^*)] > 0. \tag{18}$$

Therefore, if a solution exists, then $\beta > 0$. This means that the particles must attract each other in order for the system to be stable, in agreement with our predictions that motivated this Letter. This is also important because it allows for stable systems that have a zero net charge, $q_1 + q_2 = 0$.

Next, we show that the ratio of reduced masses $\delta > 0$. We use that $f(\alpha^*) - \alpha^* g(\alpha^*) > 0$ to solve for a bound on δ to get

$$\delta > \frac{3\gamma - 4\gamma(1+\gamma)\alpha^*}{3\gamma - 4(1+\gamma)\alpha^*} > 0, \tag{19}$$

because the denominator and numerator are both necessarily negative if $\gamma > 0$ and $\alpha^* > 1$. This demonstrates that if $m_2 > 0$, then $m_1 > 0$. In the Supplemental Material [33], we extend this to show that stable doublets can exist only in the $m_2 > 0$ and $m_1 > 0$ case and the symmetric case when buoyancy dominates over gravity $m_2 < 0$ & $m_1 < 0$.

Moreover, the upper particle must have a larger radius than the lower particle

$$\gamma < 1. \tag{20}$$

The demonstration is somewhat tedious, so it is given in the Supplemental Material [33].

If we divide both sides of Eq. (19) by γ^3, we can use $\gamma < 1$ and Eq. (17) to show that the middle term in Eq. (19) will be larger than 1. Therefore,

$$\delta/\gamma^3 > \frac{3 - 4(1+\gamma)\alpha^*}{(3\gamma - 4(1+\gamma)\alpha^*)\gamma^2} > 1. \tag{21}$$

This means that the lower particle has to be more dense than the upper one. This has the interesting implication that in our model stable doublets only form between particles of different material.

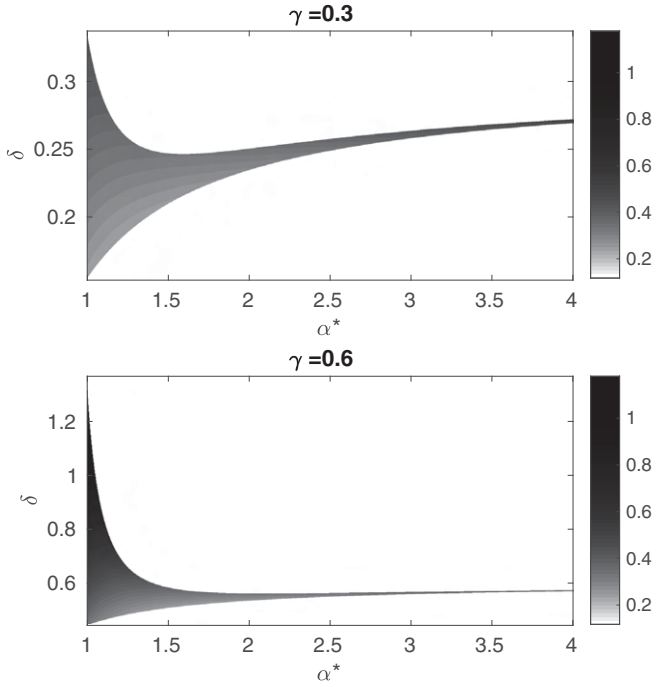

FIG. 2. Regions of stable steady states in parameter space are plotted. Given γ and δ, the shade at a point is chosen by characteristic force ratio β necessary to stabilize the system at α^*. If no amount of charge would stabilize a system with the given parameters, the point is left white.

With these bounds in mind, we give Fig. 2 in order to illustrate the way α^* and the parameters δ, γ, and β are interrelated. These plots visually demonstrate that the set of parameters that allow a feasible stable steady state is large. One can also see that there exist stable stationary configurations in the "tail" where α^* gets large. Examination of this tail introduces some facts of physical interest. By expanding the relations [Eqs. (14)–(17)] in powers of $1/\alpha^*$, we deduce that, in the tail, the upper particle must have a slightly greater Stokes velocity than the lower one: $1 - (\delta/\gamma) \approx 3(1-\gamma)/[4(1+\gamma)](1/\alpha^*) \ll 1$. Looking at the ratio of forces, we see that $\beta \approx 3\gamma(1-\gamma)/[4(1+\gamma)^2]\alpha^* \gg 1$ in the tail. This means that in the tail electrostatic interactions are strong relative to gravitational force. This demonstrates how electrostatic forces can stabilize a doublet even when the distances involved are large.

In another limit, we keep α^* constant and move values of δ and γ closer and closer to unity. In this limit, the ratio of Stokes velocities δ/γ and relative densities δ/γ^3 approach 1—that is, the particles get more similar. As a consequence of Eq. (14), β scales down to $\beta \ll 1$. We are seeing therefore that a small charge can be expected to stabilize the system in this limit.

In order to aid physical intuition in interpreting the above results, we will demonstrate the role of charge in stabilizing

a system of settling particles. For an uncharged system, the analog of Eq. (14) is $3\gamma(1-\delta)-2(\gamma-\delta)(1+\gamma)\alpha^*=0$. The first and second terms are the contributions of gravity to the mutual and self-parts of velocity. The semistability condition—the analog of Eq. (16)—can be combined with the analog of Eq. (14) to get $-2(\gamma-\delta)(1+\gamma)<0$. Therefore the semistability condition entails the ratio of Stokes velocities $\delta/\gamma<1$, so that the self-term tends to bring the particles together. We also have that $\delta<1$; therefore the mutual term must tend to push the particles apart. These contributions to the velocity balance exactly at a certain distance α'. However, if the particles are perturbed even slightly in the horizontal direction, the story is different. The analog of Eq. (16) is $3\gamma(1-\delta)<0$, which cannot be satisfied if $\delta<1$. The horizontal velocity—which contains only this mutual term—is tending to push the particles apart. There is no asymptotically stable α^*. At α' the system is "semi-stable"—it is stable only to perturbations in the vertical direction. For example, $\alpha'\approx 5.21\ldots$ in the uncharged system H', which has the same mass ratio δ and ratio of radii γ as system H given in Table I and illustrated in Fig. 1.

Now consider adding a very slight charge to the system so that $\beta=0.009\,97\ldots$, in other words system H. In a vertical arrangement, the electrostatic force adds to the self and mutual contributions to velocity without changing their signs, so that the first thing we find is that the stationary configuration of the system contracts to $\alpha^*\approx 2.33\ldots$. Now consider horizontal perturbations. There are two electrostatic contributions to the horizontal motion. A mutual term, $12\gamma\beta=0.118\ldots$, which tends to push the particles apart and a self term, $-4(1+\gamma)^2\beta\alpha^*=-0.367\ldots$, which tends to bring them back. As before, the gravitational contribution to horizontal velocity, $3\gamma(1-\delta)\alpha^2=0.225\ldots$, tends to push the particles apart. The restoring term dominates. Therefore, system H is stable.

In this way, we have demonstrated ostensively how settling charged particle systems (even with small charge) can have qualitatively new behavior (local asymptotic stability) absent in their uncharged counterparts. It applies also to semidiluted polydispersed suspensions of microparticles.

The core prediction of the model presented in this Letter is the formation of stable asymmetric doublets. The existence of such doublets is experimentally testable. These doublets are not stable without charge, indicating the novelty of the settling dynamics explored here.

In future work, we will expand the model to include electrostatic screening and precise treatment of hydrodynamic interactions between hard spheres with stick boundary conditions, applying the multipole expansion corrected for lubrication [36]. We will also investigate the influence of charge on essential features of the dynamics, such as existence of periodic motions [32].

This Letter was supported in part by Narodowe Centrum Nauki under Grant No. 2014/15/B/ST8/04359. We acknowledge scientific benefits from COST Action MP1305.

*Corresponding author.
mekiel@ippt.pan.pl

[1] S. Earnshaw, Trans. Cambridge Philos. Soc. **7**, 97 (1842).
[2] Y. Levin, Physica (Amsterdam) **352A**, 43 (2005).
[3] W. Jones, Eur. J. Phys. **1**, 85 (1980).
[4] A. Bondarenko, M. Karchevskiy, and L. Kozinkin, J. Phys. Conf. Ser. **643**, 012103 (2015).
[5] R. G. Nazmitdinov, A. Puente, M. Cerkaski, and M. Pons, Phys. Rev. E **95**, 042603 (2017).
[6] F. Mohammad-Rafiee and R. Golestanian, Phys. Rev. E **69**, 061919 (2004).
[7] V. Kantsler and R. E. Goldstein, Phys. Rev. Lett. **108**, 038103 (2012).
[8] K. Kang and J. K. G. Dhont, Phys. Rev. Lett. **110**, 015901 (2013).
[9] Y. Liu, B. Chakrabarti, D. Saintillan, A. Lindner, and O. du Roure, Proc. Natl. Acad. Sci. U.S.A. **115**, 9438 (2018).
[10] A. Perazzo, J. K. Nunes, S. Guido, and H. A. Stone, Proc. Natl. Acad. Sci. U.S.A. **114**, E8557 (2017).
[11] S. Pawłowska, P. Nakielski, F. Pierini, I. K. Piechocka, K. Zembrzycki, and T. A. Kowalewski, PLoS One **12**, e0187815 (2017).
[12] D. E. Smith, H. P. Babcock, and S. Chu, Science **283**, 1724 (1999).
[13] L. E. Becker and M. J. Shelley, Phys. Rev. Lett. **87**, 198301 (2001).
[14] M. C. Lagomarsino, I. Pagonabarraga, and C. P. Lowe, Phys. Rev. Lett. **94**, 148104 (2005).
[15] Y.-N. Young and M. J. Shelley, Phys. Rev. Lett. **99**, 058303 (2007).
[16] M. Harasim, B. Wunderlich, O. Peleg, M. Kröger, and A. R. Bausch, Phys. Rev. Lett. **110**, 108302 (2013).
[17] A. Farutin, T. Piasecki, A. M. Słowicka, C. Misbah, E. Wajnryb, and M. L. Ekiel-Jeżewska, Soft Matter **12**, 7307 (2016).
[18] M. Gruziel, K. Thyagarajan, G. Dietler, A. Stasiak, M. L. Ekiel-Jeżewska, and P. Szymczak, Phys. Rev. Lett. **121**, 127801 (2018).
[19] M. Bukowicki and M. L. Ekiel-Jeżewska, Soft Matter **14**, 5786 (2018).
[20] J. K. Nunes, K. Sadlej, J. I. Tam, and H. A. Stone, Lab Chip **12**, 2301 (2012).
[21] D. A. Edwards, J. Hanes, G. Caponetti, J. Hrkach, A. Ben-Jebria, M. L. Eskew, J. Mintzes, D. Deaver, N. Lotan, and R. Langer, Science **276**, 1868 (1997).
[22] C. A. Coutinho and V. K. Gupta, J. Colloid Interface Sci. **333**, 457 (2009).
[23] G. G. Stokes, Trans. Cambridge Philos. Soc. **9**, 8 (1851).
[24] G. K. Batchelor, *An Introduction to Fluid Dynamics* (Cambridge University Press, Cambridge, England, 2000).
[25] S. Kim and S. J. Karrila, *Microhydrodynamics: Principles and Selected Applications* (Butterworth-Heinemann, Boston, 1991).

[26] R. E. Caflisch, C. Lim, J. H. Luke, and A. S. Sangani, Phys. Fluids **31**, 3175 (1988).
[27] N. Lecoq, F. Feuillebois, N. Anthore, R. Anthore, F. Bostel, and C. Petipas, Phys. Fluids A **5**, 3 (1993).
[28] M. L. Ekiel-Jeżewska, Phys. Rev. E **90**, 043007 (2014).
[29] M. Bargiel and E. M. Tory, Powder Technol. **264**, 519 (2014).
[30] G. Saggiorato, J. Elgeti, R. G. Winkler, and G. Gompper, Soft Matter **11**, 7337 (2015).
[31] L. Hocking, J. Fluid Mech. **20**, 129 (1964).
[32] E. Wacholder and N. Sather, J. Fluid Mech. **65**, 417 (1974).
[33] See Supplemental Material at http://link.aps.org/supplemental/10.1103/PhysRevLett.121.254502 for theoretical derivations.
[34] M. D. Graham, *Microhydrodynamics, Brownian Motion, and Complex Fluids* (Cambridge University Press, Cambridge, England, 2018).
[35] P. Glendinning, *Stability, Instability and Chaos: An Introduction to the Theory of Nonlinear Differential Equations* (Cambridge University Press, Cambridge, England, 1994), p. 37.
[36] B. Cichocki, M. L. Ekiel-Jeżewska, and E. Wajnryb, J. Chem. Phys. **111**, 3265 (1999).

Correction

Table I should read

Table 1: Positions and parameters of the stable stationary configurations shown in Fig.1.

	α^*	β	δ	γ	δ/γ	δ/γ^3
A	2.5	0.160...	0.075	0.1	0.75	75
B	1.2	0.45	0.5	0.5	1	4
C	12.4	1.12...	0.5	0.51	0.980...	3.76...
D	3	0.360...	0.5	0.54	0.925...	3.17...
E	1.03	0.930...	1.1	0.6	1.83...	5.09...
F	2.5	0.212...	0.72	0.75	0.960...	1.70...
G	1.24... 4.13...	0.125	0.875	0.885	0.988...	1.26...
H	2.33...	0.00997...	0.986	0.988	0.997...	1.02...

"Cases E & F give examples" should be "Case E gives an example".

Stable Configurations Of Charged Sedimenting Particles: Supplemental Material

C I Trombley & M L Ekiel-Jeżewska
Institute of Fundamental Technological Research,
Polish Academy of Sciences,
Pawińskiego 5b, 02-106 Warsaw, Poland

1 Searching For Feasible Stable Stationary States When Particle 2 Is Not More Dense Than The Surrounding Fluid

In the text we assumed that the reduced mass m_2 of particle 2 was greater than zero - i.e. particle 2 was more dense than the fluid. In this section, we will examine the dynamics for $m_2 \leq 0$. When particle 2 is not more dense than the fluid, the normalization scheme used in the text is not applicable because the characteristic velocity scale must be positive and finite. We now will consider four remaining cases: Case 1 $m_2 \leq 0$ & $m_1 < 0$, Case 2 $m_2 < 0$ & $m_1 \geq 0$, Case 3 $m_2 = 0$ & $m_1 > 0$ and Case 4 $m_1 = m_2 = 0$.

Table 1: We summarize our results in this table. First we show whether there exist feasible stable stationary state. Next, we give where to find a proof.

		m_2		
		<0	$=0$	>0
m_1	<0	Yes: Case 1	No: Case 1	No: Main Text
	$=0$	No: Case 2	No: Case 4	No: Main Text
	>0	No: Case 2	No: Case 3	Yes: Main Text

Case 1: $m_2 \leq 0$ & $m_1 < 0$

We choose our new characteristic velocity as follows:

$$V' = -\frac{m_1 g}{6\pi\mu L} \tag{S.1}$$

And choose our non-dimensional parameters to be

$$\gamma' = \frac{a_2}{a_1} \tag{S.2}$$

$$\delta' = \frac{m_2}{m_1} \tag{S.3}$$

$$\beta' = \frac{kq_1q_2}{L^2 m_1 g} \tag{S.4}$$

This makes the dynamics of the system evolve according to the non-dimensional ordinary differential equation

$$\begin{aligned}\dot{\boldsymbol{\alpha}} &= \frac{3}{2|\boldsymbol{\alpha}|^3}\beta' \boldsymbol{\mathcal{G}}\cdot\boldsymbol{\alpha} + \frac{3}{4}(1-\delta')\,\boldsymbol{\mathcal{G}}\cdot\hat{\mathbf{z}} - \beta'\frac{(1+\gamma')^2}{\gamma'|\boldsymbol{\alpha}|^3}\boldsymbol{\alpha} \\ &- \frac{(\gamma'-\delta')(1+\gamma')}{\gamma'}\hat{\mathbf{z}}\end{aligned} \tag{S.5}$$

This equation is formally the same as the original equation (9), so the analysis can be repeated in exactly the same way as in the text with the appropriate reinterpretation of parameters. In particular, there exist feasible stable stationary state with the conditions analogous to those in the main text.

We can derive $\beta' > 0$ & $\delta' > 0$ as necessary conditions for stability as in the main text. This rules out feasible stable stationary states when $m_2 = 0$ & $m_1 < 0$. There can exist feasible stable stationary states when $m_2 < 0$ & $m_1 < 0$ and the charges are opposite in sign. In fact, there is a one-to-one correspondence between the feasible stable stationary states in the $m_2 < 0$ & $m_1 < 0$ case and those that exist in the main text - i.e. in the $m_2 > 0$ & $m_1 > 0$ case. In both cases, particle 2 is "above" particle 1 with respect to the sum of gravitational and buoyancy force.

Case 2: $m_2 < 0$ & $m_1 \geq 0$

If particle 2 is less dense than the fluid and particle 1 not less dense - then there again needs to be a change of parameters. We choose our new characteristic velocity and characteristic force ratio:

$$V'' = -\frac{m_2 g}{6\pi\mu L} \tag{S.6}$$

$$\beta'' = \frac{kq_1q_2}{L^2 m_2 g} \tag{S.7}$$

And choose the other parameters as before. We now get

$$\begin{aligned}\dot{\boldsymbol{\alpha}} &= \frac{3}{2|\boldsymbol{\alpha}|^3}\beta''\,\boldsymbol{\mathcal{G}}\cdot\boldsymbol{\alpha} - \frac{3}{4}(1-\delta)\,\boldsymbol{\mathcal{G}}\cdot\hat{\mathbf{z}} - \beta''\frac{(1+\gamma)^2}{\gamma|\boldsymbol{\alpha}|^3}\boldsymbol{\alpha} \\ &+ \frac{(\gamma-\delta)(1+\gamma)}{\gamma}\hat{\mathbf{z}} \end{aligned} \tag{S.8}$$

The stability conditions for this differential equation can be worked out as in the main text. It will now be shown that there is no feasible stable stationary state in this case. This will be a proof by contradiction. We start by finding the conditions analogous to equation and inequalities (14) - (17) for our new equation. The new dynamics will be of the form

$$\dot{\epsilon} = G(\alpha)\epsilon \tag{S.9}$$
$$\dot{\alpha} = F(\alpha) \tag{S.10}$$

where G is analogous to g in (12) and F is analogous to f in (13). Explicitly:

$$G(\alpha) = \frac{12\gamma\beta'' - 4(1+\gamma)^2\beta''\alpha - 3\gamma(1-\delta)\alpha^2}{4\gamma\alpha^4} \tag{S.11}$$
$$F(\alpha) = \frac{6\gamma\beta'' - 2(1+\gamma)^2\beta''\alpha - 3\gamma(1-\delta)\alpha^2 + 2(\gamma-\delta)(1+\gamma)\alpha^3}{2\gamma\alpha^3} \tag{S.12}$$

Just as before, the necessary and sufficient conditions for a feasible vertical asymptotically stable stationary state are

$$F(\alpha^*) = 0 \tag{S.13}$$
$$G(\alpha^*) < 0 \tag{S.14}$$
$$F'(\alpha^*) < 0 \tag{S.15}$$
$$1 < \alpha^* \tag{S.16}$$

The first task is showing that if such an α^* obtains, then $\beta'' > 0$. Exactly as (18) in the main text, we get

$$\frac{3\beta''}{\alpha^{*3}} = 3F(\alpha^*) - \alpha^*(2G(\alpha^*) + F'(\alpha^*)) > 0 \tag{S.17}$$

Where the last inequality comes from combining all four conditions (S.13) - (S.16). By (S.16), this entails $\beta'' > 0$.

Next we partition equation (S.13) into $0 = 2\gamma\alpha^{*3}F(\alpha^*) = \frac{2}{3}\gamma\alpha^{*4}F'(\alpha^*) + r_1(\alpha^*) + r_2(\alpha^*)$ where $r_1(\alpha^*) = -\gamma(1-\delta)\alpha^{*2}$ and $r_2(\alpha^*) = -\frac{2}{3}\beta''(2(1+\gamma)^2\alpha^* - 9\gamma)$. Notice that, since $\gamma > 0$ and $\delta < 0$, $r_1 < 0$. This and (S.15) imply $r_2 > 0$, therefore

$$\alpha^* < \frac{9}{2}\frac{\gamma}{(1+\gamma)^2} < \frac{9}{8} \tag{S.18}$$

This also gives us a bound on γ

$$\frac{1}{2} < \gamma < 2 \tag{S.19}$$

We will now derive a bound on $1-\delta$ and show that the bound cannot be satisfied if $\delta \leq 0$. Let $A = \frac{\gamma}{(1+\gamma)^2}$ and $B = \frac{\gamma}{1+\gamma}$. The above bounds then entail $\frac{2}{9} < A < \frac{1}{4}$ and $\frac{1}{3} < B < \frac{230}{3}$. To eliminate β'', we rewrite (S.13) as $2\beta''(\alpha^* - 3A)(1+\gamma) = 2\alpha^{*2}\big[(1-\delta)(\alpha^* - \frac{3}{2}B) + (\gamma-1)\alpha^*\big]$ Notice that $(\alpha^* - 3A) > 0$. Therefore, inequality (S.15) becomes $\alpha^*\big[(1-\delta)(\alpha^* - \frac{3}{2}B) + (\gamma - 1)\alpha^*\big] > 3(\alpha^* - 3A)\big[(1-\delta)(\alpha^* - B) + (\gamma-1)\alpha^*\big]$ Collecting the $1-\delta$ terms on one side gives

$$-2(\gamma-1)\alpha^*(\alpha^* - \frac{9}{2}A) > (1-\delta)\big[3(\alpha^* - B)(\alpha^* - 3A) - (\alpha^* - \frac{3}{2}B)\alpha^*\big] \tag{S.20}$$

The term in the square brackets on the RHS is an increasing function of α^* in the relevant range. Therefore, the term in the square brackets is lower bounded by its value at $\alpha^* = 1$, i.e. $3(1-B)(1-3A) - (1 - \frac{3}{2}B)$. This can be seen numerically to be positive over the relevant range. Since the RHS of (S.20) is positive, the LHS must also be positive. By (S.18), $-2(\alpha^* - \frac{9}{2}A) > 0$. Combining this with (S.20) gives $\gamma > 1$. Further, the term inside of the square brackets of (S.20) is positive, so we can get a function of γ and α^* which bounds $1-\delta$

$$1 - \delta < \frac{-2(\gamma-1)\alpha^*(\alpha^* - \frac{9}{2}A)}{3(\alpha^* - B)(\alpha^* - 3A) - (\alpha^* - \frac{3}{2}B)\alpha^*} \tag{S.21}$$

We will examine this bound by first showing the RHS is a decreasing function of α^* in the relevant range. The derivative of the numerator is $-2(\gamma-1)(2\alpha^* - \frac{9}{2}A)$, which is negative. The derivative of the denominator is $4\alpha^* - 9A - \frac{3}{2}B$, which is positive. Putting these together in the usual quotient rule - along with the already established fact that the numerator and denouement are positive - one sees that the whole derivative is negative. Therefore the right hand side is upper bounded by its value at $\alpha^* = 1$, giving a bound on $1-\delta$

$$1 - \delta < \frac{-2(\gamma-1)(1 - \frac{9}{2}A)}{3(1-B)(1-3A) - (1 - \frac{3}{2}B)} \tag{S.22}$$

Numerically, the RHS has a maximum less than one, contradicting the claim that $\delta < 0$. Therefore, there is no feasible stable stationary state in this case.

Case 3: $m_2 = 0$ & $m_1 > 0$

We choose as a new characteristic velocity & characteristic force ratio

$$V''' = \frac{m_1 g}{6\pi\mu L} \tag{S.23}$$

$$\beta''' = -\frac{kq_1q_2}{L^2 m_1 g} \tag{S.24}$$

These choices give as a nondimensional dynamic equation

$$\begin{aligned}\dot{\boldsymbol{\alpha}} &= \frac{3}{2|\boldsymbol{\alpha}|^3}\beta'''\,\boldsymbol{\mathcal{G}}\cdot\boldsymbol{\alpha} - \frac{3}{4}\,\boldsymbol{\mathcal{G}}\cdot\hat{\mathbf{z}} - \beta'''\frac{(1+\gamma')^2}{\gamma'|\boldsymbol{\alpha}|^3}\boldsymbol{\alpha} \\ &+ (1+\gamma')\hat{\mathbf{z}}\end{aligned} \tag{S.25}$$

This equation is the same as (S.8) with $\delta \to 0$, $\beta'' \to \beta'''$ and $\gamma \to \gamma'$. Therefore there is no feasible vertical stable stationary state in this case.

Case 4: $m_2 = m_1 = 0$

If both particles are neutrally buoyant we have as a dimensional dynamic equation

$$\dot{\mathbf{d}} = \frac{1}{8\pi\mu}\left(-\frac{2kq_1q_2}{|\mathbf{d}|^3}\,\boldsymbol{G}\cdot\mathbf{d}\right) - \frac{1}{6\pi\mu}\left(-\frac{kq_1q_2}{|\mathbf{d}|^3}(\frac{1}{a_1}+\frac{1}{a_2})\mathbf{d}\right)$$

Owing to the rotational symmetry of this system, there is clearly no feasible stable stationary state in this case.

2 Necessity And Sufficiency Of Stability Conditions

We now examine formally the local stability conditions for a class of systems that evolve according to equation (9). We will show that (14) - (16) are necessary and sufficient conditions for the stability of equilibria of the form $\boldsymbol{\alpha}^* = \alpha^*\hat{z}$. We denote the relative position of the particles by $\boldsymbol{\alpha} = \alpha_z\hat{\boldsymbol{z}} + \epsilon\hat{\boldsymbol{x}}$. We assume that $\epsilon \ll 1$ so that third and higher order terms in ϵ of (9) are neglected. In this approximation the dynamics are

$$\dot{\alpha}_z = f(\alpha_z) - \epsilon^2 r(\alpha_z) \tag{S.26}$$

$$\dot{\epsilon} = g(\alpha_z)\epsilon \tag{S.27}$$

where the algebraic form of f and g are given in equations (13) & (12) and the forms of r is

$$r(\alpha_z) \quad = \quad \frac{6\beta}{\alpha_z^5} - \frac{3\beta(1+\gamma)^2}{2\gamma\alpha_z^4} + \frac{3(1-\delta)}{2\alpha_z^3} \tag{S.28}$$

The dynamic equations (S.26) & (S.27) are valid for $\epsilon \ll 1$ and any α_z. However, it will become necessary to assume $|\alpha_z - \alpha^*| \ll 1$ to complete the proof. It is important to notice that if $\alpha_z > 0$, then $f(\alpha_z)$ is continuously differentiable and g is continuous in an open neighborhood of a steady state $\boldsymbol{\alpha}^*$.

That equation (14) and inequalities (15) & (16) are necessary for an stable steady state $\boldsymbol{\alpha}^*$ is clear. If equation (14) does not hold, the system isn't even in a steady state. We now move on to the inequalities. Use the fact that, by continuity, if these inequalities hold at $\boldsymbol{\alpha}^*$ then they hold approximately in an open neighborhood of $\boldsymbol{\alpha}^*$. Suppose, for contradiction, one of the inequalities (15) & (16) is violated. If we perturb the system in whichever direction the relevant function is nonnegative, there will not be a restoring force in that direction. This contradicts the claim that the system is stable.

We now check the sufficiency of inequalities (15) and (16). Call a system "locally Lypunov stable" if the so-called Lypunov function V has a root at the given stationary state $\boldsymbol{\alpha}^*$, is positive off of the stationary state and has negative time derivative in an open set around the stationary state. We examine the simple Lypunov function $V(\boldsymbol{\alpha}) = (\boldsymbol{\alpha} - \boldsymbol{\alpha}^*)^2$. This obviously has the desired properties $V(\boldsymbol{\alpha}^*) = 0$ and $V(\boldsymbol{\alpha}) > 0$ if $\boldsymbol{\alpha} \neq \boldsymbol{\alpha}^*$. Taking the non-dimensional time derivative one finds

$$\dot{V}(\boldsymbol{\alpha}) = 2(\alpha_z - \alpha^*)\dot{\alpha_z} + 2\epsilon\dot{\epsilon} \tag{S.29}$$

We will now show that this is negative in an open neighborhood containing $\boldsymbol{\alpha}^*$. We will do so by relating the above equation to the dynamics (S.26) & (S.27). Start with the $\dot{\epsilon}$ term. Combining (S.27) with (S.29), one sees that

$$\dot{V}(\boldsymbol{\alpha}) = 2(\alpha_z - \alpha^*)\dot{\alpha_z} + 2g(\alpha_z)\epsilon^2 \tag{S.30}$$

We now move on to work out the $\dot{\alpha_z}$ term. From (S.26), one finds that (S.30) becomes

$$\dot{V}(\boldsymbol{\alpha}) = 2(\alpha_z - \alpha^*)f(\alpha_z) + 2g(\alpha_z)\epsilon^2 - r(\alpha_z)(\alpha_z - \alpha^*)\epsilon^2 \tag{S.31}$$

Finally we must assume that α_z is approximately α^* so that $(\alpha_z - \alpha^*)\epsilon^2 \approx 0$. Therefore the remainder term $r(\alpha_z)$ disappears and one has

$$\dot{V}(\boldsymbol{\alpha}) = 2(\alpha_z - \alpha^*)f(\alpha_z) + 2g(\alpha_z)\epsilon^2 \tag{S.32}$$

If (15) holds, then the second term is negative. If (14) & (16) holds, then the first term is negative in a neighborhood of α^*. This demonstrates the sufficiency of (14) - (16).

Therefore, (14) - (16) are necessary and sufficient conditions for this system to have a locally asymptotically stable configuration at $\alpha^*\hat{\mathbf{z}}$.

3 Bounds For Ratio Of Particle Radii When The Particles Are In Feasible Stable Stationary States

We will now show that in the $m_1 > 0$ and $m_2 > 0$ case there are stable configurations only if the higher particle 2 is larger in radius than the lower particle 1 - i.e. the ratio of radii $\gamma = \frac{a_1}{a_2} < 1$. This will be a proof by contradiction. We will start by showing that there cannot be a solution when $\gamma = 1$. Following this, we will establish that if $\gamma > 1$ then a feasible, asymptotically stable steady state does not exist.

3.1 Radii Cannot Be Equal

By way of contradiction, assume both $\gamma = 1$ and there exists at least one feasible attractive steady state configuration $\boldsymbol{\alpha}^* = \alpha^* \hat{\boldsymbol{z}}$. We can now write (14) as

$$f(\alpha^*) = (4\alpha^* - 3)((\delta - 1)\alpha^{*2} - 2\beta) = 0. \tag{S.33}$$

The first term cannot be zero because of the feasibility condition (17). By inequality (18), we know that $\beta > 0$. Therefore, $\alpha^{*2} = \frac{2\beta}{\delta - 1}$. Therefore in order for a feasible stable steady state to exist in the $\gamma = 1$ case, one must have $\delta > 1$. Take the derivative of (S.33) to find

$$f'(\alpha^*) = 4((\delta - 1)\alpha^{*2} - 2\beta) + 2(\delta - 1)\alpha^*(4\alpha^* - 3) \tag{S.34}$$

The first term is zero by (S.33) and the second term is positive by $\delta > 1$ & (17). This contradicts inequality (16). Therefore, there cannot be a feasible stable stationary state in this case.

3.2 Upper Particle Cannot Be Smaller Than The Lower One In Feasible Stable Steady State

We move on to the $\gamma > 1$ case. We will use proof by contradiction, supposing that we have a set α^*, β, δ, γ where $\gamma > 1$ and conditions (14) - (17) obtain. Recall that β and δ must both be positive by inequalities (18) & (19). We will start the demonstration by showing that $\gamma > 1$ implies that $\delta > 1$. Then we will show that conditions (14) and (15) combine in a way that contradict condition (17).

We start by taking advantage of the fact that, by equation (14) and inequalities (15) (17), $f(\alpha^*) - \alpha^* g(\alpha^*) > 0$. Simplifying, we find

$$(1 - \delta)(3\gamma - 4\alpha^*(1 + \gamma)) - 4\alpha^*(\gamma^2 - 1) > 0 \tag{S.35}$$

Because of condition (17), $3\gamma - 4\alpha^*(1 + \gamma) < 0$. Further, if $\gamma > 1$, then $\gamma^2 > 1$ so the second term is negative. Therefore, in order for the above relation to hold, $\delta > 1$.

Now that we have $\delta > 1$, we aim toward eliminating β by writing (14) as

$$-2\beta(1+\gamma)^2(\alpha^* - \frac{3\gamma}{(1+\gamma)^2}) = \Big(2(\gamma-\delta)(1+\gamma)\alpha^* + 3\gamma(\delta-1)\Big)\alpha^{*2} \quad \text{(S.36)}$$

The left hand side is negative, therefore the right hand side must be negative, in other words

$$(\gamma-1)\alpha^* < (\delta-1)(\alpha^* - \frac{3}{2}\frac{\gamma}{1+\gamma}) \quad \text{(S.37)}$$

Because $\gamma > 1$, the left hand side is positive. Therefore, $\alpha^* > \frac{3}{2}\frac{\gamma}{1+\gamma}$. We now use equation (S.36) to eliminate β from (16). This gives that

$$(\delta-1)\left(2\alpha^{*2} - \frac{3\gamma(7+\gamma)}{2(1+\gamma)^2}\alpha^* + \frac{9\gamma^2}{(1+\gamma)^3}\right) < 2(\gamma-1)\alpha^*(\alpha^* - \frac{9\gamma}{2(1+\gamma)^2}) \quad \text{(S.38)}$$

The left hand side must be positive or non positive. Because $\delta > 1$, if the the left hand side in the above inequality is positive, then one can combine the above with (S.37). Simplifying, one finds $\alpha^* < \frac{3\gamma}{(1+\gamma)^2}$ which violates condition (17). Therefore the left hand side must be nonpositive:

$$2\alpha^{*2} - \frac{3\gamma(7+\gamma)}{2(1+\gamma)^2}\alpha^* + \frac{9\gamma^2}{(1+\gamma)^3} \leq 0 \quad \text{(S.39)}$$

Notice that if α^* is very large then the polynomial in (S.39) is positive and, speaking formally, if $\alpha^* = 0$ it is also positive. Therefore the above can only be negative for $\alpha^* > 1$ if the polynomial has two distinct positive real roots. We now look at the discriminant, which must be positive for the roots to be real and distinct

$$0 < \Delta = \frac{9\gamma^2(\gamma-1)(\gamma-17)}{4(1+\gamma)^4} \quad \text{(S.40)}$$

We therefore have $\gamma > 17$. Further, notice that the only negative term in (S.39) is the middle term. Therefore, we have

$$\alpha^{*2} + \frac{9\gamma^2}{2(1+\gamma)^3} \leq \frac{3\gamma(7+\gamma)}{4(1+\gamma)^2}\alpha^* \quad \text{(S.41)}$$

$$\alpha^* < \frac{3\gamma(7+\gamma)}{4(1+\gamma)^2} \quad \text{(S.42)}$$

But right hand side in (S.42) is less than 1 for all $\gamma > 17$. This is a contradiction to condition (17). Therefore conditions (14) & (16) and condition (17) cannot be simultaneously satisfied if $\gamma > 1$. Thus we have $\gamma \leq 1$.

3.3 Conclusion

We have established $\gamma \neq 1$ and that $\gamma \leq 1$. This establishes that $\gamma < 1$, that the upper particle in the feasible stable steady state must have a larger radius than the lower particle.

Journal of Physics Communications

Relative trajectories of two charged sedimenting particles in a Stokes flow

To cite this article before publication: Chris I Trombley *et al* 2021 *J. Phys. Commun.* in press https://doi.org/10.1088/2399-6528/ac060c

Relative Trajectories Of Two Charged Sedimenting Particles In A Stokes Flow

Chris I. Trombley, Maria L. Ekiel-Jeżewska‡

Institute of Fundamental Technological Research, Polish Academy of Sciences, Pawińskiego 5b, 02-106 Warsaw, Poland

Abstract. We study the dynamics of two charged point particles settling in a Stokes flow. We find what ranges of initial relative positions and what ranges of system parameters lead to formation of stable doublets. The system is parameterized by the ratio of radii, ratio of masses and the ratio of electrostatic to gravitational force. We focus on opposite charges. We find a new class of stationary states with the line of the particle centers inclined with respect to gravity and demonstrate that they are always locally asymptotically stable. Stability properties of stationary states with the vertical line of the particle centers are also discussed. We find examples of systems with multiple stable stationary states. We show that the basin of attraction for each stable stationary state has infinite measure, so that particles can capture one another even when they are very distant, and even if their charge is very small. This behavior is qualitatively different from the uncharged case where there only exists a bounded set of periodic relative trajectories. We determine the range of ratios of Stokes velocities and ratio masses which give rise to non-overlapping stable stationary states (given the appropriate ratio of electrostatic to gravitational force). For non-overlapping stable inclined or vertical stationary states the larger particle is always above the smaller particle. The non-overlapping stable inclined stationary states exist only if the larger particle has greater Stokes velocity, but there are non-overlapping stable vertical stationary states where the larger particle has higher or lower Stokes velocity.

‡ Email: mekiel@ippt.pan.pl

1. Introduction

Motion of particles in a Stokes flow, such as sedimentation, [1–3] has applications including medical technology [4–6], microfluidics [7–11], swimming of microorganisms [12–14], deformation of vesicles [15], waste water treatment [16], marine snow [17], mantle plums [18] and motion within volcanic magma [19, 20]. There are many introductions to the physics of Stokes flows, introduced in [21], such as [22–30] and the included references.

There has recently been interest in bound states of particles in viscous flows. For example, formation of doublets and other bound states of particles in viscous flows have been explored for drops [31], pairs of magnetically active rollers near a repelling wall [32] and for pairs of identical rigid spheres in a background flow with walls [33]. There are also results about large scale spontaneous self-organization into ordered structures with many drops [34] or many rollers [35].

There is also a rich literature in bound states of sedimenting particles. A fundamental problem for the motion of a group of particles close to each other is understanding whether they stay together for a long time or disperse and what are the physical mechanisms responsible for keeping them together, see [36–45]. To make the notion of capturing precise, we define a capturing state of two particles as a configuration whose relative trajectories do not go to infinity in future time. The capturing set is then the set of all capturing states.

In [46] it is shown that there can exist a capturing set of a finite non-zero measure for two uncharged spherical particles of different radii and different masses settling under gravity in a Stokes flow. This set consists of neutrally stable periodic orbits. Because of the neutral stability, there are no basins of attraction, so that even a small perturbation can have a destabilizing effect. Further, because the capturing set has finite measure, if particles begin very distantly they come closer to each other but later move away, and are not trapped. This structure of the capturing set is often used to predict that trajectories of two captured particles are likely to be disturbed by the presence of other particles in a suspension, and therefore capture will probably have no significant effect on the dynamics of sedimenting suspensions e.g. [47–50].

In this paper we study pairs of charged sedimenting particles, in order to see if the charge can create large basins of attraction for bound states. Our interest in electrostatic forces originates from the simple observation that systems of charged particles settling in viscous fluids are common, and therefore stable doublets of charged particles could be potentially used in many practical applications. In a vacuum, electrostatic interactions are destabilizing. This fact is known as Earnshaw's Theorem. However, in [51] it was shown that even a very small charge can stabilize pairs of sedimenting particles; two charged spherical particles of different radii and different masses settling under gravity in a Stokes flow can have locally asymptotically stable stationary states with particle centers in line with gravity.

The stability result in [51] is local. To understand the practical significance of this

local result, in this paper we will investigate how two charged point particles sedimenting in a Stokes flow can capture one another, depending on the characteristic parameters of the system: the ratios of the particle radii and masses. We will determine the regions in the phase space of these parameters where stable stationary states of a given interparticle distance can exist. We will determine the capturing set and its structure. We will also find a new class of stable stationary states with particle centers inclined with respect to gravity. We will show that the capturing set of a stable stationary state for two charged point particles settling in a Stokes flow is infinite in measure and consists of one or several basins of attraction to a stable stationary state. These findings open the path toward future experimental observation of these stable doublets. Such doublets could have relevance in dilute charged suspensions [52], for particles in flows at non-zero Reynolds number [53–55] and in plasma [56].

We start our investigation with the mathematical model of point-like particles in section 2. We examine the benchmark case of uncharged pairs of sedimenting point particles (as in [46]) in section 3. In section 4 we present the stability conditions by looking at the linearized dynamics near three kinds of stationary states: centers of particles aligned with gravity with larger particle up, centers of particles aligned with gravity with larger particle down and stationary states where centers of particles are inclined with respect to gravity. In section 5 we discuss generic examples of the relative motion. The vector field of the particle relative velocities and relative trajectories determined numerically on a grid of initial conditions for the case when the larger particle has a greater Stokes velocity. We find the capturing set in physical space of the relative positions using the Poincare-Bendixson theorem. The other case - when the smaller particle has a greater Stokes velocity - is examined in section 6. In section 7 we give the phase diagram for non-overlapping stable stationary states in terms of the ratio of Stokes velocities and ratio of particle radii. We conclude with a summary of our results.

2. Mathematical & Physical Model

We investigate the dynamics of pairs of charged spherical particles of different radii and masses settling under gravity in a viscous fluid, in the range of the Reynolds number much smaller than unity. A schematic of the system is shown in figure 1. Our goal is to construct the simplest possible analytical model. Therefore, we assume that the particles are point-like and use Coulomb force to model their electrostatic interactions. We also use the point-like model to describe the hydrodynamic interactions. It means that the two-particle mutual mobility is given by the Oseen tensor [26], taken at the relative position of the particles, and self-mobility follows from the Stokes law. The hydrodynamic point-like model is valid when the particles are distant. Further, the electrostatic point-like Coulomb force does not describe effects of, e.g., anisotropic distribution of mobile charges on the particle surface, nor electrostatic screening. Therefore, our approach is an approximation.

The particle pair is labeled so that radius a_1 of particle 1 is greater than or equal to the radius a_2 of particle 2. Via the Stokes equations, we will arrive at equations of motion in terms of the electrostatic and gravitational forces. These are then non-dimensionalized, parameterized and expressed in terms of coordinates.

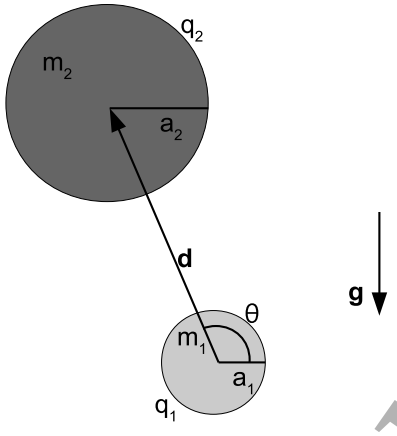

Figure 1: A representation of the geometry of two charged particles with different reduced masses m_1 & m_2 and radii a_1 & a_2 settling under gravity in a viscous fluid. The directions of $\mathbf{g}$ & $\mathbf{d}$ are the directions of the gravitational and electrostatic forces respectively. The angle θ of the interparticle position $\mathbf{d}$ from the direction perpendicular to gravity is shown.

2.1. Force Diagram and Dynamics in the Point-Force Approximation

2.1.1. External Forces We start our diagram of forces with gravity. Let $\hat{\mathbf{z}}$ be a unit vector pointing anti-parallel to the constant gravitational field $\boldsymbol{g}$. Further, let m_i be the reduced mass of particle $i = 1, 2$. This means that the particle weight is corrected for the buoyancy force of the fluid. If the fluid has density ρ and the particle has radius a_i and mass M_i, $m_i = M_i - \frac{4}{3}\pi a_i^3 \rho$. The gravitational force on particle i is

$$\mathbf{f}_{m,i} = -m_i g \hat{\mathbf{z}} \tag{1}$$

In this paper, we will assume that $m_i > 0$. The case of $m_i \leq 0$ can be studied in an analogous way as seen in the supplemental materials of [51]. Now we move on to the electrostatic field. Let $\mathbf{r}_1$ and $\mathbf{r}_2$ be the positions of the centers of particle 1 and 2, so that the relative position is

$$\mathbf{d} = \mathbf{r}_2 - \mathbf{r}_1 \tag{2}$$

We now move on to the electrostatic forces. We denote the charge on particle i by q_i. Then the Coulomb electrostatic force which acts on particle i is

$$\mathbf{f}_{q,i} = (-1)^i k q_i q_j \frac{\mathbf{d}}{|\mathbf{d}|^3} \tag{3}$$

where k is Coulomb's constant and $j = 3 - i$. The sum of the external forces acting on particle i is

$$\mathbf{f}_i = \mathbf{f}_{m,i} + \mathbf{f}_{q,i}. \tag{4}$$

2.1.2. Fluid Forces And Point Force Dynamics We now move on to discuss the fluid forces. We assume that the particles are suspended in an infinite fluid with viscosity μ. We assume that Brownian motion, fluid compressibility and inertia are irrelevant and we describe the fluid flow by the Stokes equations.

$$\mu\nabla^2\mathbf{u} - \nabla p = 0 \tag{5}$$

$$\nabla \cdot \mathbf{u} = 0 \tag{6}$$

where p is the pressure and $\mathbf{u}$ is the velocity field of a fluid [22, 23]. Physically, modeling fluid interactions by equations (5) & (6) entails that the external forces on the particles in a Stokes fluid are in balance with the resistance forces exerted on the particles by the fluid so that inertia may be neglected.

In the point particle approximation, the hydrodynamic interactions between the particles are described by a linear dependence of the particle velocities $\dot{\mathbf{r}}_i$ on the external forces $\mathbf{f}_j$ acting on them. The mutual interaction is determined by the Oseen Tensor [26]

$$\mathbf{G}(\mathbf{d}) = \frac{1}{|\mathbf{d}|}(\mathbf{I} + \frac{\mathbf{d} \otimes \mathbf{d}}{|\mathbf{d}|^2}) \tag{7}$$

where $|\mathbf{d}|$ is the length of the vector $\mathbf{d}$, $\mathbf{I}$ is the identity tensor and $\otimes$ is the tensor product. We assume the self-interaction is determined by the Stokes Velocity for the particle given by the external forces the particle is experiencing. To sum up, our dynamic equation will be of the form

$$\dot{\mathbf{r}}_i = \frac{1}{8\pi\mu}\mathbf{G}(\mathbf{d}) \cdot \mathbf{f}_j + \frac{1}{6\pi\mu a_i}\mathbf{f}_i \tag{8}$$

where $j = 3 - i$. Notice the above dynamics are first order, which means that the velocities of the particles are given by their positions. This is the mathematical expression of the irrelevance of inertia.

2.2. Characteristic Dimensions

In order to aid our analysis we will choose characteristic dimensions. In particular, we choose

$$L = a_1 + a_2, \tag{9}$$

$$V = \frac{m_2 g}{6\pi\mu L} \tag{10}$$

as our characteristic length and velocity scale. The time scale is therefore $T = L/V$. We will use the non-dimensional separation vector

$$\boldsymbol{\alpha} = \frac{\boldsymbol{d}}{L} \tag{11}$$

and the time normalized by T to nondimensionalize (8). We further define three independent non-dimensional numbers

$$\beta = -\frac{kq_1q_2}{L^2m_2g} \tag{12}$$

$$\gamma = \frac{a_1}{a_2}, \tag{13}$$

$$\delta = \frac{m_1}{m_2} \tag{14}$$

which parameterize our equation of motion. One can see that β is the ratio of characteristic electrostatic force to characteristic gravitational force, γ is the ratio of particle radii and δ is the ratio of reduced particle masses. Our assumption that $m_i > 0$ entails that $\delta > 0$ and our labeling convention entails $\gamma \leq 1$. An important physical parameter is also the ratio δ/γ of the particle Stokes velocities.

2.3. Dimensionless Equations Of Motion And Their Basic Properties

Having set up our diagram of forces and nondimensionalization choices, starting from the point-force model (8) we arrive at the following non-dimensional dynamical equation [51]

$$\dot{\boldsymbol{\alpha}} = \frac{3}{2\alpha^3}\beta\,\boldsymbol{\mathcal{G}}\cdot\boldsymbol{\alpha} - \beta\frac{(1+\gamma)^2}{\gamma\alpha^3}\boldsymbol{\alpha} + \frac{3}{4}(1-\delta)\,\boldsymbol{\mathcal{G}}\cdot\hat{\mathbf{z}} - \frac{(\gamma-\delta)(1+\gamma)}{\gamma}\hat{\mathbf{z}} \tag{15}$$

where dot denotes the non-dimensional time derivative, $\alpha = |\boldsymbol{\alpha}|$ and $\boldsymbol{\mathcal{G}}$ is the non-dimensional Green tensor given by

$$\boldsymbol{\mathcal{G}}(\boldsymbol{\alpha}) = \frac{1}{\alpha}(\mathbf{I} + \frac{\boldsymbol{\alpha}\otimes\boldsymbol{\alpha}}{\alpha^2}) \tag{16}$$

It is helpful to write equation (15) in terms of coordinates of $\boldsymbol{\alpha}$. To give a convenient geometry to work in, we will choose x and y axes of the coordinate system so that the particle centers are in the plane $y=0$ (the direction of gravity has been already chosen along the z axis). Any orbit with an initial condition in this plane will never experience a force pointing out of this plane, so we will suppress the y-coordinate for the rest of the paper. Using these conventions, equation (15) transformed into Cartesian co-ordinates becomes

$$\dot{\alpha}_x = 3\beta\frac{\alpha_x}{\alpha^4} - \beta\frac{(1+\gamma)^2}{\gamma}\frac{\alpha_x}{\alpha^3} + \frac{3(1-\delta)}{4}\frac{\alpha_x\alpha_z}{\alpha^3} \tag{17}$$

$$\dot{\alpha}_z = 3\beta\frac{\alpha_z}{\alpha^4} - \beta\frac{(1+\gamma)^2}{\gamma}\frac{\alpha_z}{\alpha^3} + \frac{3(1-\delta)}{4}\frac{\alpha_x^2+2\alpha_z^2}{\alpha^3} - \frac{(\gamma-\delta)(1+\gamma)}{\gamma} \tag{18}$$

A few words can be said about what writing the dynamics in these coordinates entails. First of all, (17) entails that if the particles begin with their centers vertically aligned there are no forces pushing the particles off vertical. This means that, for instance, there is never a periodic orbit which intersects the z-axis. Looking at the signs, we see that (17) is anti-symmetric in α_x and α_z while (18) is symmetric in α_x. Because the dynamics in this coordinate system are given by analytic functions, the pole and the zeros are always isolated points. Further, away from the pole at the origin

the dynamics are differentiable, so that orbits never intersect. Finally, the stationary states are given when the LHS of (17) & (18) are both zero, which provides limits on the count of stationary states. When examining the dynamics it is useful to also write the equations in polar co-ordinates and θ the angle from the x-axis. We use polar rather than cylindrical coordinates because there are no forces in the y-direction. These defined so that

$$\alpha_x = \alpha\cos(\theta) \tag{19}$$

$$\alpha_z = \alpha\sin(\theta) \tag{20}$$

where $\alpha > 0$. This definition entails that the positive x-axis is the ray such that $\theta = 0$, the positive z-axis is $\theta = \frac{\pi}{2}$, the negative x-axis is $\theta = \pi$ and the negative z-axis is $\theta = \frac{3\pi}{2}$. We could also use $\psi = \frac{\pi}{2} - \theta$, the angle from the z-axis. Applying this definition to equation (15), we derive

$$\dot{\alpha} = \frac{\beta}{\alpha^2}\left(\frac{3}{\alpha} - \frac{(1+\gamma)^2}{\gamma}\right) + \left(\frac{3(1-\delta)}{2\alpha} - \frac{(\gamma-\delta)(1+\gamma)}{\gamma}\right)\sin(\theta) \tag{21}$$

$$\alpha\dot{\theta} = \left(\frac{3(1-\delta)}{4\alpha} - \frac{(\gamma-\delta)(1+\gamma)}{\gamma}\right)\cos(\theta) \tag{22}$$

Writing the dynamics in these coordinates also has a few obvious implications worth making explicit. First of all, the stationary states are given when the LHS of (21) & (22) are both zero. Therefore, equation (22) means that any stationary state must have either $\cos(\theta) = 0$ (i.e., the line of the particle centers must be parallel with gravity) or have radial coordinate α equal to

$$\alpha^\dagger = \frac{3(1-\delta)\gamma}{4(\gamma-\delta)(1+\gamma)} \tag{23}$$

Because $\alpha > 0$, this second option exists only if

$$(1-\delta)(\gamma-\delta) > 0 \tag{24}$$

3. Dynamics Of Uncharged Particles

We begin our enumerative strategy by considering the case when at least one particle is uncharged and there is no electrostatic interactions between them. Our analysis will demonstrate the importance of non-stable stationary states in establishing the qualitative global dynamics as well as allow us to discuss later the limit of $\beta \to 0$. We will also compare the output of this model to the classical results [46].

We start by giving the dynamical equations. If there is at least one uncharged particle, then $\beta = 0$ and the equations of motion (21) & (22) become

$$\dot{\alpha} = \left(\frac{3(1-\delta)}{2\alpha} - \frac{(\gamma-\delta)(1+\gamma)}{\gamma}\right)\sin(\theta) \tag{25}$$

$$\alpha\dot{\theta} = \left(\frac{3(1-\delta)}{4\alpha} - \frac{(\gamma-\delta)(1+\gamma)}{\gamma}\right)\cos(\theta) \tag{26}$$

There are a few trivial cases we will quickly deal with. If $\delta = 1$ then a stationary state only exists if $\gamma = 1$ also. In this case, the particles are totally identical and there is no relative motion no matter where the particles begin. Similarly, if $\delta = \gamma$, either $\delta = \gamma = 1$ as before or no finite separation can be a stationary state. Either way, this would eliminate any interesting behavior such as bounded orbits. Moreover, only if (24) holds can there be stationary α.

Finally we come to the non-trivial cases, those in which the above inequality is satisfied. Solving for the stationary states gives four solutions: two horizontal and two vertical. The vertical cases haves $\theta^* = \frac{\pi}{2}$ or $\frac{3\pi}{2}$ and give

$$\alpha^* = \frac{3(1-\delta)\gamma}{2(\gamma-\delta)(1+\gamma)} \tag{27}$$

The horizontal cases have $\theta^\dagger = 0$ or π and lie at a distance (23) from the origin. A few points can be established about these stationary states just from equations (23) and (27). First we note that $\alpha^* = 2\alpha^\dagger$. Next, if $\delta > 1$, then the right hand side of (27) is an increasing function of γ in our range of $0 < \gamma \leq 1$. Therefore we have that $\alpha^* < 1$ in this case. Stationary states of particles with different radii or different masses can be feasible, i.e., non-overlapping and non-touching, with $\alpha^* > 1$, only if $\delta < \gamma < 1$.

We illustrate these parameter space results in figure 2(a). The solid line is $\delta/\gamma = 1$, when the particles have equal Stokes velocities. The short dashed line is equal reduced masses $\delta = 1$. Below this line and above the solid line stationary states do not exist (region D), while above this line stationary states exist but are infeasible (region E). As we have already shown, there is no stationary states on the solid line and short dashed lines except at $\delta = \gamma = 1$ where every separation is a stationary state.

The dash-dot line is $\alpha^\dagger = 1$, so that above this line but below the solid line (region C) all stationary states are feasible. On the long dashed line is $\alpha^* = 1$, so that above this line but below the dash-dot line (region B) vertical stationary states are feasible but the horizontal ones are not feasible. Below dashed line (region A) all stationary states are not feasible. Properties of the regions are outlined in table 1.

With the locations of the stationary states in mind, we now turn to characterizing the orbits in the large. We can do this by solving exactly a few special cases of the equations of motion. If our initial condition involves $\alpha = \alpha^*$ but θ is non-vertical, then the system evolves along the curve given by

$$\dot{\theta} = -\frac{(\gamma-\delta)^2(1+\gamma)^2}{3\gamma^2(1-\delta)}\cos(\theta) \tag{28}$$

This differential equation has the solution

$$\theta + \frac{\pi}{2} = 2\tan^{-1}\left[k_1 \exp\left(-\frac{(\gamma-\delta)^2(1+\gamma)^2}{3\gamma^2(1-\delta)}t\right)\right] \tag{29}$$

where k_1 is from the initial condition. This solution forms two heteroclinic curves, so designated because each connect two stationary states in infinite time.

Table 1: Properties of stationary states of uncharged particles.

region		do stationary states exist?	are vertical stationary states feasible?	are horizontal stationary states feasible?
(A)	$\frac{\delta}{\gamma} \leq \frac{2\gamma-1}{2-\gamma}$	yes	no	no
(B)	$\frac{2\gamma-1}{2-\gamma} < \frac{\delta}{\gamma} \leq \frac{4\gamma+1}{4+\gamma}$	yes	yes	no
(C)	$\frac{4\gamma+1}{4+\gamma} < \frac{\delta}{\gamma} < 1$	yes	yes	yes
(D)	$1 \leq \frac{\delta}{\gamma} \leq \frac{1}{\gamma}$ and $\gamma \neq 1$	no	N/A	N/A
(E)	$\frac{\delta}{\gamma} > \frac{1}{\gamma}$	yes	no	no

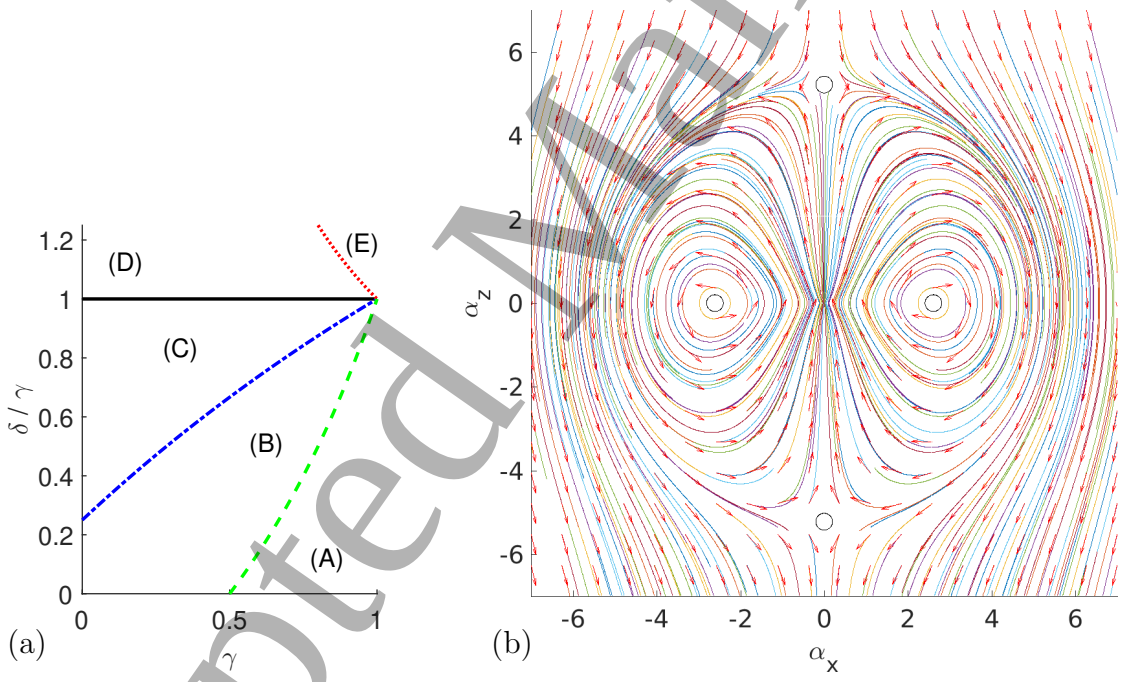

Figure 2: Dynamics of uncharged particles. (a) Phase space of the ratio γ of particle radii and the ratio δ/γ of the particle Stokes velocities, with the indicated regions defined by equations in Table 1. Feasible horizontal and feasible vertical stationary states exist only in region (C). Properties of other regions are given in Table 1. (b) Example of relative trajectories for $\delta = .986$ & $\gamma = .988$. The orbits of the larger particle, labeled 2, are shown in the reference frame of particle 1, located at the origin. The open circles represent not stable stationary states. The colors are used to facilitate tracing streamlines close to each other.

The other pair of heteroclinic curves are vertical, $\theta^* = \frac{\pi}{2}$ or $\frac{3\pi}{2}$. These heteroclinic are symmetric. In this case the equations of motion are

$$\dot{\alpha} = \pm\left(\frac{3(1-\delta)}{2\alpha} - \frac{(\gamma-\delta)(1+\gamma)}{\gamma}\right) \tag{30}$$

These differential equations have the implicit solutions

$$\pm t = k_2 - \frac{\gamma}{(\gamma-\delta)(1+\gamma)}\alpha - \frac{3(1-\delta)\gamma^2}{2(\gamma-\delta)^2(1+\gamma)^2}\ln\left|\alpha - \frac{3(1-\delta)\gamma}{2(\gamma-\delta)(1+\gamma)}\right| \tag{31}$$

where k_2 is from the initial conditions. This form of the solution makes it clear that a particle approaches θ^* in infinite time.

Collectively, the curves sketched out by these four heteroclinic orbits make two half circles. The interior of the curves contain two neutrally stable stationary states at (23). Finally, the two vertical stationary states at (27) are not stable but rather saddle points.

We can now fully characterize the orbit traced out by any initial position. By the Poincare-Bendixson Theorem every point on the interior of those closed heteroclinic curves will move in periodic motion: moving toward a stable fixed point is ruled out by linear stability analysis, the heteroclinics have all been found and wandering to infinity is impossible because they cannot touch the closed curves which initially bound them. Finally, every point not vertical and exterior to the circle with radius α^* will go to infinity, by similar reasoning.

We complete the analysis by returning to figure 2 (a) in order to characterize the qualitative dynamics as a function of the parameters. Regions (A) - (C) & (E) have qualitatively similar dynamics: in all cases there is periodic behavior. Region (D) has no stationary states and therefore all orbits are unbounded. Region (C) has the special property that some of the periodic orbits found are non-overlapping. This case is the most physically interesting and the corresponding relative trajectories are illustrated in figure 2(b). This completes the analysis of the qualitative behavior of uncharged point particles settling in a Stokes flow.

We will now briefly compare the results in this section to those in [46]. This seminal paper uses a precise model of hydrodynamic interactions, allowing for more realistic treatment of finitely sized particles. For reference, figure 2(a) can be compared directly to figure 5 in [46].

The essential similarity between the results of both approaches is that there appear such regions of the phase space γ & δ/γ that all the trajectories are unbounded, and such regions that some of the trajectories are unbounded, but the other ones are bounded. In case of the point-particle model, one should focus on the orbits (or their parts) outside the particle "surface" determined by its radius. For the point-particle model, region (A) and regions (D) and (E) of figure 2(a) contain only unbounded feasible orbits. Regions (D) and (E), where the larger particle moves slower than the smaller one, are the same as the region of unbounded orbits in [46]. Region (A), in which the larger particle moves faster than the smaller one, is smaller than the region of unbounded orbits in [46].

In the region labeled (C) the feasible point-particle orbits are periodic or unbounded. Analogous (but lager) range was also found in [46] for the more

precise hydrodynamic model. In the point-particle region (B) there are feasible unbounded orbits and feasible parts of periodic orbits, bounded owing to the non-overlapping vertical stationary states while the horizontal stationary states responsible for periodicity are overlapping. For the more precise hydrodynamic interactions used in [46], the analogous (but smaller) range exists. However, in this range there are no horizontal stationary states and the bounded orbits are not periodic. Rather, the bounded orbits are heteroclinics going from one vertical stationary state to the other. This comparison suggests that the existence of periodic or bounded orbits is predicted by the point-particle and the more precise hydrodynamic model in a qualitatively similar way when all or at least some of the stationary states are feasible.

4. Linear Stability Analysis Of Pairs Of Charged Sedimenting Particles

We now move on to charged systems of particles. We will find conditions for stationary states and, in order to investigate stability properties, gather information from the dynamics linearized around the stationary states. This information will then be used to understand global dynamics in the next sections.

Following the discussion of equation (22), we have divided all the stationary arrangements into three categories. In the first, the particle centers are aligned vertically and the larger particle is above the smaller particle, i.e. $\theta = \pi/2$ (see figure 1 for illustration). We will call these larger up vertical stationary states. In the second case, the particle centers are also aligned vertically but the larger particle is below the smaller particle, therefore $\theta = 3\pi/2$. We will call this second configurations larger down vertical stationary states. Finally, there are the inclined stationary states where θ takes on any other value.

The conditions for stability of vertical stationary states were found in [51]. Here we add a systematic analysis of vertical stationary states§, both stable and not stable. In this section we also investigate a new class of stationary states: the inclined configurations, focusing on their stability.

4.1. Vertical Larger Up Stationary States

We will first analyze properties of vertical stationary states with the larger particle above the smaller one, i.e. $\theta = \pi/2$. In this case equation (21) becomes

$$\alpha^3\dot{\alpha} = 3\beta - \beta\frac{(1+\gamma)^2}{\gamma}\alpha + \frac{3(1-\delta)}{2}\alpha^2 - \frac{(\gamma-\delta)(1+\gamma)}{\gamma}\alpha^3 \tag{32}$$

This equation gives rise to the following condition (equivalent to (14) in [51]) for a stationary state $\alpha = \alpha^*$ and $\theta = \frac{\pi}{2}$

$$0 = 6\gamma\beta - 2\beta(1+\gamma)^2\alpha^* + 3\gamma(1-\delta)\alpha^{*2} - 2(\gamma-\delta)(1+\gamma)\alpha^{*3} \tag{33}$$

§ Though [51] used Cartesian co-ordinates, the resulting stability conditions of vertical stationary states are of course the same as in polar coordinates.

It follows from this condition that it is possible to choose a β to make any particular α^* stationary. Therefore, there are stationary states that have no analogue with the uncharged case. We will return to the parameter space (γ, δ) behavior of vertical stationary states in a later section. For instance, in the range $1 > \delta > \gamma$, there are no stationary states for uncharged particles, but there are some if a charge is added. We now address linear stability of a stationary state $(\alpha^*, \frac{\pi}{2})$, given by equation (33). If we assume that $\alpha = \alpha^* + \epsilon_r$ and $\theta = \frac{\pi}{2} + \epsilon_\theta$, then the dynamics linear in epsilon are

$$\dot{\epsilon}_r \approx -\frac{1}{\gamma\alpha^{*3}}\big(\beta(1+\gamma)^2 - 3\gamma(1-\delta)\alpha^* + 3(\gamma-\delta)(1+\gamma)\alpha^{*2}\big)\epsilon_r \tag{34}$$

$$\dot{\epsilon}_\theta \approx -\frac{1}{4\gamma\alpha^{*2}}\big(3\gamma(1-\delta) - 4(\gamma-\delta)(1+\gamma)\alpha^*\big)\epsilon_\theta \tag{35}$$

Because the matrix of coefficients is diagonal, the constants within the parentheses must be positive in order for the system to be linearly stable. That is,

$$0 < \beta(1+\gamma)^2 - 3\gamma(1-\delta)\alpha^* + 3(\gamma-\delta)(1+\gamma)\alpha^{*2} \tag{36}$$

$$0 < 3\gamma(1-\delta) - 4(\gamma-\delta)(1+\gamma)\alpha^* \tag{37}$$

It can be shown by Lypunov's method that equation (33) and inequalities (36) & (37) form necessary and sufficient conditions for a stationary stable state.

4.2. Vertical Larger Down Stationary States

We will now discuss the stationary states with the larger particle below the smaller one. Similarly to equation (32), on the ray $\theta = 3\pi/2$, equation (21) becomes

$$\alpha^3\dot{\alpha} = 3\beta - \beta\frac{(1+\gamma)^2}{\gamma}\alpha - \frac{3(1-\delta)}{2}\alpha^2 + \frac{(\gamma-\delta)(1+\gamma)}{\gamma}\alpha^3 \tag{38}$$

This gives rise to the following equations for the stationary state $(\alpha^*, \frac{3\pi}{2})$

$$0 = 6\gamma\beta - 2\beta(1+\gamma)^2\alpha^* - 3\gamma(1-\delta)\alpha^{*2} + 2(\gamma-\delta)(1+\gamma)\alpha^{*3} \tag{39}$$

and for the local dynamics

$$\dot{\epsilon}_r \approx -\frac{1}{\gamma\alpha^{*3}}\big(\beta(1+\gamma)^2 + 3\gamma(1-\delta)\alpha^* - 3(\gamma-\delta)(1+\gamma)\alpha^{*2}\big)\epsilon_r \tag{40}$$

$$\dot{\epsilon}_\theta \approx -\frac{1}{4\gamma\alpha^{*2}}\big[-3\gamma(1-\delta) + 4(\gamma-\delta)(1+\gamma)\alpha^*\big]\epsilon_\theta \tag{41}$$

In order to be linearly stable, the constants within the parentheses must be positive. That is,

$$0 < \beta(1+\gamma)^2 + 3\gamma(1-\delta)\alpha^* - 3(\gamma-\delta)(1+\gamma)\alpha^{*2} \tag{42}$$

$$0 < -3\gamma(1-\delta) + 4(\gamma-\delta)(1+\gamma)\alpha^* \tag{43}$$

We have previously shown in [51] that there are no stable stationary states with the larger particle below the smaller one if we also require the particles do not overlap ($\alpha^* > 1$). However, conditions (42) & (43) will still aid in our understanding of the global dynamics because of the properties of non-stable stationary states.

4.3. Inclined Stationary States

In the previous section, we showed how to count and classify the vertical stationary states of charged particles. We will now show how to do the same for non-vertical stationary states, which have a simpler form, given by equations (21), (22) & (23). This simplicity will allow us also to easily analyze typical behaviors in the parameter space (γ, δ).

We can discuss the stationary states of charged particles using figure 2(a) and relations in Table1. The same parameter space curves and regions are of interest but require new interpretations when conceived as relating to charged inclined stationary states. We start from considering two special cases. The short dashed line in figure 2(a) represents equal reduced masses, $\delta = 1$. Equation (22) entails that there exists an inclined stationary state of charged particles only if further $\delta = \gamma = 1$. Similarly, the solid line, the special case of equal Stokes velocities $\delta/\gamma = 1$, has an inclined stationary state only if further $\delta = 1$. That is to say, those lines are consistent with the existence of an inclined stationary state only on their intersection point. However, the interpretation of that point is different between the uncharged and the charged inclined case. In the uncharged case, all the relative positions of identical particles are stationary, while in the charged case only stationary states of identical particles must have separation distance $\alpha^\dagger = \frac{3\gamma}{(1+\gamma)^2}$ (and an arbitrary orientation). This never feasible distance is the same for all $\beta \neq 0$. Moving on to the general case of unequal Stokes velocities & unequal reduced masses, a general inclined stationary state must have

$$\sin(\theta^\dagger) = \beta \frac{16(\gamma-\delta)(1+\gamma)^2(1+3\delta-3\gamma-\delta\gamma)}{9\gamma^2(1-\delta)^3} \tag{44}$$

$$\alpha^\dagger \quad = \frac{3(1-\delta)\gamma}{4(\gamma-\delta)(1+\gamma)} \tag{45}$$

Equation (45), identical to (23), corresponds to $\dot{\alpha}_\theta = 0$. Therefore, the RHS of (45) cannot be negative, and there are no inclined stationary states of charged particles in the region (D) defined in table1 and shown in figure 2(a). Moreover, the distance between the particles in an inclined stationary state is independent of the charge/mass ratio β. However, unlike the uncharged case, the condition (44) for $\dot{\alpha}_r = 0$ has a nontrivial form that does not allow for stationary states if charges are too large, because the sine of the stationary angle $\theta^\dagger$ is proportional to charge/mass ratio β. In terms of phase diagram as in figure 2(a), equation (45) entails that all and only values of the parameters γ and δ in region (C), given in table 1 have feasible inclined stationary states of charged particles, providing that value of β is sufficiently small to satisfy (44). Horizontal stationary states, generic for the dynamics of uncharged particles, are exceptional for charged systems. One can see from equation (44) that there is a horizontal stationary state with the particle centers aligned perpendicular to gravity (i.e $\sin(\theta) = 0$) if and only if either a) the particles are uncharged ($\beta = 0$) or b) the particles have Stokes velocity ratio given by the relation $\frac{\delta}{\gamma} = \frac{3\gamma-1}{\gamma(3-\gamma)}$ (and they overlap with $\alpha^\dagger = \frac{3\gamma}{(1+\gamma)^2}$). Because the curve traced by this relation is lower than the dash dot line representing the boundary of feasible

inclined stationary states (except at their intersection $\delta = \gamma = 1$) the angular part of an inclined feasible stable stationary is always less than π, which means that the larger particle is higher than the smaller one.

We now analyze the conditions for linear stability of inclined stationary states. Let $\alpha = \alpha^\dagger + \epsilon_r$ and $\theta = \theta^\dagger + \epsilon_\theta$ where ϵ_r and ϵ_θ are first order perturbations. One finds that to a first order

$$\dot{\epsilon}_r \approx -\frac{3\beta}{\alpha^{\dagger 4}}\epsilon_r + \frac{(\gamma-\delta)(1+\gamma)}{\gamma}\cos(\theta^\dagger)\epsilon_\theta \tag{46}$$

$$\dot{\epsilon}_\theta \approx -\frac{(\gamma-\delta)(1+\gamma)}{\alpha^{\dagger 2}\gamma}\cos(\theta^\dagger)\epsilon_r \tag{47}$$

The above linearized dynamics can be easily analyzed. A linear system of ODE with a matrix of constant coefficients is called stable if and only if the real parts of eigenvalues of the matrix are negative. Recall that the determinant is the product of the eigenvalues and the trace is the sum. Therefore, a necessary and sufficient condition for this stationary state to be linearly stable is the determinant to be positive and the trace negative. The determinant

$$\frac{(\gamma-\delta)^2(1+\gamma)^2}{\alpha^{\dagger 2}\gamma^2}\cos^2(\theta^\dagger) \tag{48}$$

is positive if and only if the particles have different Stokes velocities (recall that $\cos(\theta^\dagger) \neq 0$ for inclined stationary states),

$$\frac{\delta}{\gamma} \neq 1 \tag{49}$$

Further, the trace is equal to

$$-\frac{3\beta}{\alpha^{\dagger 4}}, \tag{50}$$

which is negative if and only if

$$\beta > 0 \tag{51}$$

Inequalities (49) & (51) entail that if the charges on the particles are opposed then the stationary states are stable whenever they exist: off of the solid and short dashed line in figure 2(a) and with β small enough that equation (44) has a solution. It is interesting to note that the particles having opposite charges, expressed in the inclined case by inequality (51), is also a necessary condition for a vertical stable steady state [51]. Therefore in the next sections we will focus on systems with oppositely charge particles (i.e. $\beta > 0$).

5. Example Dynamics Of Systems Of Pairs Of Charged Particles

The local information derived in the previous section can be used to find the qualitative behavior of pairs of charged particles sedimenting in a Stokes flow. For instance, as just mentioned, we have shown that the local analysis entails that if there is to be a stable stationary state then the charges on the particles must be opposed. In this section we

show some generic examples of the dynamics of charged sedimenting particle doublets with large capturing sets. It means that starting from a wide range of initial relative positions, both particles and will not separate from each other, and, on the contrary, they will decrease their distance for ever.

We choose four sets of parameters to demonstrate a variety of behaviors with the above capturing property. In this section we will choose parameters with $\beta > 0$ and $\delta/\gamma < 1$, so that the particles have opposite charges and the larger particle has greater Stokes velocity when the particles are well separated. The dynamics for when $\delta/\gamma > 1$ will be discussed in the next section. We organize by the count and arrangement of stable stationary states: one stable vertical stationary state, two stable vertical stationary states, two stable inclined stationary states and finally two stable inclined stationary states with one stable vertical stationary state.

Example orbits solving the nonlinear vector ordinary differential equation (15) are plotted in figure 3. Each orbit describes the relative motion of the larger particle 2 with the origin as the center of the smaller particle 1, and with the given initial relative positions of the larger particle. The orbits were calculated using a fourth order Runga-Kutta method with constant step size $\Delta t = .1$. We have decided to use (α_x,α_z) space in this figure and this section for easy comparison with observations. One can see visually that the basins of attraction in our characteristic cases are large. We have also provided in figure 4 a visual way of demonstrating the local stability (or instability) of vertical stationary states. The solid curves are the vertical velocity $\dot{\alpha}_z$ of particle 2 relative to particle 1 when their line of centers is vertically aligned and the relative vertical position is α_z. On vertical axis, $\dot{\alpha}_z = \dot{\alpha}$ which can be obtained from (32) & (38). When the solid curve goes down through the horizontal dash-dot line (which corresponds to $\dot{\alpha}_z = 0$) when α_z is increased, then separation between the particle centers is a stationary state which is vertically stable as given by inequalities (36) & (42). The two dashed lines capture the angular stability conditions (37) & (43) for the given parameters, separately for $\alpha_z > 0$ and $\alpha_z < 0$. In each of these ranges of α_z, if a stationary state is to the left of a dashed line, then it is horizontally stable. In the following we will demonstrate that using properties of the stationary states we are able to determine basic features of the dynamics and qualitatively describe the boundary of the basin of attraction in all of these generic cases.

5.1. One Vertical Stable Stationary State

We will now apply the results we have derived to find a typical phase portrait of the relative dynamics. As an example, we look at a system with a single stable stationary configuration. We choose the parameters $\delta = 0.986$ & $\gamma = 0.988$ from the region (C) and $\beta = 0.01$ too large for the existence of inclined stationary states. In this case all of the stationary states have particle centers aligned in the direction of gravity. Relative orbits for different initial positions are illustrated in figure 3(a). It seems that there are two generic classes of orbits visible in this figure, a capturing set and a separating set.

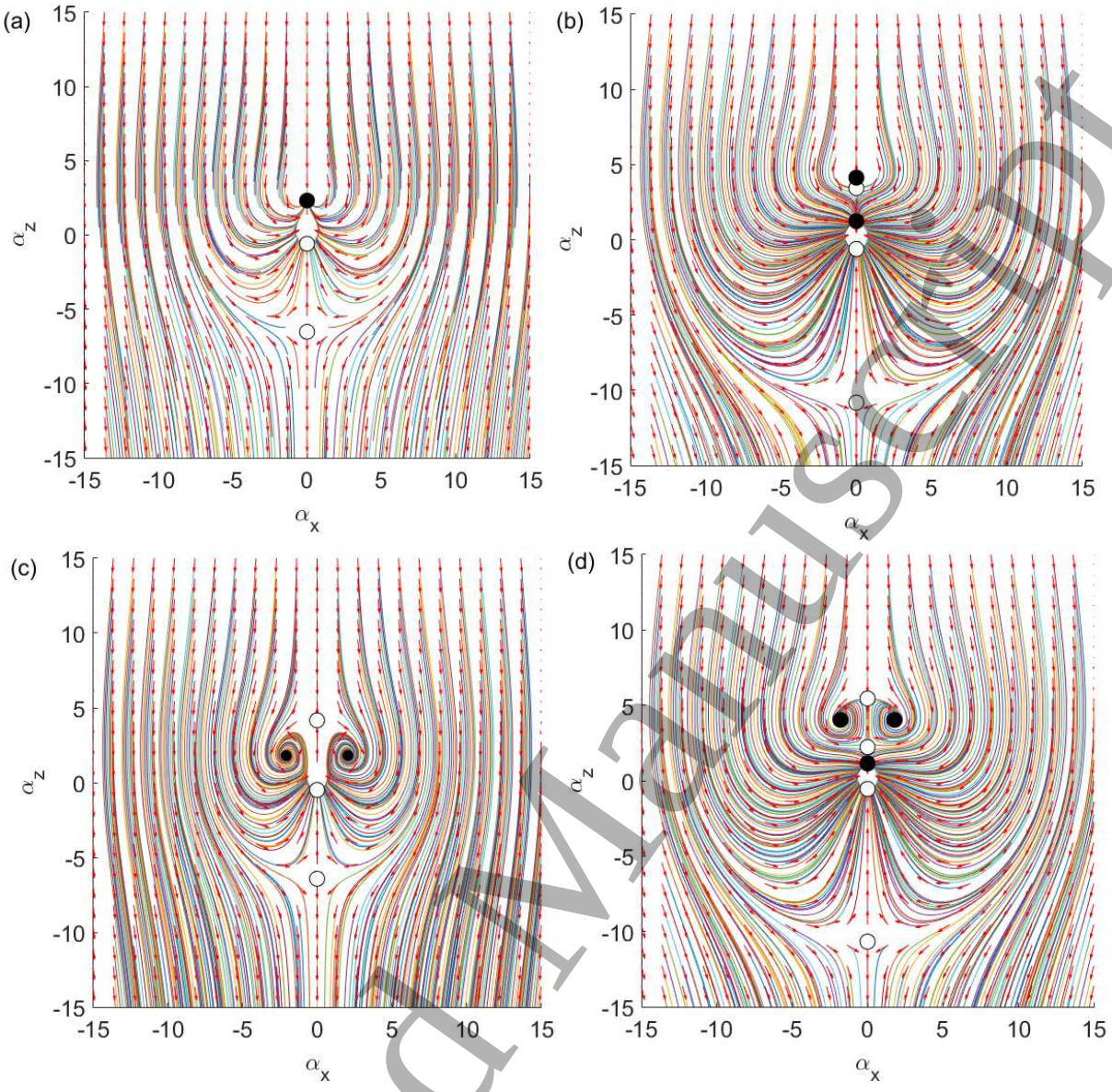

Figure 3: These orbits illustrate the relative motion of the larger particle with the origin defined as the center of the smaller particle. The parameters are (a) $\beta = .01$, $\delta = .986$ & $\gamma = .988$, (b) $\beta = .125$, $\delta = .875$ & $\gamma = .885$, (c) $\beta = 0.22$, $\delta = 0.45$ & $\gamma = 0.5$ and (d) $\beta = .42$, $\delta = .47$ & $\gamma = .5$. The colors are used to facilitate tracing streamlines close to each other.

In the first one, the particle come closer to each other. In the second one, the particles separate from each other. This informal visual analysis can be deduced by classifying the local behavior of the stationary states and examining the behavior of separatrix and other special orbits.

Figure 4(a), which illustrates the behavior of the system when the particle centers are aligned vertically, is helpful for classifying the stationary states. There are three

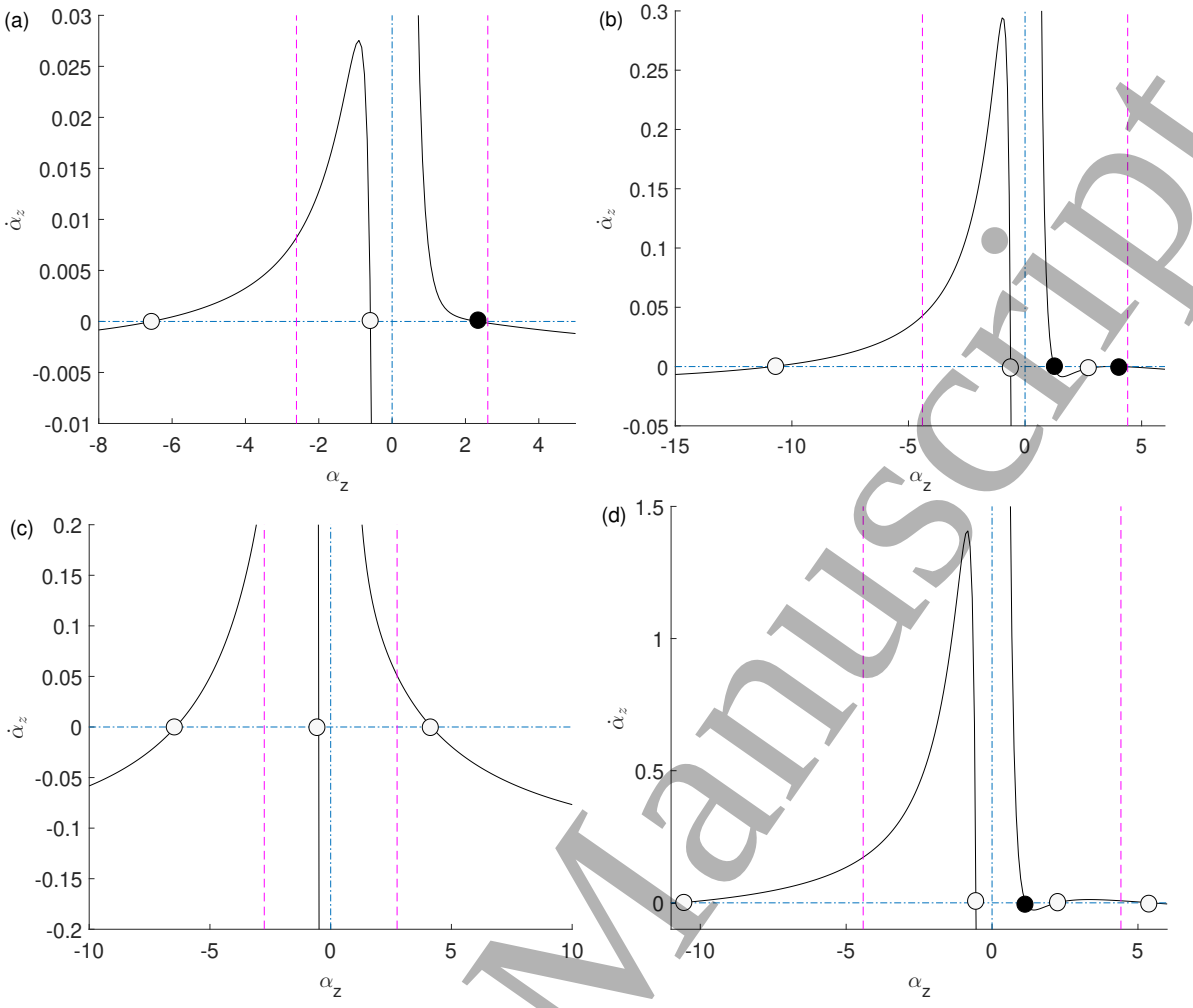

Figure 4: Stability analysis of the vertical stationary configurations shown in figure 3. The dash-dot lines are axes; the horizontal one corresponds to the stationary condition $\dot{\alpha}_z = 0$. The solid curves are the vertical relative velocities $\dot{\alpha}_z = \dot{\alpha}$, evaluated as functions of α_z from (32) & (38). When the solid curve goes down through the horizontal dash-dot line when α_z increases from the stationary position, then that stationary state is vertically stable. In each of the ranges $\alpha_z > 0$ or $\alpha_z < 0$, if a stationary state is to the left of a dashed line, given by (37) or (43), then it is horizontally stable.

stationary states and a discontinuity at the origin. The stationary state with the larger particle directly above the smaller is $\alpha_z = 2.31....$ This is the sole "larger up" stationary state. The stationary states with the larger particle directly below the smaller one are $\alpha_z = -6.56...$ and $\alpha_z = -.588....$ We will call these the "far" and "close" larger down stationary states respectively. We can now classify the stationary states based on their local behavior. Again referring to 4(a), we see the larger up stationary state is stable while the stationary states on the negative z-axis are saddle points. Further, one can see that the far larger down state is stable with respect to horizontal perturbations and unstable with respect to vertical perturbations. Similarly, the close larger down state

is unstable with respect to horizontal perturbations and stable with respect to vertical perturbations. Finally, if we briefly and informally consider the origin by considering a point in a punctured neighborhood of the origin we see that it is unstable in the sense that all arrows sufficiently near the origin lead away from the origin.

Now we supplement the local information by considering some special orbits. To simplify language, we will use "end" to mean the limit in positive infinite time and "begin" to mean the limit in negative infinite time, taking care to only use this language when it makes sense. There are four special orbits which end on the saddle points. Two vertical special orbits end on the close larger down stationary state: one which begins on the origin and one which begins on the far larger down stationary state.

The most important special orbits, however, are the pair which end on the far larger down stationary state. These non-vertical orbits form the separatrix curve of the system. We use "separatrix" informally to mean a curve which separates the plane into two sets where the interior and exterior have different qualitative behavior. It is clear to the eye from figure 3(a) that the separatrix cuts the plane into two sets. In fact, the separation property follows from the local information about saddle stationary states.

The separatrix and its interior form the capturing set of the system. In fact, the topology of the vector field shows us a stronger result: all orbits on separatrix or in its interior must go to a stationary state. We start by considering the off vertical orbits on the interior of the separatrix. Such an orbit cannot go to infinity because the orbit cannot cut the separatrix. The orbit cannot be periodic, as a closed orbit in the plane must have a stationary state in its interior - the Poincare-Bendixson Theorem - and there are no stationary states off the vertical axis. With periodic motion and separation eliminated, we have shown that all non-vertical orbits on the interior of the separatrix go to a stationary state. Mopping up the remaining special orbits, by examining 4(a) we see the vertical orbits on the interior of the separatrix go to the close larger down stationary state or the stable stationary state. Finally, the orbits that make up the separatrix end on the far larger down stationary state by definition. We have now shown that all orbits in the capturing set go to a stationary state. The demonstration that all orbits in the exterior of the separatrix have the particles drift apart is similar.

This is already a powerful qualitative characterization of the orbits. The local information tells us even more than this. In fact, because any state close to the higher larger down stationary state with non-zero horizontal component is repelled, we see that the vertical special orbits that end on the higher larger down stationary state are the only orbits on the interior of the separatrix which end on the higher larger down stationary state at all. Therefore, almost all points on the interior of the separatrix end on the stable stationary state. This includes, for instance, those orbits on the interior of the curve formed by special orbits which begin on the close larger down stationary state and end on the stable stationary state, which appears as a teardrop shape in figure 3(a).

We have now shown the manner in which the local behavior of the stable and not stable stationary states come together to give us the global dynamics by applying some

simple topological reasoning. This completes the description of the qualitative dynamics for this example. We end by again noting that any set of parameters which gives rise to the same structure of stationary states will result in the same qualitative dynamics.

5.2. Two Stable Vertical Stationary States

Similar to the previous example, we can give the global dynamics for when all stationary states are vertical and there are two stable stationary states. As an example of such a system we choose $\beta = .125$, $\delta = .875$ & $\gamma = .885$. Orbits of particle 2, relative to particle 1, in such a system are illustrated in figure 3 (b). One can see that the capturing set is still large in this case.

In figure 4(b), we plot the relative vertical velocity of the system when the particle centers are aligned vertically, find all vertical stationary configurations and determine their stability against vertical and horizontal perturbations. As before, we can reason from the local information about the stationary states to the global dynamics. The larger up stationary states at $\alpha_z = 1.242...$ and $\alpha_z = 4.130...$ are stable. We will call them the near and far stable stationary states, respectively. The stationary state at $\alpha_z = 3.429...$ is a saddle point not stable to vertical perturbations, so we will call it the not stable larger up stationary state. Similarly, the two larger down stationary states at $\alpha_z = -10.829...$ and $\alpha_z = -0.615...$ are saddle points and will be called near and far larger down stationary states, respectively.

We shall soon see that all orbits in the capturing set go to a stationary state and furthermore almost all go to a stable steady state. We do this by examining some important orbits and the curves they trace. Once again, the curve made up of orbits which end on the far larger down stationary state is the separatrix that forms the boundary of the capturing set. One can use the argument from the last section to show the separatrix is unbounded. Another important curve is made of the orbits that end in the not stable larger up stationary state. All points on the interior of this curve go to the far stable stationary state and, more obviously, no point on its exterior goes to the far stable stationary state. This curve is also a separatrix, since it is the boundary between basins of attraction of both stable stationary states. It's easy to see that all the orbits off the vertical go to one of these two stable stationary states. From figure 4(b) it is clear that some vertical orbits go to the far larger up stable stationary state, and others go to the near larger down unstable stationary state. This gives us all the qualitative dynamics for systems with two stable vertical stationary states.

5.3. Inclined Stable Stationary States

We will now examine a characteristic example of dynamics when there are inclined stable stationary states, and they are the only stable stationary states. We choose as our parameters $\beta = 0.22$, $\delta = 0.45$ and $\gamma = 0.5$. This results in a stable stationary state with $\alpha = 2.75...$, $\theta = 0.722...$ and another one symmetric across the z-axis. One can see

by figure 4(c) that these parameters entail there are no vertical stable stationary states. All vertical stationary states are saddle points.

Orbits are illustrated in figure 3(c). Once again, the capturing set is quite large, even though there are no vertical stable stationary states.

We now discuss how the global dynamics is related to the local properties of the stationary states. Once again all orbits in the capturing set go to a stationary state and almost all go to a stable stationary state. However because there are inclined stationary states we must use a new method to show this. Consider pair of orbits that begin on the close larger down saddle point and end on an inclined stable stationary state. These prevent periodic orbits, because any periodic orbit would have to contain an inclined stationary state and therefore cut one of these orbits which is impossible. Further we once more see the boundary of the capturing set is a separatrix coming from infinity and going into the far larger down saddle point. With periodic and unbounded orbits eliminated as possibilities for orbits in the capturing set, the Poincare-Bendixson theorem entails they must all go to some stationary state. The only orbits in the capturing set that do not go to an inclined stationary state are those with initial conditions such that the particle centers are aligned with gravity, which separate the orbits that go to different stable stationary states. We have see again the importance of saddle stationary states in characterizing the qualitative dynamics of particle motion. In this case, the orbits coming out of a saddle point prevented periodic motion. Further, we have repeatedly seen that the seperatrices that form the boundary of the capturing set contain a saddle stationary state. We will see this pattern again in the next case.

5.4. Dynamics With Both Inclined And Vertical Stable Stationary States

Inclined and vertical stable stationary states can coexist. For example, the parameters $\beta = .42$, $\delta = .47$ & $\gamma = .5$ have inclined and vertical stationary states. The dynamics of this case can be seen in figure 3(c). We analyze the vertical dynamics in figure 4(d). This example has five vertical and two inclined stationary states. The only vertical stable stationary state has the large particle over the smaller one at $\alpha_z = 1.15....$ The inclined stable stationary states are at $\alpha = 4.41..$ and $\theta = 1.15....$ The not stable stationary states are the far larger down stationary state at $\alpha_z = -10.6...$, the close larger down stationary state at $\alpha_z = -.548...$, the close larger up stationary state at $\alpha_z = 2.22..$ and the far larger up stationary state at $\alpha_z = 5.45....$ All the not stable stationary states are saddle points.

All orbits in the capturing set go to some stationary state, for the same reason as the previous case. In particular, the orbits coming out of the far larger up stationary state approach the inclined stable stationary states and therefore prevent periodic orbits as seen in figure 3(c). As before, the separatrix which bounds the capturing set is made up of the orbits which end in the far larger down stationary state. The orbits coming from infinity and ending at the the close larger up stationary state form the boundary between the basins of attraction of the inclined and vertical stable stationary states. This

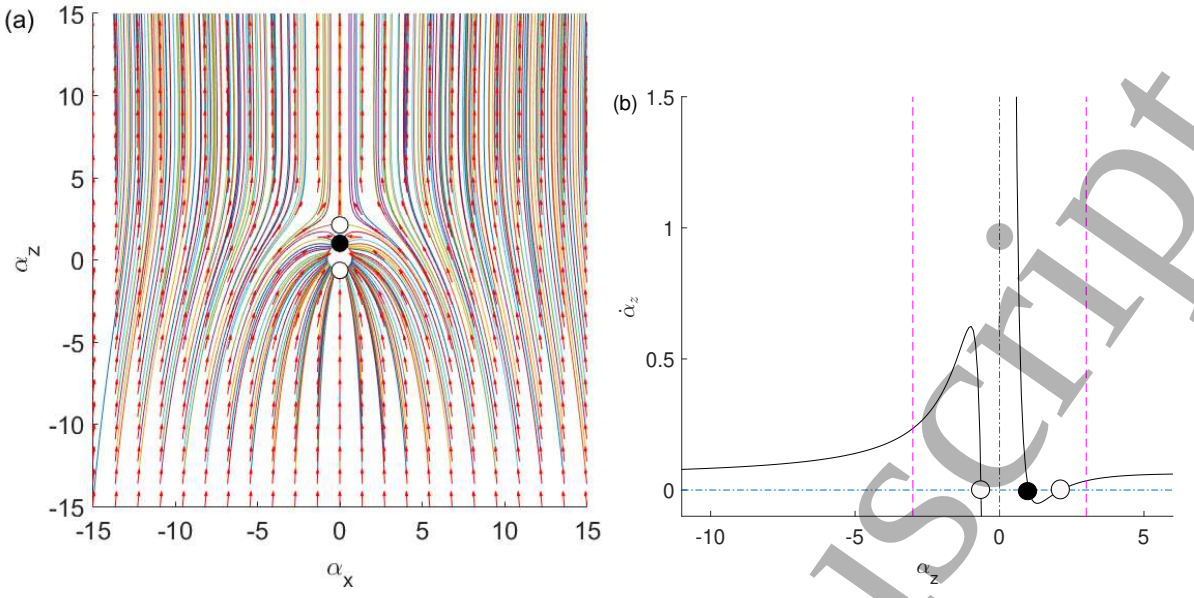

Figure 5: An example system with inverted Stokes velocity ratio $\delta/\gamma \geq 1$. One can see from the example orbits in (a) that the larger particle moves against gravity relative to the smaller particle when the separation between them is large. The dynamics when the particle centers are aligned with gravity can be read from (b). The parameters chosen are $\beta = .293...$ $\delta = .82$ & $\gamma = .8$.

completes our analysis of the global dynamics from the local behavior of the stationary states for a system with both stable and inclined stable stationary states.

6. Inverted Stokes Velocity Ratio Dynamics

In all the cases of the previous section, when particle separation is large the larger particle moves in the direction of gravity relative to the smaller particle. This is because in all the cases examined the ratio of Stokes Velocities $\delta/\gamma < 1$. It is also possible to have $\delta/\gamma \geq 1$, so that the larger particle moves against gravity relative to the smaller particle when the particle separation is large. We will call this case that of 'inverted Stokes velocity ratio". The stability considerations from section 4 do not change in form for Inverted Stokes velocity ratios. We will see by example that the Poincare-Bendixson theorem used throughout the previous section still allows us to make qualitative conclusions about the global dynamics.

As our example, we choose parameters $\beta = .293...$ $\delta = .82$ & $\gamma = .8$. This corresponds to the range (D) of the phase space γ & δ/γ, see figure 2(a) and table 1. The corresponding orbits of the larger particle (with the label 2) relative to the smaller particle (with the label 1) are illustrated in figure 5(a). One can see that even though the stable stationary state is still "larger up" ($\alpha_z > 0$), the part of the capturing set when the larger particle is above the smaller particle is now bounded, whereas in figure 3 it was not bounded. The part of the capturing set with the larger particle below

the smaller particle is now unbounded, whereas before it was bounded. This property of the capturing set corresponds to the inverted direction of the relative trajectories, which have now vertical components coming from $-\infty$ while in the previous section, they arrived from $+\infty$, in agreement with the inverted Stokes velocity ratio.

We can now extract qualitative information about the dynamics of this system. The dynamics when the particle centers are aligned with gravity are displayed in figure 5(b). The stationary state at $\alpha_z^* = 1.01...$ is stable and the stationary states at $\alpha_z^* = 2.12$ and $\alpha_z^* = -0.63$ are saddle points. There are no inclined stable stationary states. The separatrix coming into the larger up saddle point must come in from infinity. This is due to the Poincare-Bendixson theorem: the only other place the separatrix could begin is the larger down saddle point, but this would require a closed curve of orbits without a steady state in the interior. The heteroclinics coming out of the larger down saddle point must go to the stable stationary state. This is also an application of the the Poincare-Bendixson theorem: the orbit cannot diverge without crossing over the heteroclinic coming into the larger up saddle point and cannot be closed because there is no inclined stationary state to be on a closed orbit's interior. Therefore it must end in a stationary state and the only choice is the sole stable one. The curve ending in the larger saddle point is the boundary of the capturing set. Almost all the orbits on the interior of these curves end up on the stable stationary state. All the orbits on its exterior diverge, which corresponds to separation of the particles.

7. Phase Diagram For Stationary States

In section 3, we gave a phase diagram of the potential stationary states of the pair of uncharged point-particles as a function of the ratio δ/γ of Stokes velocities and the ratio γ of particle radii. Further, in subsection 4.3, we demonstrated how to reinterpret this graph in the case of inclined stationary states of charged particles. In this section we will give the phase diagram appropriate to the case of "larger up" vertical stationary states, including a heatmap with information about the separation of particle centers at the stable stationary state. We concentrate on such stationary states because we have already shown that "larger down" vertical stationary states are never stable [51]. We will also compare the phase diagrams and heat maps for vertical and inclined stationary states.

In the remainder of this section we will consider particles of the opposite charges,

$$\beta > 0, \tag{52}$$

because only in this case there exist stable stationary states, as shown in [51]. We will also assume, again following [51], that at the stationary state the particles are non-overlapping (feasible), that is,

$$1 < \alpha^* \tag{53}$$

This inequality along with equation (33) and inequalities (36) & (37) form necessary

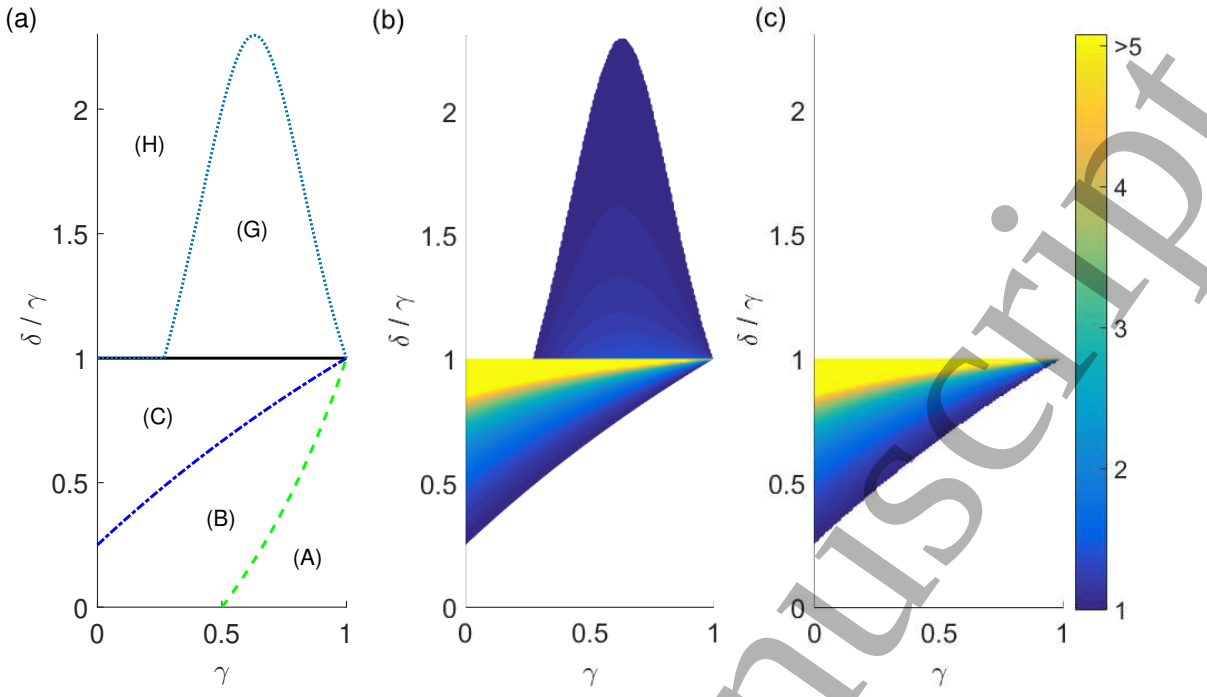

Figure 6: Phase diagrams of stationary states in the parameter space of the ratio of particle radii γ and the ratio of the particle Stokes velocities δ/γ. (a) Non-overlapping "larger up" stable stationary states exist in regions (C) and (G) but not in (A), (B) and (H). See table 2 for the properties of "larger up" stationary states in different regions. Vertical and inclined stable stationary states exist in the colored regions of (b) and (c), respectively. Brighter colors correspond to greater values of the maximum distance α_{max} between the particle centers at the stationary state, as indicated in the color bar.

and sufficient conditions for a "larger up" feasible locally asymptotically stable vertical stationary state.

To complete the list of the bounds imposed on the parameters, we remind that

$$0 < \gamma \leq 1, \qquad \delta > 0. \tag{54}$$

Our goal is to identify the characteristic regions in the parameter space of δ/γ and γ appropriate for feasible vertical "larger up" stable stationary states of charged point particles, for certain values of β & α^*. In fact, we will start by solving equation (33) for β as a function of α^*

$$\beta = \frac{3\gamma(1-\delta) - 2(\gamma-\delta)(1+\gamma)\alpha^*}{2(1+\gamma)^2\alpha^* - 6\gamma}\alpha^{*2} \tag{55}$$

The conditions (52) and (55) give the following bound on δ/γ as a function of α^* and γ,

$$\delta/\gamma > \frac{2(1+\gamma)\alpha^* - 3}{2(1+\gamma)\alpha^* - 3\gamma}. \tag{56}$$

Because the right hand side of (56) is an increasing function of α^*, the greatest lower bound for the ratio of Stokes velocities of oppositely charged particles at a feasible

stationary state is reached at $\alpha^* = 1$. This bound is

$$\delta/\gamma > \frac{2\gamma - 1}{2 - \gamma}. \tag{57}$$

The bound $\delta/\gamma = 2\gamma - 1/2 - \gamma$ is plotted by dashed line (green online) in Figure 6(a). Below this line, in the range (A), there are no feasible stationary states.

We now analyze angular stability of stationary states. We write inequality (37) as

$$\frac{\delta}{\gamma} > \frac{4(1+\gamma)\alpha^* - 3}{4(1+\gamma)\alpha^* - 3\gamma} \tag{58}$$

The minimum of the right hand side, reached at $\alpha^* = 1$, is the greatest lower bound in the phase space $(\delta/\gamma, \gamma)$ for existence of feasible stationary states stable against angular perturbations,

$$\frac{\delta}{\gamma} > \frac{4\gamma + 1}{4 + \gamma} \tag{59}$$

The bound is plotted by dash-dot line (blue online) in Figure 6(a). Below this line, in the range (B), all feasible stationary states are angularly unstable. We now analyze radial stability of stationary states. We use equation (55) to eliminate β from (37). After a careful analysis of signs we obtain

$$\frac{\delta}{\gamma} < P(\gamma, \alpha^*) \tag{60}$$

where

$$P(\gamma, \alpha^*) = \frac{18\gamma + 4(1+\gamma)^3\alpha^{*2} - 3(1+\gamma)(1+7\gamma)\alpha^*}{18\gamma^2 + 4(1+\gamma)^3\alpha^{*2} - 3\gamma(1+\gamma)(7+\gamma)\alpha^*}. \tag{61}$$

It leads to the following least upper bound in the phase space $(\delta/\gamma, \gamma)$ for existence of stationary states stable against radial perturbations,

$$\delta/\gamma < R(\gamma), \tag{62}$$

where

$$R(\gamma) = \begin{cases} 1 & \text{for } \gamma \le 2-\sqrt{3} \\ P(\gamma, 1) & \text{for } \gamma > 2-\sqrt{3} \end{cases} \tag{63}$$

The bound (62)-(63) is plotted in Figure 6(a) as the sum of the boundaries between regions (C) and (H) & regions (G) and (H). Above it, in the range (H), all stationary states are radially unstable.

Basic properties of "larger up" vertical stationary states in the regions (A)-(H) are outlined in table 2. Recall that the ratio of forces $\beta > 0$ has been eliminated using the stationary condition (33) and so remarks about stability should be interpreted with the β so derived. For $\delta/\gamma < 1$ the requirement of the opposite charges (56) and the angular stability condition (58) give the upper bounds on the interparticle distance at a stationary state, $\alpha^* < 2M(\delta/\gamma, \gamma)$ and $\alpha^* < M(\delta/\gamma, \gamma)$, respectively, with

$$M(\delta/\gamma, \gamma) = \frac{3\gamma(\frac{1}{\gamma} - \frac{\delta}{\gamma})}{4(1 - \frac{\delta}{\gamma})(1+\gamma)}. \tag{64}$$

Table 2: Properties of "larger up" non-overlapping vertical stationary states (each with a certain value of $\beta > 0$).

	region	properties of stationary states
(A)	$0 < \frac{\delta}{\gamma} \leq \frac{2\gamma - 1}{2 - \gamma}$ or $\gamma = 1$	There are no stationary states with $\alpha^* > 1$.
(B)	$\frac{2\gamma - 1}{2 - \gamma} < \frac{\delta}{\gamma} \leq \frac{4\gamma + 1}{4 + \gamma}$	For any $1 < \alpha^* < 2M(\delta/\gamma, \gamma)$ there exists a stationary state. There are no stationary states with $\alpha^* > 2M(\delta/\gamma, \gamma)$. Each stationary state is unstable with respect to angular perturbations.
(C)	$\frac{4\gamma + 1}{4 + \gamma} < \frac{\delta}{\gamma} < 1$	For any $1 < \alpha^* < 2M(\delta/\gamma, \gamma)$ there exists a stationary state. There are no stationary states with $\alpha^* > 2M(\delta/\gamma, \gamma)$. For $1 < \alpha^* < M(\delta/\gamma, \gamma)$ there exist stable stationary states. For $M(\delta/\gamma, \gamma) \leq \alpha^* < 2M(\delta/\gamma, \gamma)$ stationary states are angularly unstable.
(G)	$1 \leq \frac{\delta}{\gamma} < R(\gamma)$ and $2 - \sqrt{3} < \gamma < 1$	For any $\alpha^* > 1$ there exists a stationary state. Each stationary state is stable against angular perturbations. There exist stable stationary states.
(H)	$R(\gamma) \leq \frac{\delta}{\gamma}$	For any $\alpha^* > 1$ there exists a stationary state. Each stationary states is radially unstable and angularly stable.

In general, for a given β, γ and δ/γ there might be several stable "larger up" vertical stationary states with different values of the distance α^*. We focus on the largest of them. We find the upper bound on the separation of particle centers, which is graphed in figure 6(b), where the regions of increasingly bright color correspond to regions of increasing separations. The white space corresponds to regions which do not have feasible stable stationary states. Analytically, we choose α_{max} as the least upper bound of the α^* which satisfy inequalities (58) & (60) and we derive the following relation in region (C),

$$\frac{\delta}{\gamma} = \frac{3 - 4(1+\gamma)\alpha_{max}}{3\gamma - 4(1+\gamma)\alpha_{max}} \tag{65}$$

In region (G) this relation is

$$\frac{\delta}{\gamma} = \max\left[1, P(\gamma, \alpha_{max})\right] \tag{66}$$

For comparison, we graph in figure 6(c) the separations of particles for inclined stationary states given by equation (45). As we previously noted, these are feasible only in region (C). One must take care during interpretation because what is plotted in this figure is the exact value rather than merely an upper bound. One can see that for inclined equilbria the lines of constant interparticle separation are monotonically functions of γ, that is that it takes an increasing ratio of Stokes velocities to balance a system with increasing reduced masses at the same separation distance.

8. Conclusions

We have shown that coexistence of hydrodynamic and electrostatic interactions between particles sedimenting in Stokes flows leads to the dynamics essentially different than in the absence of charge or in the absence of fluid. Using the point-particle model, we demonstrated analytically that charged particles can form stable doublets with basins of attraction in the space of the particle relative positions which are very large in comparison to particle radius. This result indicates that charged sedimenting particles can capture one another, even if the initial distance between them is large. The captured particles tend to a certain stable relative position, where the distance between the particle centers is larger than the sum of their radii, so that their surfaces are separated from each other by a fluid. In particular, there exist stable stationary configurations of charged particles separated by large distances, with large basins of attraction, within the range where the hydrodynamic interactions can be approximated as point-like.

Moreover, even if the ratio β of electrostatic to gravitational forces is very small, the dynamics of pairs of charged particles is both quantitatively and qualitatively different from the dynamics in the absence of any electrostatic interactions. The main qualitative difference is the structure of the capturing set in the space of relative positions. For charged particles, the capturing set consists of trajectories tending to a stationary state while for uncharged particles, it consists of neutrally stable periodic orbits.

The existence of a capturing set in the space of the relative positions is associated with the existence of stable stationary configurations of two charged sedimenting particles. However, stable stationary states are formed only for certain ranges of the ratio of particle radii γ and the ratio of Stokes velocities δ/γ. Therefore, we have determined the region in the parameter space of γ and δ/γ where stable stationary configurations exist for certain values of β, and for a certain range of values of the distance $\alpha^* > 1$ between the particles at the stable stationary state. In this way, we have shown that the capturing of charged particles takes place in a large region in the parameter space of γ and δ/γ. Interestingly, for some values of β, γ and δ/γ there exist multiple stable stationary states inside the capturing set.

We have found stable stationary states with the line-of-centers at an angle ψ inclined with respect to gravity. In the point-particle model, $\cos(\psi)$ is proportional to the ratio β of electrostatic to gravitational force while the particle-to-particle separation distance $\alpha^\dagger$ at the inclined stationary state does not depend on β.

By analyzing examples of capturing sets, we have found that the basin of attraction of all stable stationary states has a boundary which is a surface of revolution of a trajectory which ends on a saddle point stationary state with the particle centers vertically aligned. It seems that the difference between vertical positions of the particles at this stationary state can be used as an estimate of "the cross-section" of the capturing set. For example, in figure 3(b) and 3(d) the cross section is more than 10 times the sum of the particle radii $a_1 + a_2$, and particle at the stable stationary configuration are separated by more than $4(a_1 + a_2)$. For large capturing sets and large particle separations, the particle dynamics is well-approximated by the point- particle model. Therefore, the analysis presented here suggests that the existence of stable doublets could be confirmed by future experiments.

Acknowledgements

This work was supported in part by the National Science Centre under grant UMO-2018/31/B/ST8/03640.

[1] Witten T A and Diamant H 2020 A review of shaped colloidal particles in fluids: Anisotropy and chirality Reports on Progress in Physics **83** 116601
[2] Ramaswamy S 2001 Issues in the statistical mechanics of steady sedimentation Advances in Physics **50** 297–341
[3] Guazzelli E and Hinch J 2011 Fluctuations and instability in sedimentation Annual review of fluid mechanics **43** 97–116
[4] Fabry T L 1987 Mechanism of erythrocyte aggregation and sedimentation Blood **70** 1572–1576
[5] Peltomäki M and Gompper G 2013 Sedimentation of single red blood cells Soft Matter **9** 8346–8358
[6] Rallabandi B, Nunes J K, Perazzo A, Gershtein S and Stone H A 2019 Representative subsampling of sedimenting blood Proc. Math. Phys. Eng. **475** 20190223
[7] Stone H A and Kim S 2001 Microfluidics: basic issues, applications, and challenges AIChE J **47** 1250–1254
[8] Link D, Anna S L, Weitz D and Stone H 2004 Geometrically mediated breakup of drops in microfluidic devices Phys. Rev. Lett. **92** 054503
[9] Stone H A, Stroock A D and Ajdari A 2004 Engineering flows in small devices: microfluidics toward a lab-on-a-chip Annu. Rev. Fluid Mech. **36** 381–411
[10] Squires T M and Quake S R 2005 Microfluidics: Fluid physics at the nanoliter scale Rev. Mod. Phys. **77** 977
[11] Whitesides G M 2006 The origins and the future of microfluidics Nature **442** 368–373
[12] Lauga E and Powers T R 2009 The hydrodynamics of swimming microorganisms Rep. Prog. Phys. **72** 096601
[13] Rizvi M S, Peyla P, Farutin A and Misbah C 2020 Deformable microswimmer in an external force field Phys. Rev. Fluids **5**(3) 033101
[14] Stark H 2016 Swimming in external fields Eur Phys J Spec Top **225** 2369–2387
[15] Huang Z, Abkarian M and Viallat A 2011 Sedimentation of vesicles: from pear-like shapes to microtether extrusion New Journal of Physics **13** 035026
[16] Coutinho C A, Harrinauth R K and Gupta V K 2008 Settling characteristics of composites of pnipam microgels and tio2 nanoparticles Colloids Surf, A Physicochem Eng Asp **318** 111–121
[17] Alldredge A L and Silver M W 1988 Characteristics, dynamics and significance of marine snow Prog. Oceanogr. **20** 41–82
[18] Kerr R C, Mériaux C and Lister J R 2008 Effect of thermal diffusion on the stability of strongly tilted mantle plume tails J. Geophys. Res. Solid Earth **113**

[19] Schwindinger K R 1999 Particle dynamics and aggregation of crystals in a magma chamber with application to kilauea iki olivines J Volcanol Geotherm Res **88** 209–238
[20] Kerr R C and Lister J R 1991 The effects of shape on crystal settling and on the rheology of magmas J. Geol **99** 457–467
[21] Stokes G G 1851 On the effect of the internal friction of fluids on the motion of pendulums Trans. Camb. Phil. Soc. **9** 8–94
[22] Lamb H 1895 Hydrodynamics (Cambridge University Press)
[23] Batchelor G K 2000 An introduction to fluid dynamics (Cambridge University Press)
[24] Russel W B, Russel W, Saville D A and Schowalter W R 1991 Colloidal Dispersions (Cambridge University Press)
[25] Pozrikidis C 1992 Boundary integral and singularity methods for linearized viscous flow (Cambridge University Press)
[26] Kim S and Karrila S J 2013 Microhydrodynamics: principles and selected applications (Courier Corporation)
[27] Guazzelli E and Morris J F 2011 A physical introduction to suspension dynamics (Cambridge University Press)
[28] Happel J and Brenner H 2012 Low Reynolds number hydrodynamics: with special applications to particulate media vol 1 (Springer Science & Business Media)
[29] Duprat C and Stone H A 2015 Fluid-structure interactions in low-Reynolds-number flows (Royal Society of Chemistry)
[30] Graham M D 2018 Microhydrodynamics, Brownian motion, and complex fluids (Cambridge University Press)
[31] Shen B, Leman M, Reyssat M and Tabeling P 2014 Dynamics of a small number of droplets in microfluidic Hele–Shaw cells Exp. Fluids **55** 1–10
[32] Delmotte B 2019 Hydrodynamically bound states of a pair of microrollers: A dynamical system insight Phys. Rev. Fluids **4** 044302
[33] Fouxon I, Rubinstein B, Ge Z, Brandt L and Leshansky A 2020 Theory of hydrodynamic interaction of two spheres in wall-bounded shear flow Phys. Rev. Fluids **5** 054101
[34] Singha S, Malipeddi A R, Zurita-Gotor M, Sarkar K, Shen K, Loewenberg M, Migler K B and Blawzdziewicz J 2019 Mechanisms of spontaneous chain formation and subsequent microstructural evolution in shear-driven strongly confined drop monolayers Soft Matter **15** 4873–4889
[35] Driscoll M, Delmotte B, Youssef M, Sacanna S, Donev A and Chaikin P 2017 Unstable fronts and motile structures formed by microrollers Nat. Phys. **13** 375–379
[36] Hocking L 1964 The behaviour of clusters of spheres falling in a viscous fluid part 2. Slow motion theory J. Fluid Mech. **20** 129–139
[37] Tory E M and Kamel M T 1992 A note on the periodic motion of four spheres Powder technology **73** 95–96
[38] Jánosi I M, Tél T, Wolf D E and Gallas J A 1997 Chaotic particle dynamics in viscous flows: The three-particle stokeslet problem Phys. Rev. E **56** 2858
[39] Ekiel-Jeżewska M, Metzger B and Guazzelli E 2006 Spherical cloud of point particles falling in a viscous fluid Phys. Fluids **18** 038104
[40] Metzger B, Nicolas M and Guazzelli É 2007 Falling clouds of particles in viscous fluids J. Fluid Mech **580** 283
[41] Alabrudziński S, Ekiel-Jeżewska M L, Chehata-Gómez D and Kowalewski T A 2009 Particle clusters settling under gravity in a viscous fluid Phys. Fluids **21** 073302
[42] Mylyk A, Meile W, Brenn G and Ekiel-Jeżewska M L 2011 Break-up of suspension drops settling under gravity in a viscous fluid close to a vertical wall Phys. Fluids **23** 063302
[43] Goldfriend T, Diamant H and Witten T A 2017 Screening, hyperuniformity, and instability in the sedimentation of irregular objects Physical review letters **118** 158005
[44] Chajwa R, Menon N and Ramaswamy S 2019 Kepler orbits in pairs of disks settling in a viscous

fluid Phys. Rev. Lett. **122** 224501
[45] Chajwa R, Menon N, Ramaswamy S and Govindarajan R 2020 Waves, algebraic growth, and clumping in sedimenting disk arrays Physical Review X **10** 041016
[46] Wacholder E and Sather N 1974 The hydrodynamic interaction of two unequal spheres moving under gravity through quiescent viscous fluid J. Fluid Mech. **65** 417–437
[47] Davis R H 1984 The rate of coagulation of a dilute polydisperse system of sedimenting spheres J. Fluid Mech **145** 179–199
[48] Batchelor G 1982 Sedimentation in a dilute polydisperse system of interacting spheres. part 1. general theory J. Fluid Mech **119** 379–408
[49] Batchelor G and Wen C S 1982 Sedimentation in a dilute polydisperse system of interacting spheres. part 2. numerical results J. Fluid Mech **124** 495–528
[50] Bürger R, Karlsen K H, Tory E M and Wendland W L 2002 Model equations and instability regions for the sedimentation of polydisperse suspensions of spheres ZAMM-Journal of Applied Mathematics and Mechanics/Zeitschrift für Angewandte Mathematik und Mechanik: Applied Mathematics and Mechanics **82** 699–722
[51] Trombley C I and Ekiel-Jeżewska M L 2018 Stable configurations of charged sedimenting particles Phys. Rev. Lett. **121**(25) 254502
[52] Banchio A J, Gapinski J, Patkowski A, Häußler W, Fluerasu A, Sacanna S, Holmqvist P, Meier G, Lettinga M P and Nägele G 2006 Many-body hydrodynamic interactions in charge-stabilized suspensions Phys. Rev. Lett. **96** 138303
[53] Nie D, Guan G and Lin J 2021 Interaction between two unequal particles at intermediate Reynolds numbers: A pattern of horizontal oscillatory motion Phys. Rev. E **103** 013105
[54] Lu J, Nordsiek H and Shaw R A 2010 Clustering of settling charged particles in turbulence: theory and experiments New J. Phys. **12** 123030
[55] Saw E W, Shaw R A, Salazar J P and Collins L R 2012 Spatial clustering of polydisperse inertial particles in turbulence: Ii. comparing simulation with experiment New J. Phys. **14** 105031
[56] Nosenko V, Ivlev A, Kompaneets R and Morfill G 2014 Stability and size of particle pairs in complex plasmas Phys. Plasmas **21** 113701

8 Author Contributions

In **Article A**,

Basic Concepts of Stokes Flows

Published in *Flowing Matter* (pp. 35-50). Editors: Toschi, F. and Sega, M., Springer, Cham.

Christopher Trombley

- Wrote Examples Of Reversibility
- Created figures 2.1 & 2.3
- Analyzed Stokes paradox
- Gave interrelations between the basic concepts of Stokes Flow

Maria Ekiel-Jezewska

- Provided figure 2.2
- Provided example of accelerating fluid in Stokes flow
- Concieved and supervised the study

Both authors designed the review and wrote the manuscript.

Christopher Trombley

Christopher Trombley Maria Ekiel-Jezewska

In **Article C**,

Relative Trajectories Of Two Charged Sedimenting Particles In A Stokes Flow

Published in Journal Of Physics Communications (2021)

Christopher Trombley

- Co-concieved of the study
- Created figures
- Applied point particle model
- Found exact solutions for uncharged heteroclinics
- Found inclined stable stationary configurations of charged particles
- Performed linear stability analysis
- Applied Poincare-Bendixson theorem to find qualitative dynamics
- Found some bounds for ratio of Stokes Velocity and ratio of particle radii

Maria Ekiel-Jezewska

- Created tables
- Found some bounds for ratio of Stokes Velocity and ratio of particle radii
- Co-concieved of and supervised the study

Both authors wrote the manuscript and performed analytical calculations.

Christopher Trombley

Christopher Trombley Maria Ekiel-Jezewska

In **Article B**,

Stable Configurations of Charged Sedimenting Particles

Published in Physical Review Letters 121, 254502 (2018)

Christopher Trombley

- Co-concieved of the study
- Researched Earnshaw's Theorem for electrostatics
- Applied point particle model
- Found the perturbative dynamics to establish stationary, stability and feasibility conditions
- Co-established necessary conditions on parameters for the existence of a stable stationary state
- Created figures and table
- Performed analysis in Supplemental Materials 1 & 2

Maria Ekiel-Jezewska

- Provided applications of microparticles in a Stokes flow
- Co-established necessary conditions on parameters for the existence of a stable stationary state
- Performed asymptotic analysis in the limit of large distances
- Performed analysis in Supplemental Materials 3
- Co-concieved and supervised the study

Both authors designed the study and wrote the manuscript.

Christopher Trombley

Christopher Trombley

Maria Ekiel-Jezewska